Dissertation

Universität Bremen
Fachbereich für Physik und Elektrotechnik
Institut für Umweltphysik

Atmospheric Trace Gas Measurements in the Tropics

Zur Erlangung des akademischen Grades eines
Doktor der Naturwissenschaften (Dr. rer. nat)

vorgelegt von

Anna Katinka Petersen

Gutachter:
Prof. Dr. Justus Notholt
Prof. Dr. David Griffith

Bremen, 17. April 2009

Abstract

Fourier Transform Infrared (FTIR) spectrometry has been used for ground-based solar absorption, laboratory and flux measurements, to study the atmospheric composition, as well as physical and chemical processes in the atmosphere.

The solar absorption FTIR measurements have been performed in Paramaribo, Suriname (5.8°N, 55.2°W) between September 2004 and November 2007 and represent the first remote sensing measurements in the inner tropics over several years. These measurements are of great importance for a better understanding of global climate and physical and chemical processes of the tropical atmosphere as well as for satellite validations. Vertical profiles of carbon monoxide (CO) and ethane (C_2H_6) and total columns of methane (CH_4), hydrogen cyanide (HCN) and acetylene (C_2H_2) have been retrieved from the FTIR spectra.

The quality of the methane retrieval was limited by the available spectroscopic data. Laboratory cell-based FTIR measurements have been performed to correct the methane spectroscopy in the infrared spectral region, which significantly improved the retrieval of methane from SCIAMACHY and FTIR spectra. The retrieval of methane profiles from near-infrared FTIR spectra by optimal estimation significantly improved the results.

The FTIR observations of methane are compared with TM5 model simulations and satellite observations from SCIAMACHY, and are the first validation of the SCIAMACHY retrieval in the tropics using remote sensing techniques. The ratio CH_4/CO_2, which can be measured directly from SCIAMACHY and FTIR, compares very good, while the column averaged volume mixing ratio (XVMR(CH_4)) of SCIAMACHY do not agree with the FTIR observations. Model assumptions are used in the SCIAMACHY retrieval to derive the XVMR(CH_4) from the directly measured CH_4/CO_2 ratio. The worse agreement of SCIAMACHY XVMR(CH_4) with FTIR compared to the SCIAMACHY CH_4/CO_2 ratio with FTIR could be attributed to unrealistic model assumptions used in the SCIAMACHY retrieval that led to wrong time series of the column averaged CH_4 VMR. There is a good agreement of the FTIR XVMR(CH_4) with the TM5 model.

FTIR observations of carbon monoxide agree well with satellite data from the MOPITT instrument for all of the measurement campaigns. Simulations of CO and C_2H_6 from the MATCH-MPIC model reproduce the mean vertical structure of the FTIR observations. The model is generally not able to reproduce the extreme

enhancements seen during the specific biomass burning events by both observation instruments. Nevertheless, the model indicates that beyond the background source of CO from methane oxidation, the main contributions to the CO mixing ratios are the episodic convective injection of NMHCs and CO from South American biomass burning into the upper troposphere, along with long range transport of African biomass burning CO, particularly during spring. Revised simulation of the MATCH-MPIC model with improved biomass burning emissions still fails to reproduce most of the individual observed pollution events. It generally underestimates the observed concentrations of carbon monoxide and ethane. The revised model is in better agreement with the observations in the upper troposphere, while in the boundary layer and lower troposphere the revised model underestimates the FTIR measurements and results in underestimated total columns. Current generation atmospheric chemistry models underestimate OH is the tropical region and compensate for this part by too low isoprene emissions. It is speculated that, if a mechanism like e.g. isoprene recycling and realistic isoprene emissions would be included in current models, it would result in a powerful CO source in the boundary layer over Suriname from the isoprene oxidation. The CO oxidation rate would also increase due to higher OH concentrations. Because of the complex chemistry and transport processes, it is difficult to predict the exact changes without having done the simulations.

The last part of this work presents the development of an advanced flux measurement technique, consisting of a cell-based FTIR analyser and a Relaxed Eddy Accumulation (REA) system, to enable automated and continuous flux measurements of atmospheric trace gases. The combination of the REA technique with the FTIR analyzer was tested successfully in the lab and during a three weeks field campaign. The FTIR-REA technique offers the capacity to measure a range of gases simultaneously under field conditions and enables long-term measurements and monitoring of atmospheric greenhouse gas fluxes.

Publications

Journal Articles

Petersen, A. K., Warneke, T., Lawrence, M. G., Notholt, J., and Schrems, O.: First ground-based FTIR observations of the seasonal variation of carbon monoxide in the tropics, Geophys. Res. Lett., 35, doi:10.1029/2007GL031393, 2008.

Frankenberg, C., Bergamaschi, P., Butz, A., Houweling, S., Meirink, J.-F.,Notholt, J., Petersen, A. K., Schrijver, H., Warneke, T., and Aben, I.: Tropical methane emissions: A revised view from SCIAMACHY onboard ENVISAT, Geophys. Res. Lett., doi:10.1029/2008GL034300, 2008.

Articles in Conference Proceedings

P. Duchatelet, E. Mahieu, P. Demoulin, C. Frankenberg, F. Hase, J. Notholt , A. K. Petersen , P. Spietz , M. De Mazière and C. Vigouroux: Impact of different spectroscopic datasets on CH_4 retrievals from Jungfraujoch FTIR spectra, Proceeding ASA (Atmospheric Spectroscopy Applications) meeting in Reims (August 2008)

Presentations at Conferences

Petersen, A. K. et al., Combined FTIR-micrometeorological techniques for long term measurements of greenhouse gas fluxes from agriculture, DPG-Tagung in Hamburg, March 2009 (Poster presentation)

Petersen, A. K. et al, Carbon monoxide and ethane in the tropics, SCOUT Tropical Meeting in Manchester (GB), January 2008 (Poster presentation)

Petersen, A. K. et al., Atmospheric trace gas measurements in Suriname, Conference: Water and future development of Suriname in Paramaribo (Suriname), November 2007 (Talk)

Petersen, A. K. et al., First ground-based FTIR-observations of the seasonal variation of carbon monoxide in the tropics, Reunion Island International Symposium in La Reunion Island (F), November 2007 (Poster presentation)

Petersen, A. K. et al., First ground-based FTIR-observations of the seasonal variation of carbon monoxide in the tropics, SPARC-Meeting in Bremen, September 2007 (Poster presentation)

Petersen, A. K. et al., Methane from ground-based remote sensing measurements in the tropics, ACCENT-Symposium in Urbino (Italy), July 2007 (Poster presentation)

Petersen, A. K. et al., Ground-based solar absorption measurements of atmospheric trace gases in the tropics, NDACC-Meeting in Tenerife (Spain), May 2007 (Talk)

Petersen, A. K. et al., Ground-based solar absorption measurements of atmospheric trace gases in the tropics, EGU-conference in Vienna (Austria), April 2007 (Talk)

Petersen, A. K. et al., Ground-based solar absorption measurements of atmospheric trace gases in the tropics, DPG-Tagung in Regensburg, March 2007 (Talk)

Petersen, A. K. et al., Atmospheric trace gas measurements in the tropics by FTIR-spectrometry, STAR-Summerschool in Paramaribo, Suriname, March 2006 (Talk)

Contents

Motivation

Motivation and Objectives of this Thesis

Measurements and interpretation of atmospheric trace gas composition and the exchange of trace gases between the atmosphere, biosphere and geosphere are of significant importance for a better understanding of budgets, sources and sinks of trace gases important for atmospheric chemistry, the greenhouse effect and climate change.

Especially the composition of the tropical atmosphere and its change is of significant importance. Since several decades, rapid population growth and industrial development, along with deforestation, are increasingly changing the environment in the tropical countries. The effect of these changes on atmospheric composition and climate are quite uncertain, as the governing physical and chemical processes of the tropical atmosphere are only poorly understood.

For the understanding of physical and chemical states of the stratosphere and upper troposphere and for assessing the impact of stratospheric changes on the underlying troposphere and on global climate, remote sensing observations play an important role. Satellite observations are well suited to reveal global trace gas distributions and trends, and to deduce strength and spatiotemporal distribution of sources and sinks by inverse modeling. However, satellite observations are essential useless without validation. Aiming for high accuracy and precision, the improvement of retrieval strategies and validation by in situ and ground-based remote sensing observations is required. Ground-based FTIR solar absorption spectrometry is a well-established remote sensing technique for the measurement of atmospheric trace gases. For many important trace gases ground-based solar absorption FTIR spectrometry is the only remote sensing technique suitable for the validation of satellites.

Systematic observations of relevant atmospheric parameters are scarce over the oceans, the poles and in tropical regions. In the tropics the lack of observations is mostly due to the inaccessibility of the tropical forests and the vast tropical oceans, as well as the lower priorities given to these observations by developing countries. Before 2004, there have been no FTIR observations in the inner tropics. For many gases, FTIR spectrometry is the only ground-based remote sensing technique that can provide information with the required precision; examples are column averages

of methane and profiles of carbon monoxide. The primary objective of this work was to perform ground-based solar absorption FTIR measurements at the tropical site Paramaribo, Suriname, and to retrieve vertical profiles and total column concentrations of carbon monoxide and methane with sufficient precision to be useful for the validation of satellite retrievals and for the comparison with model simulations. Trace gas observations e.g. of CO or ethane can serve to test predictions of atmospheric transport and chemistry models and to check source strength and geographic distribution of sources of atmospheric trace gases. The vertical distribution and total columns of methane can be retrieved from solar absorption FTIR spectra. Although several retrieval approaches for methane profiles exist, the retrieved vertical profiles of methane often show large oscillations in the troposphere. The target of my work was to improve the retrieval of methane from FTIR spectra. Thus, laboratory cell-based FTIR measurements were performed to improve the spectroscopy of methane in the infrared spectral region. The tropical FTIR observations of methane are aimed to validate the SCIAMACHY retrieval.

The chance to get an research scholarship from the Endeavour Programme of the Australian Government provided me the possibility to go for six month to Wollongong, Australia. During this stay, I was involved in the construction of an in situ analyzer based on FTIR spectrometry. This FTIR in situ analyzer was used in combinations with a micrometeorological flux measurement technique. The aim of my work was the advancement of this technique with a so called "lung-system" in order to enable continuous performance and make this combined technique suitable for long-term measurements of atmospheric trace gas fluxes.

Outline of the thesis

The thesis is devided in three main parts, which can be read independently:

Part I provides the fundamental background and motivation for this work. It includes a short overview about the physics and chemistry of the atmosphere and its current changes. The tropical measurement site Paramaribo is introduced and its relevance in the global observation network for the monitoring of greenhouse gases and satellite validation is outlined. The technique of FTIR spectrometry for remote sensing and for in situ measurements using absorption spectra in the infrared is described in the last section.

Part II presents remote sensing observations using ground-based FTIR solar absorption spectrometry. It is devided into two chapters. In the first one, methane observations in the tropics are presented. First, the efforts undertaken for the improvement of the methane retrieval from FTIR solar absorption spectra are

described, including laboratory cell-based FTIR measurements for methane spectroscopy. Then, results from solar absorption FTIR measurements performed at the tropical site Paramaribo, Suriname are presented. The tropical FTIR measurements are compared with satellite observations from SCIAMACHY and TM5 model simulations for Paramaribo. Furthermore, flask surface observations of methane sampled in Paramaribo are shown and compared with the surface output from the TM5 model.

The second chapter presents tropical observations of carbon monoxide and other short-lived trace gases related to biomass burning. The FTIR observations of CO are compared with model simulations and satellite data. In the last part, revised emission scenarios for the model are discussed.

Part III gives first an overview about different flux measurement techniques and the motivation for the developement of an advanced flux measurement technique. The new method is then described in detail, including a description of its components. Results from a three weeks measurement campaign, where the technique has been tested under real conditions, are presented.

An appedix provides supplementary material.

Part I

Fundamentals

1 The Earth's Atmosphere

1.1 Composition of the Atmosphere and its Current Changes

The content of this section is largely adopted from the assessment reports of the Intergovernmental Panel on Climate Change (IPCC, 2007) and standard textbooks (e.g. Wallace and Hobbs, 2006)). A short introduction to tropospheric chemistry relevant for this work is given in the Appendix A.

The Earth's atmosphere consists of about 78 % nitrogen, 21 % oxygen and 0.9 % argon. Water vapour, which accounts for roughly 0.25 % of the mass of the atmosphere, is a highly variable constituent, with concentrations ranging from around 5 ppmv (parts per million by volume) in the coldest regions of the Earth' atmosphere up to as much as 5 % by volume in hot, humid air masses. Less than 0.1 % is formed by the so called trace gases, e.g. carbon dioxide (on average 380 ppm (parts per million)) and methane (1775 ppb (parts per billion)). Despite their low mixing ratios, the trace gases play an important role in atmospheric chemistry and physics, especially in the context of the natural and anthropogenic greenhouse effect and climate change.

The Earth's atmosphere is more transparent to incoming solar radiation than to outgoing radiation emitted by the Earth's surface. The absorption and reemission of outgoing radiation by the atmosphere, the so called greenhouse effect, keeps the Earth's surface warmer than it would be in the absence of atmospheric trace gases. Due to the presence of clouds and aerosols in the Earth's atmosphere, ∼22 % of the incoming solar radiation is backscattered to space without being absorbed. The backscattering of radiation by clouds and aerosols has in general a cooling effect on global climate, which opposes the greenhouse effect.

The most important greenhouse gases are water vapour, carbon dioxide (CO_2, methane (CH_4) and nitrous oxide (N_2O). Global atmospheric concentrations of CO_2, CH_4 and N_2O have increased markedly as a result of human activities since 1750 and now far exceed pre-industrial values determined from ice cores spanning many thousands of years (see Figure 1.1). The global increases in carbon dioxide concentration are primarily due to fossil fuel use and land use change (mainly deforestation), while those of methane and nitrous oxide are primarily due to agriculture.

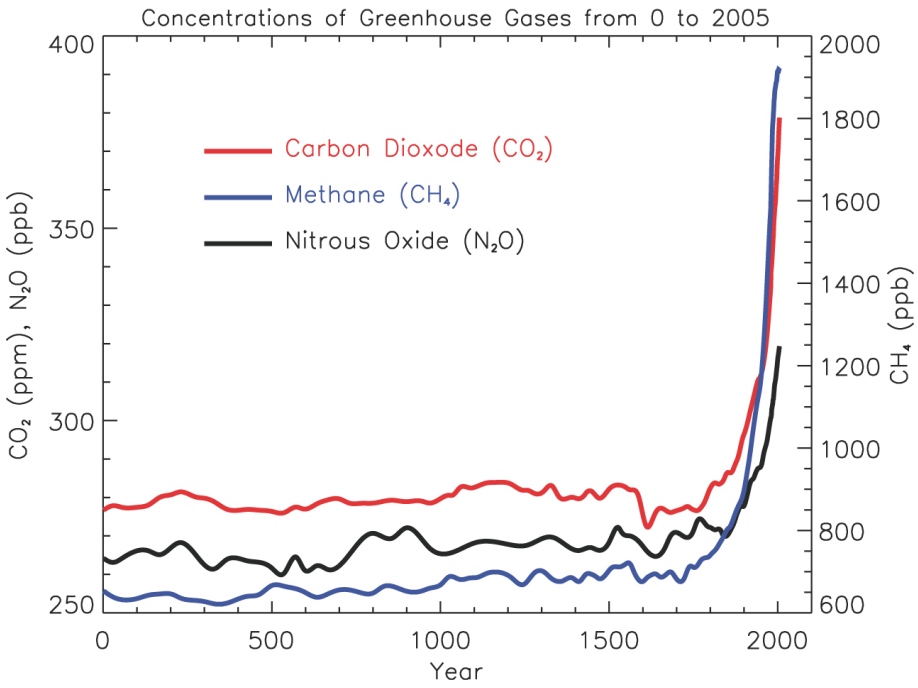

Figure 1.1: Atmospheric concentrations of the greenhouse gases CO_2, CH_4 and N_2O over the last 2,000 years. Increases since about 1750 are attributed to human activities in the industrial era. (IPCC, 2007).

The Intergovernmental Panel on Climate Change (IPCC) use the concept of radiative forcing to quantify the strength of forcing agents (natural and anthropogenic) causing climate change. Radiative forcing is a measure of the influence that a factor has in altering the balance of incoming and outgoing energy in the Earth-atmosphere system and is an index of the importance of the factor as a potential climate change mechanism. Figure 1.2 shows the components of radiative forcing of climate change since the start of the industrial era. Human activities have on global average a warming net effect, with a radiative forcing of +1.6 [+0.6 to +2.4] Wm^{-2} (IPCC: Forster et al. (2007)). Even if the greenhouse gas concentrations are held fixed at their 2005 concentration levels, the world will observe an estimated warming of 2.4°C [1.4 to 4.3°C] above preindustrial temperatures, which is the specified range where the planet is committed to widespread loss of biodiversity and widespread deglaciation. Continued greenhouse gas emissions at or above current rates would cause further warming and induce many changes in the global climate system. Even if greenhouse gas concentrations were to be stabilized, anthropogenic warming and sea level rise is expected to continue for centuries due to the time scales associated with climate processes. Large factors of uncertainty in the quantification of future global warming are potential feedback effects, e.g. the ability of the ocean and terrestrial biosphere to take up CO_2 is expected to decline as global warming continues. The consequences of the global warming, like sea level rise, changes in sea ice, precipitation and temperature patterns will have large socioeconomic impacts.

1.2 Structure of the Atmosphere

Atmospheric pressure is a direct consequence of the weight of the air column above the measurement point due to gravity. Pressure and density decrease nearly exponentially with height, i.e.,

$$p(z) \simeq p(z_0) \exp\left(-\frac{(z - z_0) M_{air} g}{RT}\right) \tag{1.1}$$

where $p(z_0)$ is the pressure at some reference level z_0, which is usually taken as sea level, T the mean temperature of the atmosphere between z and z_0, M_{air} the molar mass of dry air (28.96 g/mole), g the acceleration due to gravity (9.81 ms^{-2}) and R the universal gas constant (8.31 $\mathrm{JK}^{-1}\mathrm{mol}^{-1}$).

The atmosphere is not isotherm and can be divided into different layers according to temperature variations. Figure 1.3 shows the vertical structure of the atmosphere. The lowest layer is called the troposphere. It extends from the surface to between 7 km at the poles and 17 km at the equator and is further separated in the boundary layer and the overlying free troposphere. The maximum temperature in the troposphere is usually reached at the surface due to emission

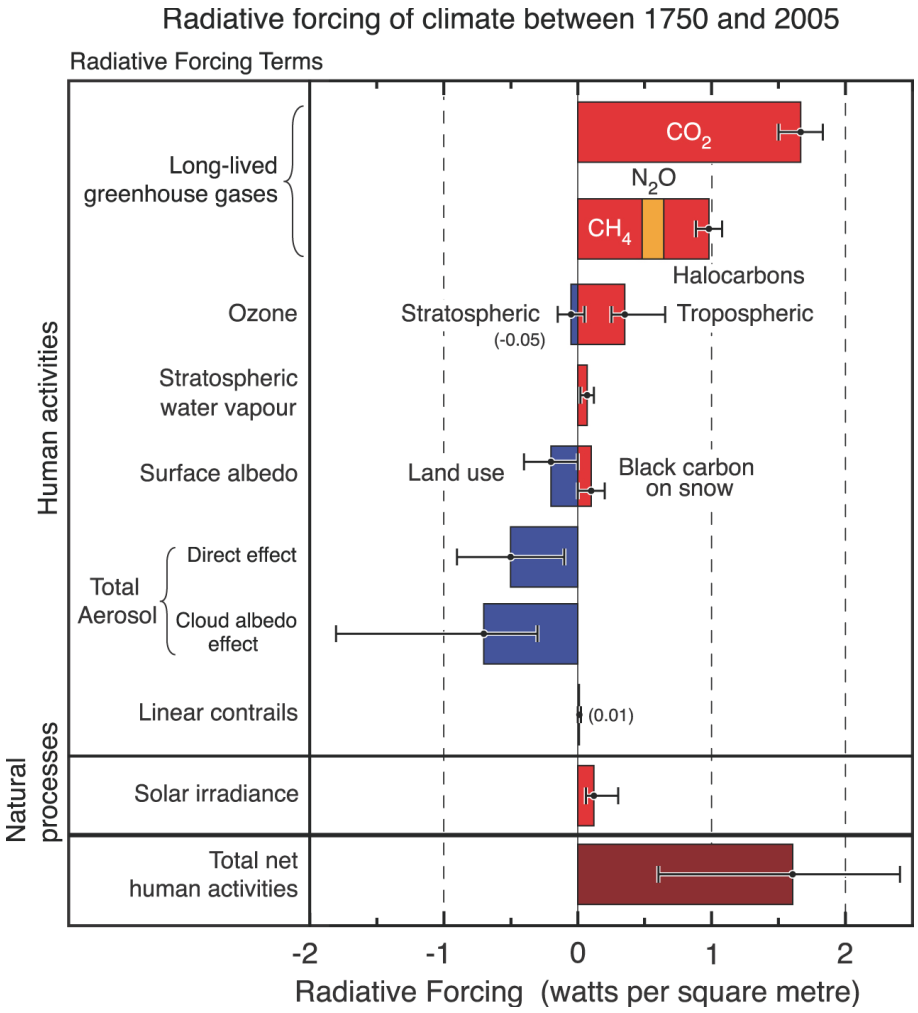

Figure 1.2: Global average radiative forcing (RF) estimates and ranges in 2005 for anthropogenic carbon dioxide (CO_2), methane (CH_4), nitrous oxide (N_2O) and other important agents and mechanisms. The net anthropogenic radiative forcing and its range are also shown. (IPCC, 2007).

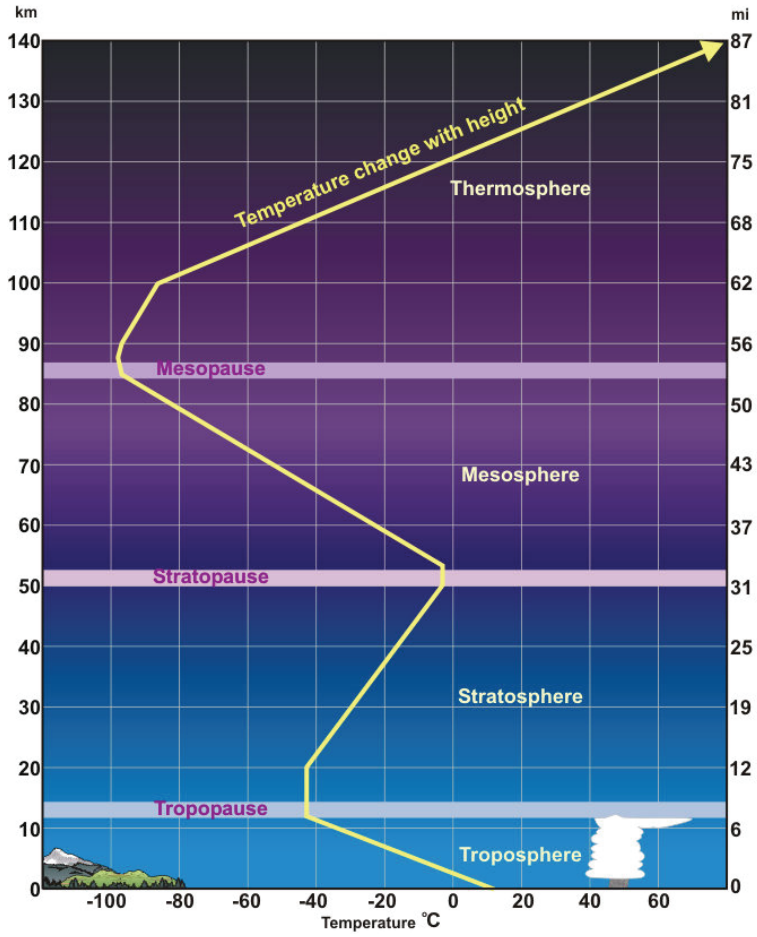

Figure 1.3: Vertical structure of the atmosphere (`http://www.srh.weather.gov/jetstream/atmos/atmprofile.htm`).

of thermal infrared radiation of the Earth and generally decreases with increasing altitude because of adiabatic cooling upon expansion which is caused by the pressure decrease with height. The heating from below leads to a relative instable thermal layering resulting in a good vertical mixing induced by convection. The troposphere is bounded from above by the tropopause and is followed by the stratosphere extending to about 50 km. In the stratosphere the temperature increases with height due to absorption of ultraviolet solar radiation by ozone, until it reaches a maximum characterizing the stratopause. The following mesosphere which extends to 80-90 km has again a negative temperature gradient. At the mesopause which separates the mesosphere from the thermosphere, the temperature reaches an absolute minimum in the atmosphere before it rises again. The outermost layer of the Earth‘s atmosphere, the exosphere, represents the smooth transition to space with continuously decreasing gas density.

Measurements and interpretation of atmospheric trace gas composition and the exchange of trace gases between the atmosphere, biosphere and geosphere are of significant importance for a better understanding of the budgets, sources and sinks of trace gases important in atmospheric chemistry, the greenhouse effect and climate change. Surface in situ measurements have the advantage that they are cost effective, very precise and easily performed also for continuous monitoring. However, in situ measurements reveal information only about concentrations at the location where they are taken. In case of aircraft or balloon measurements, information about the vertical distribution of trace gases is obtained, but they are expensive and complex and therefore sparse. Furthermore, aircraft and balloon based in situ measurements only give information up to certain altitudes. For the understanding of physical and chemical states of the stratosphere and upper troposphere and for assessing the impact of stratospheric changes on the underlying troposphere and on global climate, remote sensing observations play an important role. Satellite observations are well suited to reveal global trace gas distributions and trends, and to deduce strength and spatiotemporal distribution of sources and sinks by inverse modeling which is based on fitting the model emissions to the observations of the satellite, but need careful validation from the ground. Aiming for high accuracy and precision, the improvement of retrieval strategies and validation by in situ and ground-based remote sensing observations is required.

Ground-based FTIR solar absorption spectrometry is a well-established remote sensing technique for the measurement of atmospheric trace gases. Column densities of about 20 different trace gas species can be retrieved from the infrared spectral region and for some gases it is possible to retrieve vertical profiles from the pressure broadening of isolated absorption lines. For many important gases ground-based FTIR spectrometry is the only technique suitable for the validation of satellites, since they measure the same quantity (total column concentrations) as satellites. Especially in the tropics, where a lack of continuous atmospheric observations exists, remote sensing observations are of great importance for the understanding of atmospheric composition changes and their impact on global climate.

2 Measurements in the Tropics

2.1 Relevance of the Tropics

The Tropics are the geografic regions around the equator where the sun reaches its zenith at least once during the solar year. The tropics are limited in the North by the Tropic of the Cancer (23.5°N) and in the South by the Tropic of the Capricorn (23.5°S). The tropical seasons are dominated by the Intertropical Convergence Zone (ITCZ), a tropical cloud belt, resulting in dry and rainy seasons. Due to the solar radiation, air is ascending in the ITCZ, moving polewards in the upper troposphere and descending in the subtropical ridges. Equatorwards flowing air in the lower troposphere is deflected westwards by the Coriolis force resulting in the trade winds. This circulation pattern, driven by the solar radiation in the tropics, is known as the Hadley cell. The Hadley cell strongly affects global climate and is responsible for the transport of heat, angular momentum and trace gases from the tropical regions to mid and high latitudes.

The composition of the tropical atmosphere and its change is of significant importance for global climate. Since several decades, rapid population growth and industrial development, along with deforestation, are increasingly changing the environment in the tropical countries. The effect of these changes on atmospheric composition and climate are quite uncertain, as the governing physical and chemical processes of the tropical atmosphere are only poorly understood. Emissions within the tropics, e.g. from biomass burning or plants, contribute substantially to the global budgets of many important trace gases (Crutzen and Andreae (1990); Andreae and Merlet (2001), IPCC: Houghton et al. (2001)). Biomass burning is not restricted to the tropics, but most burning occurs in the tropics. The tropics are also the location of two important exchange processes, the interhemispheric exchange and the entry of tropospheric air into the stratosphere. Both processes are of crucial global importance and are subject of current atmospheric research. Since the entry of tropospheric air into the stratosphere takes almost exclusively place in the tropics, the composition of the tropical atmosphere also plays a critical role for stratospheric chemistry (Holton et al., 1995). For example anthropogenic emissions causing stratospheric ozone depletion, e.g. CFCs, have to pass through the tropical atmosphere. Therefore emissions within the tropics have potentially a great impact on the stratospheric chemistry (Notholt et al., 2003). The processes leading to the entry of tropospheric air into the stratosphere are not well

understood. Unlike the tropopause in higher latitudes, where a sharp transition between the troposphere and the stratosphere exists, the tropical tropopause is not sharp, but a transition layer of certain extend, called the Tropical Tropopause Layer (TTL). The TTL is the region of the tropical atmosphere that lies between the top of the main cumulus outflow layer (∼12 km) and the thermal tropopause (∼16 km), hence it is the transition layer between the dynamical control of the vertical mass flux by tropospheric convection, and by the stratospheric Brewer-Dobson circulation (Holton, 2002). The composition of the TTL, the uplift of air masses by deep convection, and the slow ascent into the stratosphere all show strong seasonal and long-term variabilities. In order to study the TTL, it is necessary to study the composition of the entire atmosphere from the surface to the stratosphere, e.g. by remote sensing techniques.

2.2 Measurements in the Tropics

Systematic observations of relevant atmospheric parameters are scarce over the oceans, the poles and in tropical regions. In the tropics the lack of observations is mostly due to the inaccessibility of the tropical forests and the vast tropical oceans, as well as the lower priorities given to these observations by developing countries.

Before 2004, there have been no FTIR observations in the inner tropics. For many gases, FTIR spectrometry is the only ground-based remote sensing technique that can provide information with the required precision. Examples are column averages of methane and profiles of carbon monoxide.

Figure 2.1 shows a world map indicating the locations of stations where FTIR measurements are performed. Most of these stations are part of the NDACC (Network for the Detection of Atmospheric Composition Change) and/or TCCON (Total Carbon Column Observing Network) networks. The only site in the tropics is the Paramaribo site, located in Suriname, at the northern coast of South America at 5.8°N and 55.2°W. The Paramaribo observatory fills in an important gap in the global atmospheric observation network, which is essential for global change research and assessment. Earth observation satellites that have been or will be launched in the near future can partly compensate for the lack of observations in the tropics. However, there is a growing need for surface observations for the validation and calibration of these satellite instruments, e.g. the atmospheric chemistry instruments onboard of the European ENVISAT satellite (SCIAMACHY and MIPAS). For many satellite data products the uncertainties are especially large in the tropics the high content of water, which interferes in many spectral regions.

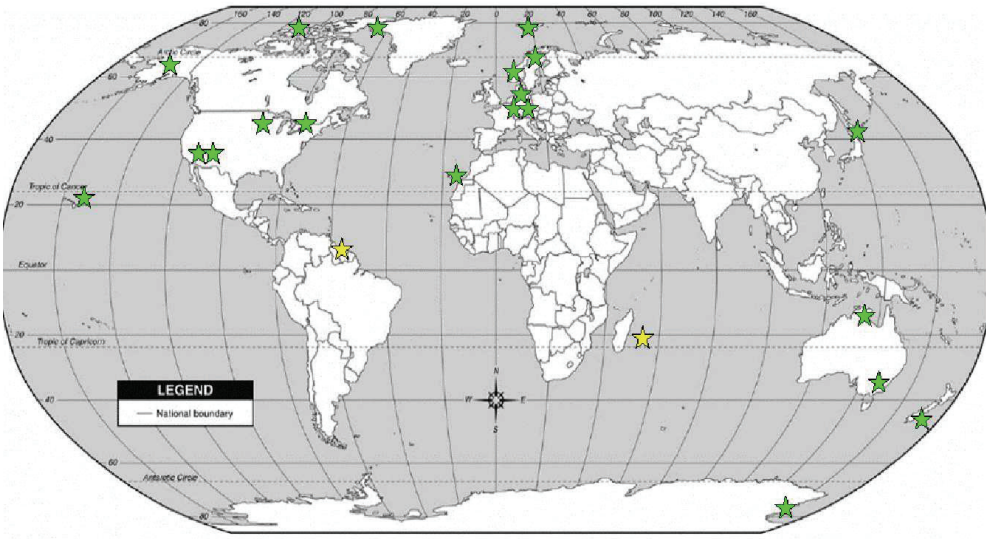

Figure 2.1: World map indicating the locations of stations where FTIR solar absorption measurements are performed (green stars). At Paramaribo and La Réunion (yellow stars) FTIR measurements are performed on campaign base.

2.3 Paramaribo Station

The solar absorption FTIR measurements presented in this work were performed at the Meteorological Service (MDS) in Paramaribo, Suriname (5.8°N, 55.2°W) during several consecutive dry seasons between September 2004 and November 2007. What makes Paramaribo station particularly interesting from a scientific point of view is the fact that it lies very close to the Equator, at a location in the middle of the annual migration range of the Inter-Tropical Convergence Zone (ITCZ). The Intertropical Convergence Zone migrates twice a year over the measurement site, resulting in the characteristical wet and dry seasons of the tropics. During the short dry season (February to March) the ITCZ is located south of Paramaribo, while during the long dry season (August to November) the ITCZ is located north of Paramaribo (see Figure 2.3). This implies that the measurement site belongs to the meteorological northern hemisphere (NH) during the short dry season, while during the long dry seasons it belongs to the meteorological southern hemisphere (SH) (Fortuin et al., 2007).

Figure 2.4 demonstrates this effect with sulfur hexafluoride (SF_6) in situ measurements performed within this PhD-work in Paramaribo. The SF_6 concentration in the NH is persistently higher if compared to the SH due to the predominate release of SF_6 in the NH, and an interhemispheric exchange time of air in the order of 1 year (Maiss and Levin, 1994). FTIR measurements in Paramaribo take place

Figure 2.2: Top: The measurement site in Paramaribo. The container on the left is used for LIDAR measurements performed by the Alfred-Wegener Institute Bremerhaven, the middle one for FTIR measurements and the right container is used for logistics and office work during the campaigns. Behind the containers, the Meteorological Service (Meteorologische Dienst van Suriname, MDS) can be seen with the measurement platform on the roof, housing meteorological instruments in cooperation with international partners.
Bottom: Solar tracker on top of the FTIR container.

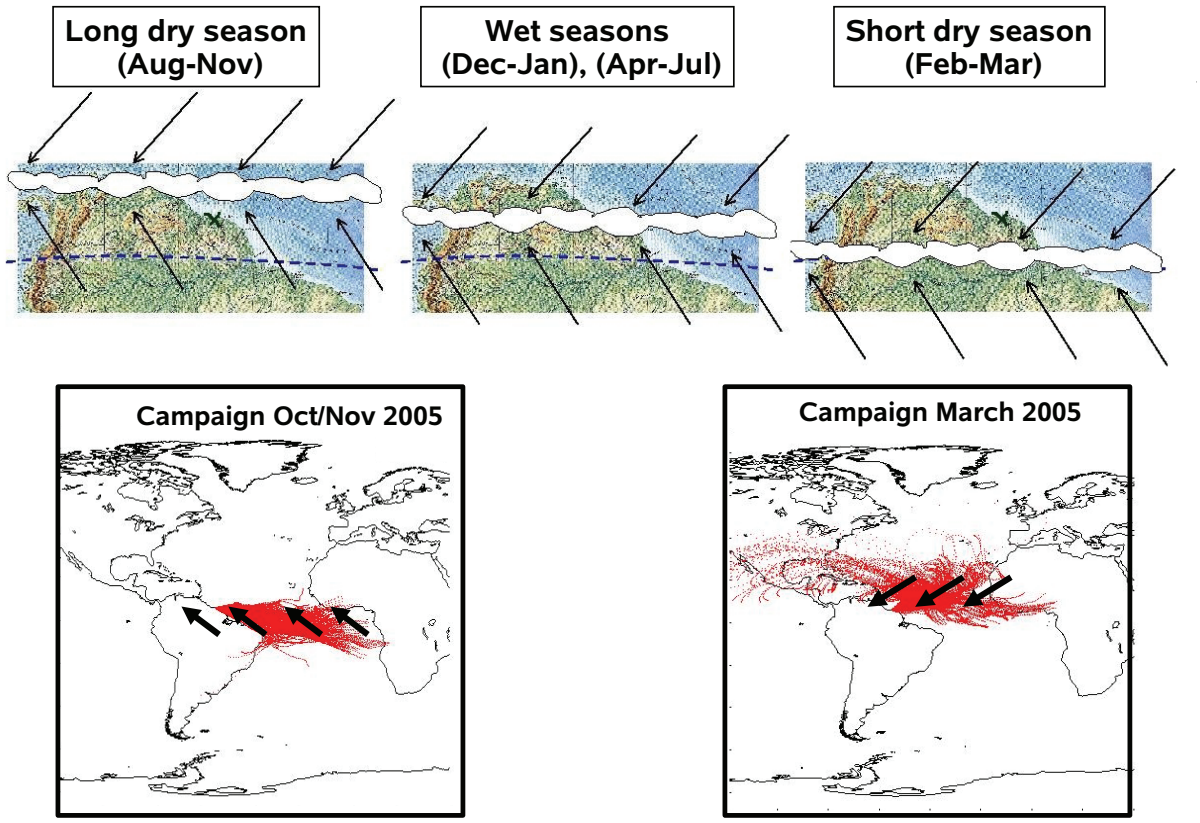

Figure 2.3: Migration of the ITCZ over Paramaribo. During the long dry seasons (LDS), the ITCZ is located north of the measurement site. During the wet seasons, Paramaribo experiences a lot of rainy weather. During the short dry seasons (SDS), the ITCZ is located south of Paramaribo. The arrows indicate the direction of the trade winds. In the lower panel, the back-trajectories (BADC) reaching Paramaribo during two different measurement campaigns are presented. One typical SDS campaign and one typical LDS campaign are shown. Clearly seen is the main wind direction during these periods (trade winds).

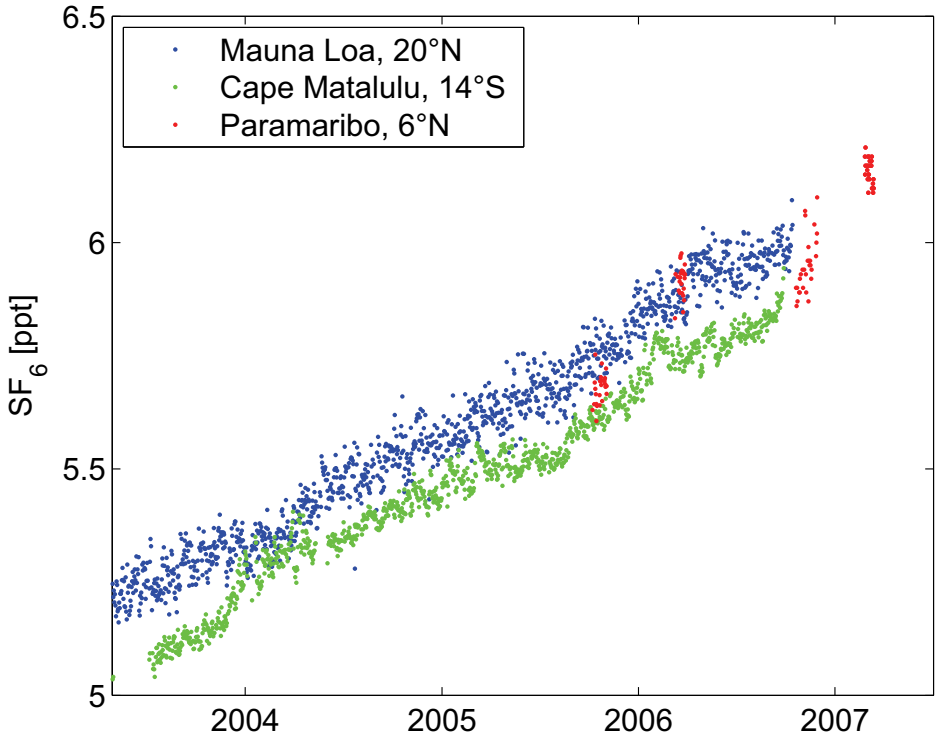

Figure 2.4: The sulfur hexafluoride (SF_6) in situ measurements at Paramaribo (magenta) demonstrate the change of the meteorological hemispheres during the different dry seasons. Apart from the measurements in Paramaribo, SF_6 measurements performed within the NOAA surface observation network from Mauna Loa (for the NH) and Cape Matalulu (or the SH) are shown. For the campaign in October-November 2006, it can be seen that during the end of the measurement campaign the SF_6 concentrations increase to those typical for the NH, indicating the change of the seasons. This was accompanied by cloudy weather and rain. The last measurements of this campaign were performed within the ITCZ.

Figure 2.5: In situ measurements by flask sampling on the platform on the MDS roof. The air samples are analysed for CO_2, CH_4, CO, SF_6, H_2, $\delta^{13}C$ and $\delta^{18}O$ in C_2O by gas chromatography and mass spectrometry at the MPI Jena.

only during dry seasons, since FTIR measurements can only be performed under clear sky conditions. Campaigns during short dry seasons (SDS, February to March) are denoted as SDS campaigns, while campaigns during long dry seasons (LDS, August to November) as LDS campaigns. Besides the FTIR measurements, atmospheric observations at MDS include LIDAR (Immler et al., 2007) and MAX-DOAS measurements, weekly ozone- and Snow-White-soundings (Fortuin et al., 2007; Verver et al., 2006; Peters et al., 2004). Since 2005, the allready mentionned surface in situ measurements were sampled at different locations in Suriname in cooperation with the MPI Jena (see Figure 2.5). The air samples are analysed for CO_2, CH_4, CO, SF_6, H_2, $\delta^{13}C$ and $\delta^{18}O$ in C_2O by gas chromatography and mass spectrometry.

3 Fourier Transform InfraRed (FTIR) Spectrometry

The solar radiation undergoes a number of modifications on its way through the atmosphere. The high energetic UV radiation is shielded by the outer layers of the atmosphere due to absorption of oxygen ($\lambda < 242.4\,\text{nm}$) and ozone ($242\,\text{nm} < \lambda < 310\,\text{nm}$). The UV-visible radiation, which arrives in the denser layers of the atmosphere is also partly absorbed by ozone, but mostly scattered by molecules and aerosols. A large part of the IR radiation, for which scattering can be neglected, is absorbed by atmospheric trace constituents like CO_2, H_2O, O_3, CH_4 and N_2O (Brasseur and Solomon, 1984). Most of the molecules in the atmosphere absorb infrared radiation. These absorption features can be used to determine the quantity of this molecule in the atmosphere. Before the method of FTIR spectrometry is described in Section 3.2, the charecteristics of an atmospheric absorption spectrum is shortly presented in the next section. A more detailed description can be found in (Haken and Wolf, 2006).

3.1 Absorption of Infrared Radiation by Molecules

Absorption or emission of photons by a molecule are caused by changes in energy. The energy changes can occur in translation or as a change in electronic, vibrational or rotational state. In the following, we will only concentrate on vibrational-rotational spectra, which can be measured in the IR spectral region. Rotational-vibrational excitation of a molecules involves changes in the vibrational and rotational states simultaneously. Generally vibrational transitions occur in conjunction with rotational transitions. Consequently, it is possible to observe both rotational and vibrational transitions in the vibrational spectrum. Although many methods are available for observing vibrational spectra, the two most common methods are infrared spectroscopy and Raman spectroscopy.

In a first approximation, the rotational and vibrational contributions to the energy of the molecule can be considered independently. For diatomic molecules the approximation of an harmonic oscillator and rigid rotor yields:

$$E_{vib,rot} = E_{vib} + E_{rot} = \left(\nu + \frac{1}{2}\right) h\nu_0 + BhcJ\,(J+1) \tag{3.1}$$

where ν is the vibrational quantum number, J is the rotational quantum number, h is Planck's constant, ν_0 is the frequency of the vibration, c is the speed of light, and B is the rotational constant. The selection rules are $\Delta\nu = 0, \pm 1$ and $\Delta J = 0, \pm 1$. For linear molecules the most commonly observed case is that only transitions with $\Delta J = \pm 1$ are observed. Vibrational-rotational spectra of diatomic molecules consists of transition branches, the P-branch with $\Delta J = -1$ and the R-branch with $\Delta J = 1$ (see Figure 3.1). The Q-branch ($\Delta J = 0$) is generally not observed, and only possible for molecules with unpaired electrons. Pure rotational transitions ($\Delta\nu = 0$) are possible if the molecule has a permanent electric dipole moment. The involved transitions are illustrated in Figure 3.1. The positions of the peaks in the spectrum can be predicted using the rigid rotor

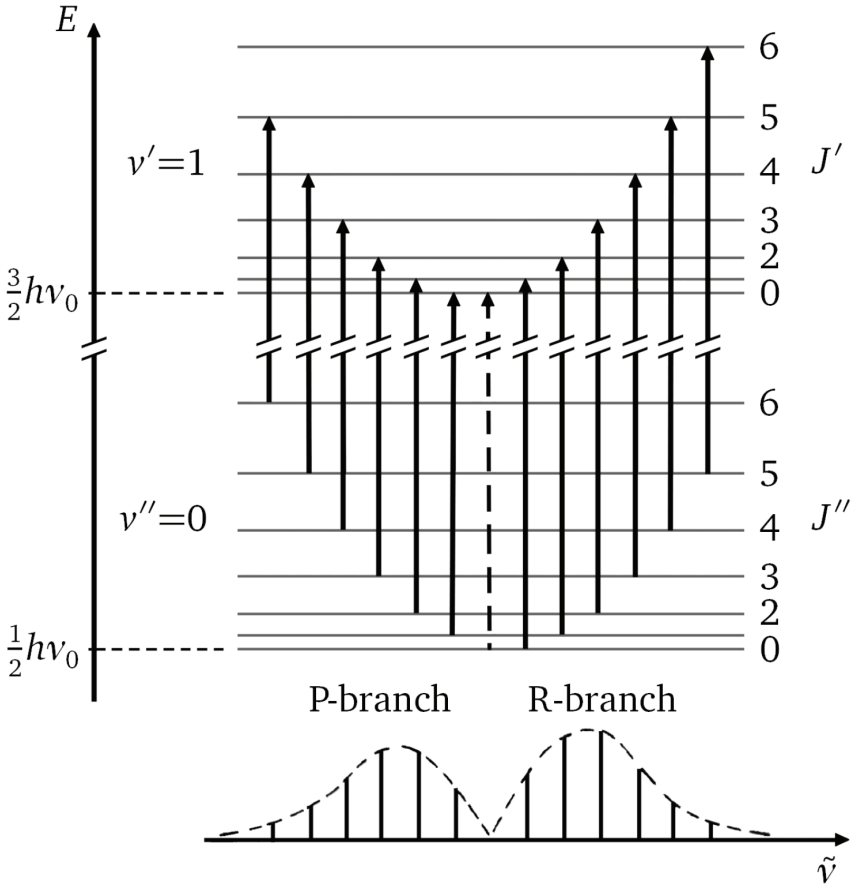

Figure 3.1: Schematic rotational-vibrational molecular spectral band and corresponding transitions (Haken and Wolf, 2006).

model. One prediction of the rigid rotor model is that the space between each of the peaks should be $2B$ where B is the rotational constant for a given molecule.

Experimentally, it is observed that the spacing between the R-branch peaks decreases as the frequency increases. Similarly, the spacing between the P-branch peaks increases as the frequency decreases. This variation in the spacing results from the bonds between the atoms in a molecule not being entirely rigid. For the most simple case of an harmonic oszillator, only transitions with $\Delta\nu = \pm 1$ are allowed. For an unharmonic potential, unharmonic termes occure in the vibrational energy. Anharmonicity additionally causes overtone bands resulting from vibrational transitions with $\Delta\nu = \pm 2, \pm 3, \pm 4, \ldots$ with decreasing intensity.

The relative amplitude of the spectral lines in the P- and R-branches depends on the population of the states. The population probability is given by the Boltzmann distribution (in thermodynamic equilibrium):

$$\frac{n_J}{n_0} = \frac{g_J}{g_0} \exp\left(-\frac{E_J - E_0}{k_B T}\right) = g_J \exp\left(-\frac{hcBJ(J+1)}{k_B T}\right) \tag{3.2}$$

where g_J, g_0 is the degeneracy (number of states having the energy E_J and E_0 respectively). k_B denotes the Boltzmann constant and T the temperature. The degeneration is given by $(2J+1)$ for linear molecules and $(2J+1)^2$ for spherical molecules. For small J, the degeneration term dominates and the population increases with J, while for larger J the population decreases exponentially with J (see Figure 3.1).

3.2 Principles of FTIR Spectrometry

The content of this section is largely adopted from (Davis et al., 2001).

The concept of Fourier Transform Infrared (FTIR) spectrometry is based on a classical Michelson interferometer. Infrared light from a point source is rendered parallel by a collimator (lens or mirror). The now plane wavefront passes to a beamsplitter and is divided 50:50. The two resultant wavefronts travel to the plane mirrors and are reflected back on themselves. The wavefronts on recombination at the beamsplitter (now acting as a recombiner) are still plane and parallel and will interfere by the principle of superposition. After focusing by a condenser, a detector will record an intensity that depends on the path difference of the two wavefronts. A schematic design of a Michelson interferometer is shown in Figure 3.2. Suppose that one mirror moves at a constant velocity v. When illuminated by a monochromatic point source, the detector will see a periodically varying signal. For an input of monochromatic light of wavenumber σ_0 and intensity $B(\sigma_0)$, the intensity at the detector as a function of the optical path difference x between the two beams is given by

$$I_0(x) = B(\sigma_0)[1 + \cos(2\pi\sigma_0 x)] \tag{3.3}$$

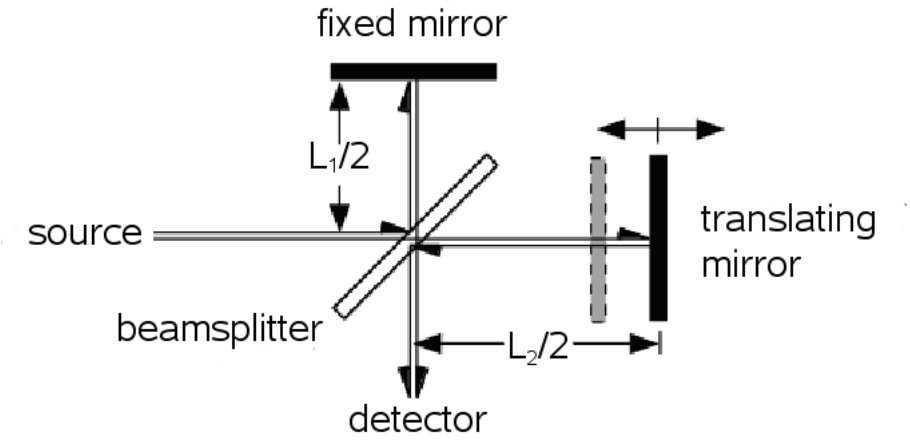

Figure 3.2: Schematic design of a Michelson Interferometer.

where the wavenumber σ is defined as $\sigma = 1/\lambda = \nu/c$, measured in reciprocal centimeters. When one mirror is moving, so x is changing, the intensity is a cosine of the wavenumber.

For polychromatic light, the detector measures a superposition of such cosines:

$$I_0(x) = \int_0^\infty B(\sigma)[1 + \cos(2\pi\sigma x)]d\sigma \tag{3.4}$$

The the constant part, the mean value $\overline{I(x)}$ can be substracted to form an expression for the intensity as a function of x, the interferogram:

$$I(x) = I_0(x) - \overline{I(x)} = \int_0^\infty B(\sigma)[\cos(2\pi\sigma x)]d\sigma \tag{3.5}$$

The right-hand side contains all the spectral information in the light and is the cosine Fourier transform of the source distribution $B(\sigma)$. The distribution can be recovered by the inverse Fourier transform,

$$B(\sigma) = \int_0^\infty I(x)\cos(2\pi\sigma x)dx \tag{3.6}$$

Mathematecilly, the Fourier transform of equation (3.5) produce not only the spectrum $B(\sigma)$ but also its mirror image, $B(-\sigma)$, at negative frequencies. Since $\cos(2\pi\sigma x) = \cos(-2\pi\sigma x)$, $B(\sigma)$ and $B(-\sigma)$ produce identical interferograms. The negative frequencies are physically unreal. For complete symmetry in transforming back and forth from the interferogram domain to the spectral domain, the integral has to extend over all frequencies from minus to plus infinity. It is possible to construct a spectral function B_e from B and change the definition to include all

frequencies:

$$B_e(\sigma) = \frac{1}{2}[B(\sigma) + B(-\sigma)] \tag{3.7}$$

$$I(x) = \int_{-\infty}^{\infty} B_e(\sigma)[\cos(2\pi\sigma x)]d\sigma \tag{3.8}$$

$$B_e(\sigma) = \int_{-\infty}^{\infty} I(x)[\cos(2\pi\sigma x)]dx \tag{3.9}$$

Suppose that one mirror moves at a constant velocity v, so the path difference is simply $x = vt$. The detector will see a periodically varying signal:

$$I(t) \propto \cos(2\pi\sigma vt) \tag{3.10}$$

Since the input beam is assumed to be stationary (steady in spectral content and average amplitude), the FTS can be regarded as a modulator that produces a frquency $f = \sigma v$ from the steady beam. The envelope of the interferogram has exactly the same shape as the original wave, but the frequencies are reduced by the factor v/c.

A Michelson interferometer can be considered as a form of frequency transducer that converts optical frequencies (which are very high and well beyond the capability of known detectors to sense) down to electrical frequencies that can, in principle, have any value we choose since the mirror velocity v is controlable by the user. The transformation is linear: the amplitude of the electrical output is directly proportional to the incoming intensity.

For more details about Fourier Transformation in general, I refer to standard text books. For more information about Fourier Transform spectrometry, (Davis et al., 2001) is recommendable.

3.3 Solar Absorption FTIR Measurements

Spectroscopic measurement techniques are well suited for remote sensing of the atmosphere. As solar radiation passes through the atmosphere, trace gases selectively absorb at specific wavelengths of the light. The measurement of the sun's spectrum at the Earth's surface thus provides a wealth of information about atmospheric composition (see Figure 3.3).

High resolution ground-based FTIR spectrometers are capable of quantifying the total column amounts of numerous tropospheric and stratospheric trace gases. Vertical profile information can also be determined from the pressure broadening of the absorption lineshapes. Tropospheric gases include CO_2, CH_4, CO, N_2O,

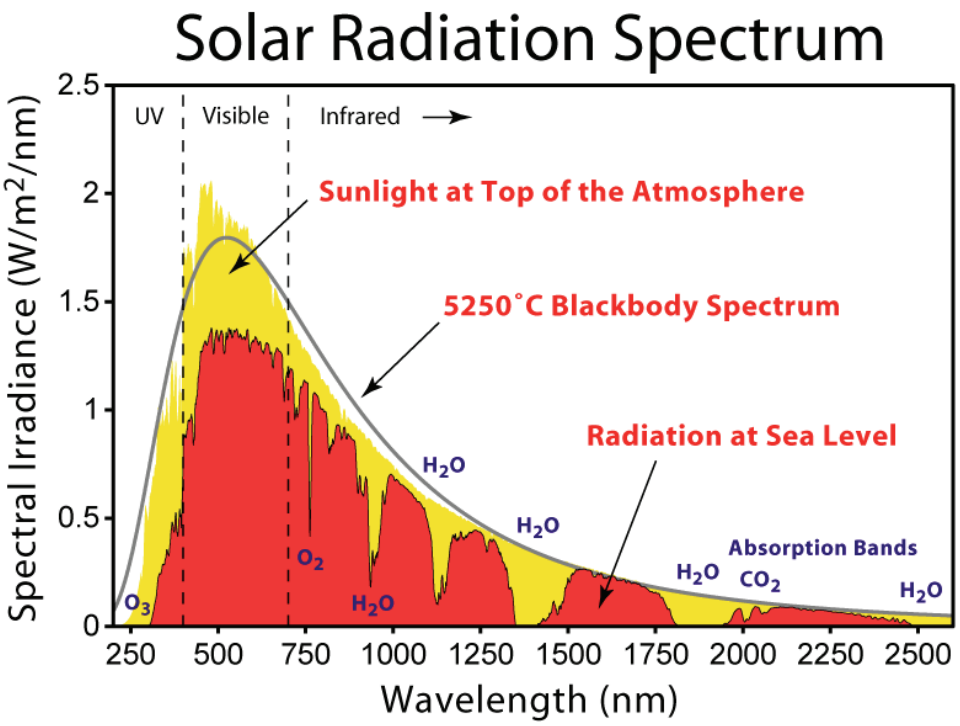

Figure 3.3: Solar spectrum at the top of the atmosphere, at sea leval, and the Planck curve of a black body at T=5250°C (temperature of the sun). Taken from `http://www.wikipedia.org`.

C_2H_2, C_2H_6, HCN, CH_2O, OCS and CFCs. Important measurable stratospheric species are O_3, HCl , HNO_3, NO, NO_2 and $ClONO_2$.

The retrieval of trace gas concentrations from absorption spectra is based on the comparison of measured with simulated spectra. For an apriori state of the atmosphere (e.g. pressure and temperature profiles) and with respect of instrumental influences, a transmission spectrum of the atmosphere is calculated. Through variation of certain parameters (e.g. trace gas concentrations) in the simulation, the calculated spectrum is fitted to the measured spectrum. Total column trace gas concentrations can be retrieved by scaling the trace gas concentration profiles during the fit. In addition to the retrieval of total column amount, for some trace gases it is possible to retrieve information about the vertical distribution from the analysis of the shape of absorption lines, e.g. by optimal estimation. The spectral line shape of an absorption line is influenced by the natural line width, Doppler broadening and pressure broadening. Since pressure decreases with height, pressure broadening dominates in the troposphere whereas in the stratosphere, Doppler broadening is dominant in the infrared.. Information about the volume mixing ratio profiles can be gained as high up as pressure broadening

is dominant. When the line shape is dominated by Doppler broadening and thus not a function of pressure and height, the residuals provide hardly any information about the profile distribution.

All solar absorption spectra presented in this work were recorded using a Bruker 120M interferometer. Total column amounts and volume mixing ratio (vmr) profiles were retrieved using the algorithm SFIT2 vs2.92 (Spectral Least Square Fitting Program) developed at NASA Langley Research Center and the National Institute for Water and Atmospheric Research in New Zealand (for further details see Rinsland et al. (1998)). Profiles of pressure, temperature and relative humidity are obtained from the NOAA Climate Diagnostics Center (CDC) based on NCEP (National Centers for Environmental Prediction) Reanalysis data (`http://www.cdc.noaa.gov/data/gridded/data.ncep.reanalysis.html`).

In Section 4 and 5 results from solar absorption FTIR measurements performed in Paramaribo, Suriname are presented. The spectra are analysed for volume mixing ratio profiles and total column concentrations of methane, carbon monoxide, ethane and other trace gases related to biomass burning.

3.4 Cell-Based FTIR Measurements

Instead of measuring the absorption of solar radiation passing through the atmosphere, the absorption of light from an artificial source through an air sample can be used to analyse trace gas concentrations in this air sample. The radiation from the infrared light source passes through the air sample, contained in a cell. In order to enhance the infrared absorption, cells with White-optics are commonly used, where the beam is reflected several times within the cell to maximize the light path. The spectrum is measured with an FTIR spectrometer and then analysed to retrieve trace gas concentrations.

In this work, I will present results of two different setups where cell-based FTIR measurements have been used successfully. In Section 4.1.1 of Chapter 4 laboratory cell-based FTIR measurements are used to improve the spectroscopy of methane. These measurements have significantly improved the retrieval of methane from ground-based solar absorption FTIR spectra as well as from SCIAMACHY low resolution spectra. In Part III cell-based FTIR spectrometry is combined with micrometeorological methods to perform flux measurements of carbon dioxide, nitrous oxide and methane. The newly developed technique allows to make flux measurement continuously and over longer terms.

The flux measurements with cell-based FTIR spectrometry have been performed with a trace gas analyser developed at the University of Wollongong. The system is able to measure trace gas concentrations automated and continuously. FTIR spectra are recorded from 1500 to 7800 cm^{-1} at 1 cm^{-1} resolution and analysed for CO_2 and its main isotopes $^{12}CO_2$ and $^{13}CO_2$, CH_4, CO, N_2O and H_2O by

a non-linear least squares fitting technique, in which the measured FTIR spectrum is fitted with an iteratively-calculated spectrum until a least squares best fit is obtained (Griffith, 2006, 1996). δ^{13}C is calculated from the measured main isotopologues of CO_2 ($^{13}CO_2$ and $^{12}CO_2$) by

$$\delta^{13}\mathrm{C} = \left(\frac{\left[\frac{^{13}\mathrm{CO_2}}{^{12}\mathrm{CO_2}}\right]_{sample}}{\left[\frac{^{13}\mathrm{CO_2}}{^{12}\mathrm{CO_2}}\right]_{standard}} - 1 \right) * 1000. \tag{3.11}$$

The least squares fitting procedure used for quantitative spectrum analysis is based on tabulated spectral data (HITRAN 2004) and requires no calibration gases. For more accurate absolute calibration, measurements can be compared to independently calibrated reference gases.

Part II

Remote Sensing Measurements

4 Methane

Global atmospheric concentrations of carbon dioxide (CO_2), methane (CH_4) and nitrous oxide (N_2O) have increased markedly as a result of human activities since 1750 and now far exceed pre-industrial values determined from ice cores spanning many thousands of years (IPCC: Forster et al. (2007)). CH_4 is the second most important anthropogenic greenhouse gas in the atmosphere and it one of the target gases of the Kyoto protocol. Its global atmospheric concentration has more than doubled since preindustrial times and was 1774 ppb in 2005 (IPCC: Forster et al. (2007)). Sources and sinks of atmospheric methane are not well quantified. In particular, in the the tropics with no ground based continuous methane measuring stations a large uncertainty in the methane budget exists. The first space-borne measurements with sufficient precision revealed unexpected features of the global distribution of atmospheric CH_4. Frankenberg et al. (2005) found significantly enhanced tropical methane enhancements, especially over tropical forests, by analysing near infrared spectra recorded by the SCanning Imaging Absorption SpectroMeter for Atmospheric ChartographY (SCIAMACHY) instrument onboard ENVISAT. These findings were confirmed by Buchwitz et al. (2006) using a different retrieval algorithm. Source inversion studies based on SCIAMACHY retrievals (Frankenberg et al., 2006) indicate significantly larger tropical emissions than estimated by inversions using surface observations only (Bergamaschi et al., 2007; Meirink et al., 2008). Warneke et al. (2006) reported ship-borne CH_4 measurements over the tropical Atlantic ocean, which were found to be consistent with surface observation based model fields, while other recent ground-based and airborne measurements indicate significant tropical emissions (Miller et al., 2007). A study by Keppler et al. (2006) surprised the scientific community by reporting hitherto unknown methane emissions from terrestrial plants under aerobic conditions, supposedly largest in the tropics, possibly contributing 10 - 30 % to the total annual CH_4 emissions into the atmosphere. However, this new release method is heavily debated, especially with respect to reported global emission estimates, which were considered too high by several studies (e.g. Houweling et al., 2006). Even this new release method has been confirmed by later studies (I.Vigano et al., 2008; Keppler et al., 2008), its importance in the global methane budget remains highly uncertain.

Within the framework of this PhD-work we have performed specific FTIR measurements in order to improve the spectroscopic linelist in the near-infrared (NIR) required for the SCIAMACHY retrieval. This work was done in close collabora-

tion with Christian Frankenberg, who analysed the measurements and applied them to the SCIAMACHY retrievals. These measurements included the laboratory cell-based FTIR measurements described in the following section and high resolution FTIR solar absorption measurements performed in Bremen and Paramaribo. The improved spectroscopic linelist achieved from the cell-based FTIR measurements resulted in a great improvement of the CH_4 retrieval from SCIAMACHY (Frankenberg et al., 2008b). The results were confirmed using ground-based FTIR solar absorption measurements performed in Bremen. The results largely reduced residuals and bias for the SCIAMACHY retrieval. Analysis of high resolution spectra from FTIR solar absorption measurement performed in Bremen and Paramaribo and the improved spectroscopic database revealed systematic errors in previous SCIAMACHY methane retrievals caused by an erroneous H_2O spectroscopic database, which resulted in systematic overestimation of tropical methane abundances (Frankenberg et al., 2008a), which resulted in systematic overestimation of tropical methane abundances. Compared to inversions based on previous SCIAMACHY retrievals, annual tropical emission estimates are reduced from 260 to about 210 Tg CH_4 but still remain higher than previously anticipated. In the following section the performed cell measurements and other attempts to improve the retrieval of methane in the mid-infrared (MIR) spectral region are discussed in detail. Unfortunately, the corrected spectroscopy of methane resulted only in slight success for the retrieval of CH_4 volume mixing ratios in the MIR. Following the successful retrieval strategy for SCIAMACHY in the NIR, FTIR spectra have been analysed in the same spectral region and with the same spectroscopic linelist as used for the retrieval from SCIAMACHY. The results are presented in Section 4.2. Solar absorption spectra, recorded during seven consecutive dry seasons between September 2004 and November 2007 at the MDS in Paramaribo, Suriname, were analysed using the SFIT2 vs2.92 algorithm to retrieve volume mixing ratio profiles and total column amounts of methane. The FTIR measurements of methane will be compared with CH_4 retrievals from low-resolution spectra from the SCIAMACHY instrument.

4.1 Improvement of Retrieval

The vertical distribution and partial or total columns of methane can be retrieved from solar absorption FTIR spectra using e.g. the SFIT2 retrieval algorithm (Rinsland et al., 1998) based on the Optimal Estimation method of Rodgers (Rodgers and Connor, 2003). Although several retrieval approaches for methane profiles, characterized by relatively high information content, exist, the retrieved vertical profiles of methane often show large oscillations in the troposphere. This might result from errors in the spectroscopic line parameters (pressure broadening coefficients, temperature dependency of the absorption lines) and wrong pressure-

temperature-profiles (pT-profiles) resulting in wrong absorption coefficients. A significant improvement of the retrieval is expected by using better spectroscopic data for CH_4. Section 4.1.1 gives insight in the effort taken to improve the quality of the CH_4-spectroscopy. In Section 4.1.2 the influence of different pT-profiles on the retrieval is investigated.

4.1.1 Cell Measurements to Improve the Spectroscopy

In order to improve the spectroscopy of methane in the mid-infrared (MIR) spectral region, we performed laboratory cell measurements in close cooperation with the Forschungszentrum Karlsruhe (FZK) with a Bruker 125HR FTS of John Burrows at the Institute of Environmental Physics, University of Bremen. All spectra were obtained using a internal tungsten lamp as IR light source, a CaF_2 beamsplitter and a liquid nitrogen cooled InSb detector. An optical filter was used to reduce the bandpass. The gas mixture has been inserted in a 140 cm cell with wedged CaF_2 windows at the front and at the back. For thermal stabilization and insulation the cell was enclosed by two coaxial quartz jackets. The inner one was temperature stabilized by a flow of ethanol from a thermostatic bath. The outer one was evacuated for thermal insulation. To avoid condensation on the windows of the cell, the frames of the CaF_2 windows have been heated. The cell was located behind the interferometer and the light passed twice through the cell before being detected (absorption path 280 cm). Spectra were recorded over the 2600-2950 cm^{-1} spectral range. Transmission spectra were deduced by dividing sample spectra by spectra obtained with the evacuated cell. To achieve constant, uniform methane mixing ratios, the cell was first filled with N_2 (or synthetic air), then with CH_4 and then again with N_2 (or synthetic air). The internal pressure could be regulated to perform measurements at different pressures. The pressure in the cell was measured with two independent capacitive pressure transducers of 500 hPa and 1000 hPa maximum range (MKS Baraton).
The measurements described above have been performed to improve the CH_4 spectroscopy in the MIR spectral region. Subsequent measurements have been done with the same measurement setup for the NIR spectral region (5600-6300 cm^{-1}) to improve the CH_4 total column retrieval in the NIR e.g. used for SCIAMACHY retrievals and solar absorption FTIR retrievals using profile scaling (Toon et al., 1992). Details and results about the improved spectroscopic data in the NIR and their impact on the SCIAMACHY retrieval can be found in Frankenberg et al. (2008b,a).

Table 4.1 indicates the different measurement conditions. To derive line positions and line intensities, methane was first measured at low pressures at room temperature. In order to derive pressure broadening parameters and pressure shifts, methane was mixed with nitrogen or synthetic air and was measured at different pressures at room temperature. To evaluate the temperature dependency of

line intensities and pressure broadening, the same experiments (with pure methane and methane-N_2 (or synthetic air) mixtures) have been performed at room temperature and -30°C. No attempt was made to achieve improved accuracy for absolute band intensities, since this would require to perform very accurate measurement of pressure and to avoid any leakage in whole measurement setup. The obtained spectra were fitted in two different ways to derive the spectral line parameters including relative line intensities, pressure-broadening coefficient and pressure shift. C. Frankenberg fitted these parameters for each individual line using multiple laboratory spectra simultaneously by applying a multi-spectrum nonlinear constrained least squares approach based on Optimal Estimation. Details can be found in Frankenberg et al. (2008b). The derived parameters were used to update the HITRAN2004 linelist in the spectral region used for the CH_4 retrieval, denoted as MsFT(Multi-spectrum Fitting Technique)-linelist in the following. The LINEFIT algorithm (Hase et al., 1999) was used as forward code to derive line positions and intensities in the spectral region used for the retrieval, the updated HITRAN2004 linelist is denoted as EFT(Emperical Fitting Technique)-linelist in the following. The relevant spectroscopic parameters for three linelists within the five used microwindows are shown in Table 4.2 and 4.3.

The impact on the retrieval of using these different linelists has been tested using the 2004 data from Paramaribo. Five microwindows for the retrieval of vertical profiles of methane have been selected within the EU-project UFTIR and used in the EU-project HYMN an within this work (see Figure 4.1). The five microwindows are fitted simultaneously and the interfering species were fitted by profile scaling (see Table 4.4), using SFIT-2 v3.90 (Rinsland et al., 1998). Solar lines are generally simulated in the retrieval.

Figure 4.2 shows the residuals for the five different microwindows used for the CH_4 retrieval. To distinguish the spectroscopic impact from the normal noise, the residuals were averaged over all spectra from Paramaribo in 2004 (64 spectra). There is a slight improvement (smaller residuals) for the updated linelists relativ to HITRAN2004. Especially in the first mircrowindow (upper panel, 2613.70 - 2615.40 cm^{-1}) the EFT- and MsFT-linelists clearly improve the fit quality.

Figure 4.3 shows the impact of using different spectroscopic data on the volume mixing ratio (VMR) profiles for Paramaribo. Shown are the deviations relative to the VMR retrieved using the HITRAN2004 spectroscopy. Both updated linelists show in general a higher VMR of 0.5 to 1.5 % in the troposphere than HITRAN2004. In the stratosphere, the MsFT-linelist results in a greater VMR, while the EFT-linelist results in a smaller VMR than HITRAN2004. The derivations from the HITRAN2004-VMR are below 2 %. In Figure 4.4 the impact on the total columns are shown. The use of the updated lineslists results in an offset of the total columns relativ to the HITRAN2004 retrieved columns. The MsFT-total columns are in general 0.65 %, the EFT-total columns 1.5 % smaller than the HITRAN2004-total columns. In general, measurements based on spectroscopy

	CH_4 Partial Pressure [mbar]	Total Pressure [mbar]	Temperature [°C]
pure CH_4	5.0	5.0	22.0
	1.0	1.0	22.0
	0.5	0.5	22.0
CH_4 + N_2	10.0	500.0	22.0
	5.0	250.0	22.0
	2.5	125.0	22.0
pure CH_4	5.0	5.0	23.0
	4.0*	4.0*	-30.0
	1.0	1.0	-30.0
CH_4 + N_2	11.0	500.0	24.5
	9.0*	420.0*	-30.0
CH_4 + synthetic air	11.0	500.0	26.5
	9.0*	420.0*	-30.0
	4.5	211.0	-30.0
	2.0	106.0	-30.0

Table 4.1: Measurement parameters to derive line intensities and shifts, pressure broadening parameters and pressure-induced shifts as well as temperature dependencies of these parameters.
* previous cell content has been maintained for low temperature measurement

	Transition frequency [cm^{-1}]			Line intensity		
	Hitr04	MsFT	EFT	Hitr04	MsFT	EFT
1.	2614.019900	2614.019900	2614.019850	$1.885 \cdot 10^{-22}$	$1.901 \cdot 10^{-22}$	$1.930 \cdot 10^{-22}$
2.	2614.778900	2614.778900	2614.778860	$3.017 \cdot 10^{-22}$	$3.057 \cdot 10^{-22}$	$3.076 \cdot 10^{-22}$
3.	2615.070400	2615.070400	2615.068000	$3.097 \cdot 10^{-23}$	$3.199 \cdot 10^{-23}$	$3.597 \cdot 10^{-23}$
4.	2615.169600	2615.169600	2615.169600	$1.224 \cdot 10^{-23}$	$1.242 \cdot 10^{-23}$	$1.470 \cdot 10^{-23}$
5.	2650.739400	2650.739400	2650.739400	$3.319 \cdot 10^{-23}$	$3.319 \cdot 10^{-23}$	$3.485 \cdot 10^{-23}$
6.	2650.774464	2650.774464	2650.770104	$6.209 \cdot 10^{-24}$	$6.209 \cdot 10^{-24}$	$6.209 \cdot 10^{-24}$
7.	2651.033100	2651.033100	2651.032990	$1.673 \cdot 10^{-22}$	$1.673 \cdot 10^{-22}$	$1.682 \cdot 10^{-22}$
8.	2835.520300	2835.520300	2835.525400	$7.216 \cdot 10^{-24}$	$5.927 \cdot 10^{-24}$	$4.329 \cdot 10^{-24}$
9.	2835.560100	2835.560100	2835.560100	$6.099 \cdot 10^{-24}$	$5.353 \cdot 10^{-24}$	$4.270 \cdot 10^{-24}$
10.	2835.676300	2835.676300	2835.676400	$1.888 \cdot 10^{-22}$	$1.914 \cdot 10^{-22}$	$1.855 \cdot 10^{-22}$
11.	2835.793110	2835.793110	2835.793110	$1.627 \cdot 10^{-24}$	$1.479 \cdot 10^{-24}$	$8.000 \cdot 10^{-25}$
12.	2835.799800	2835.799800	2835.799800	$6.891 \cdot 10^{-24}$	$6.843 \cdot 10^{-24}$	$3.450 \cdot 10^{-24}$
13.	2903.652675	2903.652675	2903.652875	$2.926 \cdot 10^{-23}$	$2.904 \cdot 10^{-23}$	$2.926 \cdot 10^{-23}$
14.	2903.780263	2903.780263	2903.780263	$1.774 \cdot 10^{-23}$	$1.738 \cdot 10^{-23}$	$1.774 \cdot 10^{-23}$
15.	2903.790089	2903.790089	2903.790089	$1.184 \cdot 10^{-23}$	$1.234 \cdot 10^{-23}$	$1.184 \cdot 10^{-23}$
16.	2903.875700	2903.875700	2903.876000	$6.009 \cdot 10^{-22}$	$5.990 \cdot 10^{-22}$	$6.010 \cdot 10^{-22}$
17.	2921.331850	2921.331850	2921.332050	$9.349 \cdot 10^{-22}$	$9.365 \cdot 10^{-22}$	$9.390 \cdot 10^{-22}$

Table 4.2: Spectroscopic parameters for the HITRAN2004 linelist and the two by laboratory measurements updated linelists

	Air-broadening width			Temp.dependence			Pressure shift		
	Hitr04	MsFT	EFT	Hitr04	MsFT	EFT	Hitr04	MsFT	EFT
1.	0.0632	0.0619	0.0623	0.63	0.63	0.80	-0.006100	-0.006660	-0.004240
2.	0.0698	0.0678	0.0668	0.65	0.65	0.87	-0.004000	-0.006667	-0.005500
3.	0.0440	0.0398	0.0400	0.65	0.65	0.65	-0.006000	-0.011005	-0.006000
4.	0.0470	0.0464	0.0470	0.65	0.65	0.65	-0.006000	-0.015516	-0.006000
5.	0.0660	0.0660	0.0660	0.80	0.80	0.80	-0.006000	-0.006000	-0.006000
6.	0.0440	0.0440	0.0440	0.65	0.65	0.65	-0.005302	-0.005302	-0.005302
7.	0.0660	0.0660	0.0660	0.80	0.80	0.85	-0.006000	-0.006000	-0.002020
8.	0.0470	0.0472	0.0470	0.63	0.63	0.63	-0.006000	+0.017901	-0.006000
9.	0.0470	0.0471	0.0470	0.63	0.63	0.63	-0.006000	-0.001271	-0.006000
10.	0.0631	0.0654	0.0631	0.80	0.80	0.80	-0.004860	-0.006709	-0.005500
11.	0.0470	0.0472	0.0470	0.63	0.63	0.63	-0.005672	-0.010557	-0.005672
12.	0.0440	0.0440	0.0440	0.63	0.63	0.63	-0.006000	-0.006000	-0.006000
13.	0.0450	0.0466	0.0450	0.75	0.75	0.75	-0.005807	-0.005456	-0.005807
14.	0.0390	0.0402	0.0430	0.75	0.75	0.75	-0.005808	-0.018502	-0.005808
15.	0.0290	0.0299	0.0380	0.75	0.75	0.75	-0.005808	+0.007727	-0.005808
16.	0.0610	0.0607	0.0605	0.73	0.73	0.73	-0.008596	-0.009862	-0.009800
17.	0.0613	0.0610	0.0610	0.72	0.72	0.72	-0.003894	-0.004879	-0.005000

Table 4.3: Spectroscopic parameters for the HITRAN2004 linelist and the two by laboratory measurements updated linelists

microwindows [cm^{-1}]	interfering species
2613.70 - 2615.40	HDO, CO_2
2650.60 - 2651.30	HDO, CO_2
2835.50 - 2835.80	
2903.60 - 2904.03	NO_2
2921.00 - 2921.60	H_2O, HDO, NO_2

Table 4.4: Microwindows used for the retrieval of CH_4 profiles including interfering species

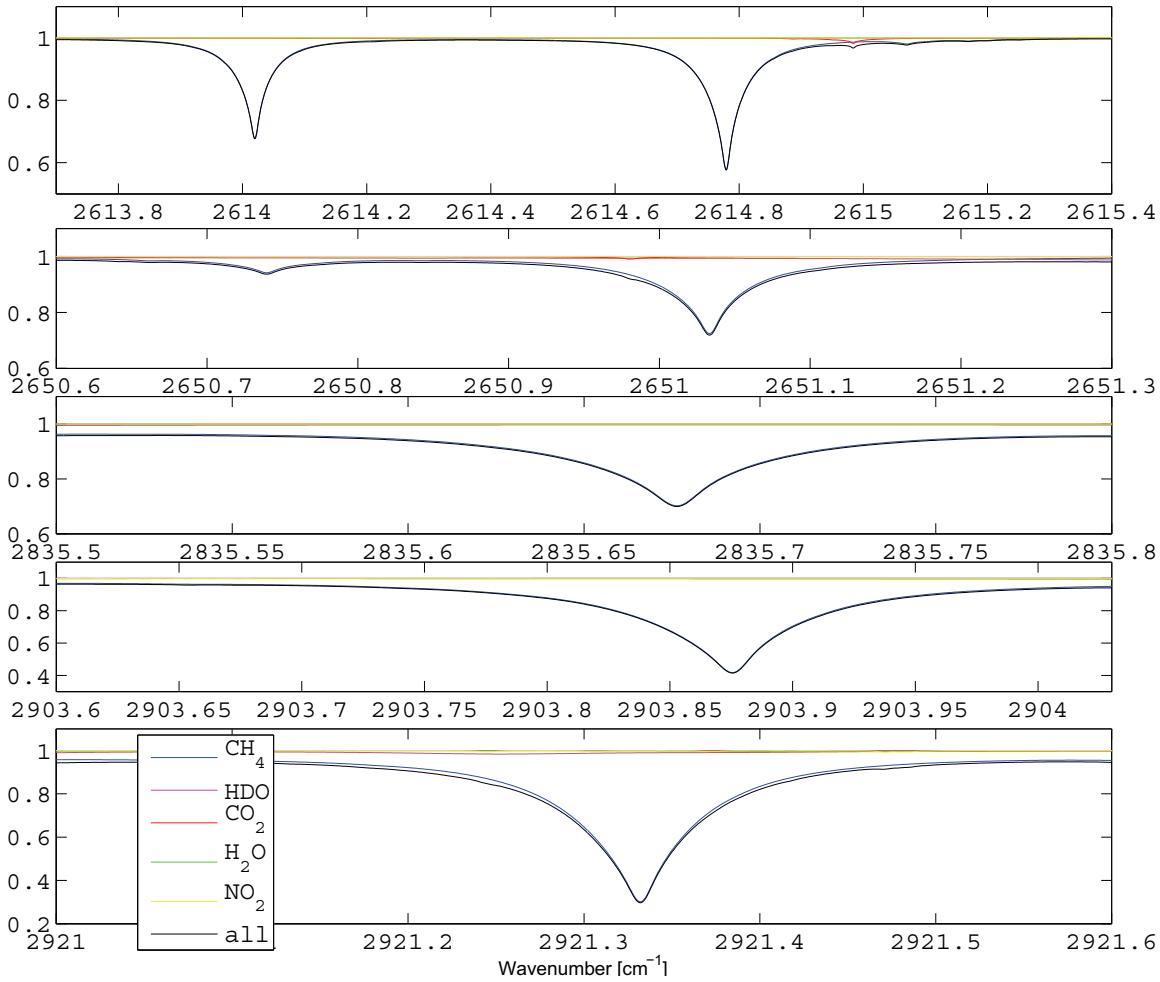

Figure 4.1: The five microwindows used for the retrieval of the vertical distribution of CH_4. Interfering species are fitted by profile scaling.

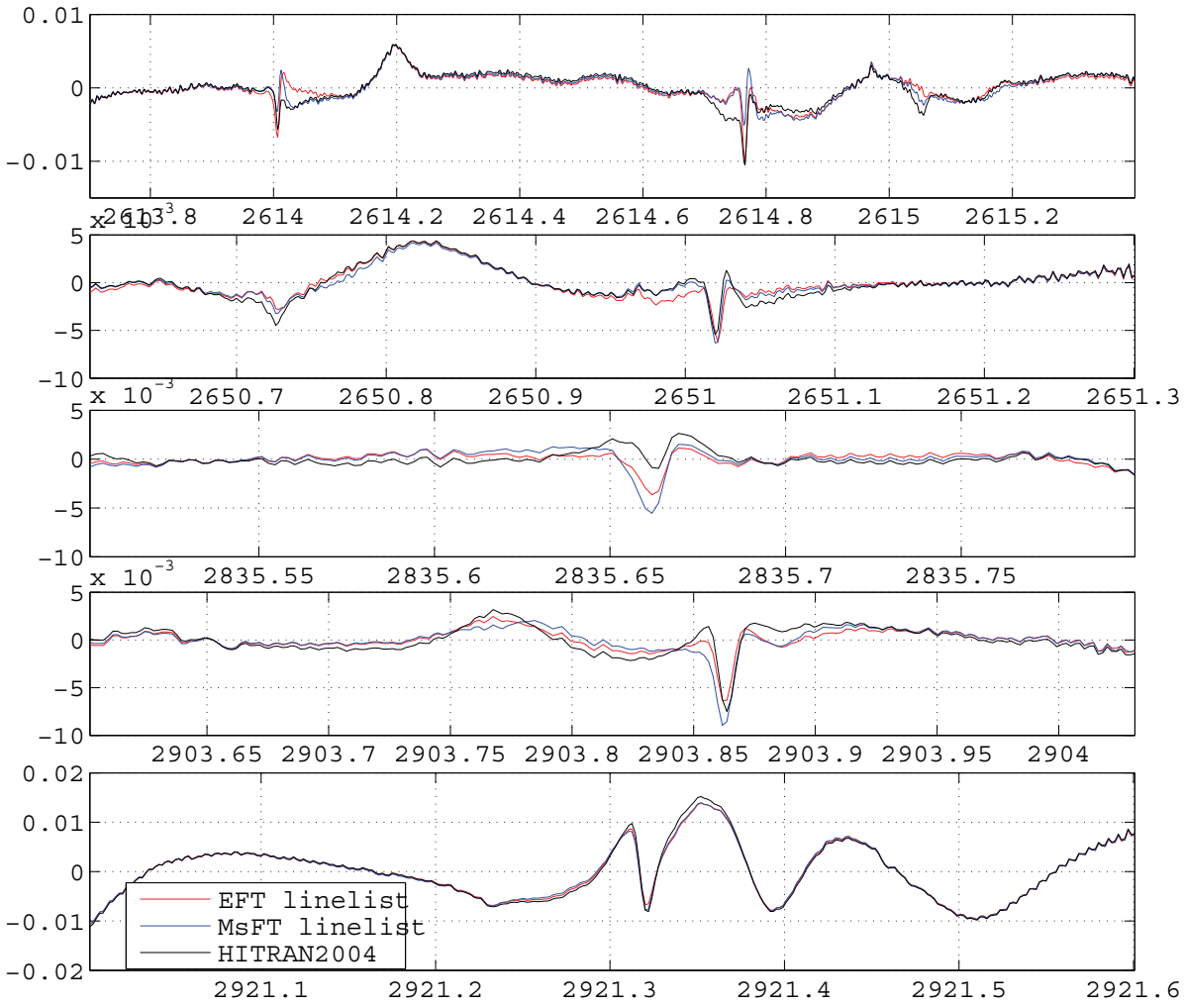

Figure 4.2: Residuals (average over 64 residuals of 2004 Paramaribo) for the five microwindows used for the CH_4 retrieval with different spectroscopic linelists Paramaribo

may have offsets resulting from different absolute intensities of the absorption lines in the spectroscopic linelists.

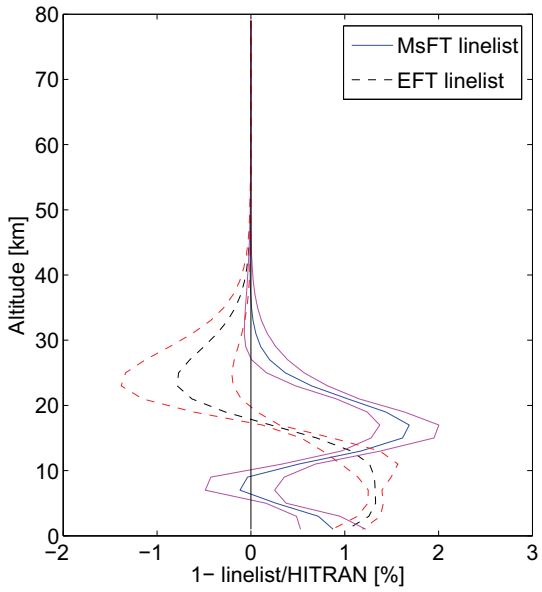

Figure 4.3: VMR profiles for Paramaribo retrieved using different spectroscopic linelists, relativ to HITRAN2004

In general, the updated lineslists show only slight improvements, the HITRAN2004 spectroscopy performs quite well in the spectral region used for the retrieval. In the NIR on the other hand, the due to the cell measurements updated linelist shows large improvements for both satellite (Frankenberg et al., 2008a) and FTIR retrieval of methane. Section 4.2 presents results of CH_4 column averaged mixing ratios retrieved from FTIR spectra in Paramaribo and from SCIAMACHY spectra.

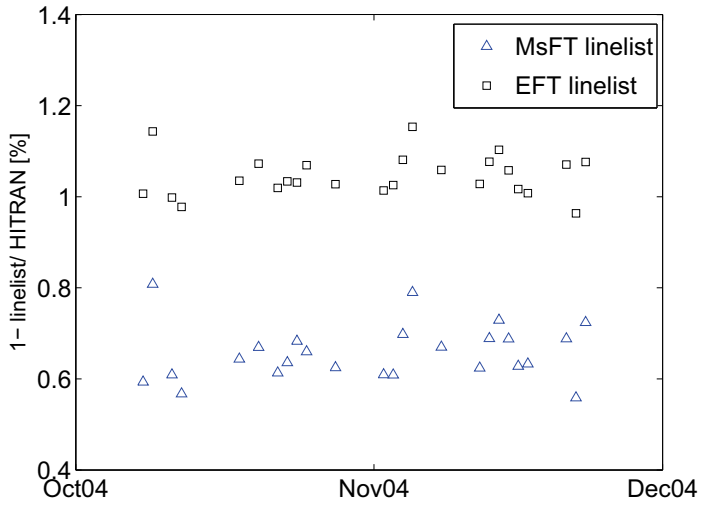

Figure 4.4: Total column for Paramaribo retrieved using different spectroscopic linelists, relative to HITRAN

4.1.2 Pressure-Temperature Profiles

Vertical profiles of pressure and temperature (pT-profiles) are required for the retrieval of vertical trace gas distributions from absorption spectra. Within the TCCON (Total Carbon Column Observing Network) and NDACC (Network for Detection of Atmospheric Composition Change, formerly NDSC) community, pT-profiles from the NOAA Climate Diagnostics Center (CDC) based on NCEP (National Centers for Environmental Prediction) Reanalysis data (see e.g.Washenfelder et al. (2006)) are used for the retrieval. European modeling groups often use pT-profiles from ECMWF (European Centre for Medium-Range Weather Forecasts) for inverse modeling systems, e.g. the TM5 model (Meirink et al., 2008; Bergamaschi et al., 2007). Also new SCIAMACHY retrieval versions use pressure, temperature and water vapour profiles from ECMWF (Frankenberg et al., 2008a). For the comparison of different CH_4 datasets from solar absorption FTIR or satellite measurements and inverse model simulations, it is important to minimize error sources like using different assumptions for pT-profiles. In this section the influence of different pT-profiles on the CH_4 retrieval from solar absorption FTIR measurements is investigated. ECMWF pT-profiles are only provided from the surface up to ∼65 km. For the analysis of solar absorption spectra, ECMWF profiles are extended above ∼65 km using the NOAA standard atmosphere. At higher latitudes (Bremen, Spitsbergen) the pT-profiles from ECMWF and NCEP agree in the troposphere and stratosphere, but tend to show higher deviations above ∼35 km. Especially in Bremen, ECMWF profiles show higher temperatures above 40 km relative to NCEP. In the tropics (Paramaribo) the differences between ECMWF and NCEP are larger than at higher latitudes. Especially in tropopause region (∼17 km) and above 35 km the differences are larger than the standard deviation. Details can be found in the Appendix (see B).

PT-profiles from NCEP, ECWMF and radio sondes have been compared and the impact on the retrieval has been tested. Figure 4.5 shows pT-profiles from NCEP, ECMWF and a radio sonde for one examplary day (29th September 2004) at Paramaribo. The ECMWF pT-profile is in nice agreement with the radio sonde. Especially in the tropopause region, the radio sonde agrees better with ECMWF, while NCEP shows larger temperatures than ECMWF and the radio sonde. In the stratosphere and stratopause region, the ECMWF profile shows large differences relativ to NCEP. Figure 4.6 shows the impact of different pT-profiles on the volume mixing ratio and 4.7 on the total column for the 2004 Paramaribo dataset. The total columns are in general 0.07 % smaller when ECMWF profiles are used compared to NCEP. Apart from one outlayer, the variation is within 0.02 % (within the errorbars). The VMR shows a systematic overestimation between 10 and 25 km when ECMWF is used relativ to NCEP.
This demonstrates that the impact of the different pT-profiles on the retrieval is small. We do not expect problems in the comparison of data sets based on

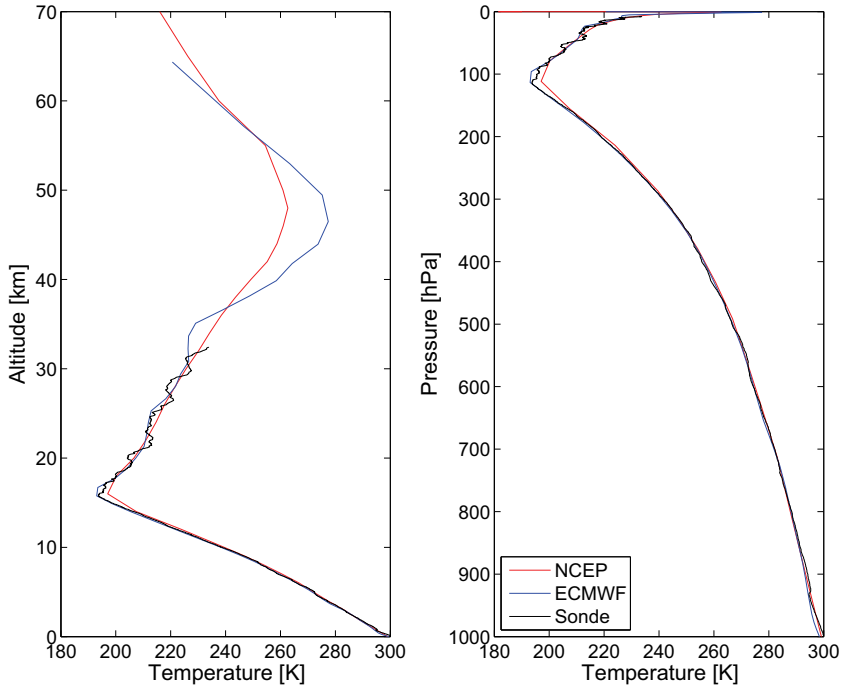

Figure 4.5: Pressure-Temperature profiles from NCEP, ECMWF and a radio sonde for the 29th September 2004 in Paramaribo

different pT-profiles.

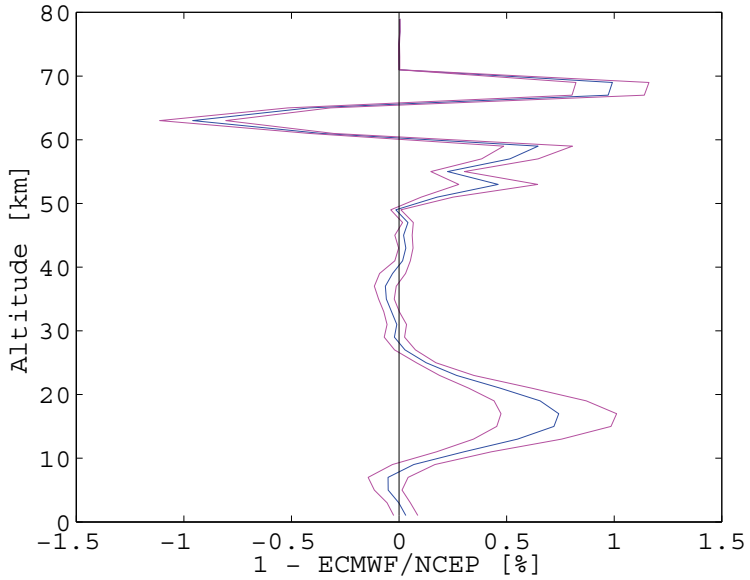

Figure 4.6: Impact of different pT-profiles on the VMR. Shown are the deviations $(\frac{(NCEP-ECMWF)}{NCEP} \cdot 100)$ of the VMR profiles for Paramaribo.

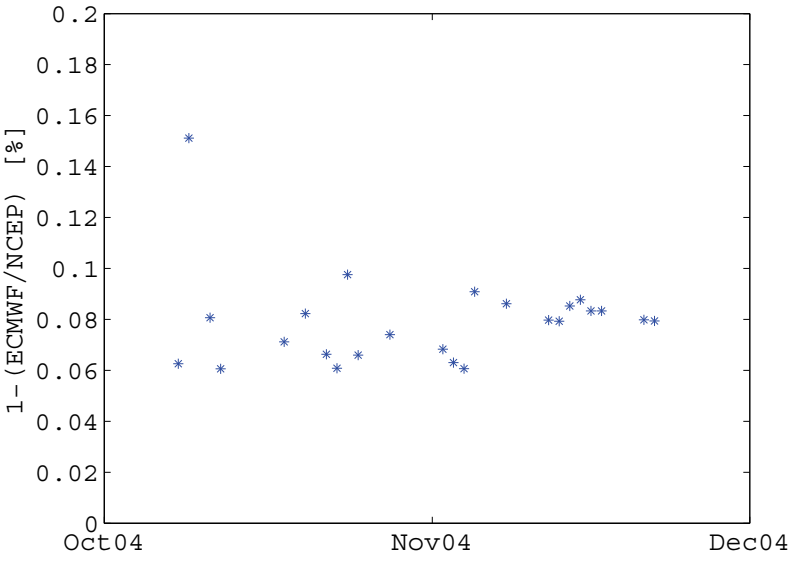

Figure 4.7: Impact of different pT-profiles on the total columns. Shown are the deviations $(\frac{(NCEP-ECMWF)}{NCEP} \cdot 100)$ of the total columns for Paramaribo.

4.2 Tropical Methane Measurements

The improvement of the retrieval of CH_4 volume mixing ratios from ground-based solar absorption measurements in the mid-infrared (MIR) is part of the EU-project HYMN. It is focused on the MIR, since not all NDACC FTIR stations perform solar absorption measurements in the near-infrared (NIR) spectral region. Within the HYMN-project, cell-based FTIR measurements have been performed in Bremen to improve the spectroscopic linelist of methane in the MIR (see Section 4 of this work). The corrected spectroscopy resulted only in marginal improvements for the retrieval of CH_4 volume mixing ratios in the MIR. Subsequent measurements have been done with the same measurement setup for the NIR spectral region (5600 - 6300 cm^{-1}) to improve the CH_4 retrieval in the NIR used for SCIAMACHY retrievals. These improved CH_4 spectroscopy data and and an update of the water spectroscopy, based on Jenouvrier et al. (2007) and high resolution FTIR spectra from Bremen and Paramaribo, resulted in a great improvement of the CH_4 retrieval from SCIAMACHY spectra (Frankenberg et al., 2008b,a). Following the successful retrieval strategy for SCIAMACHY, within this work FTIR spectra have been analysed in the same spectral region and with the same spectroscopic linelist as used for the retrieval from SCIAMACHY. Solar absorption spectra, recorded during seven consecutive dry seasons between September 2004 and November 2007 at the MDS in Paramaribo, Suriname, were analysed using the SFIT2 vs2.92 algorithm to retrieve volume mixing ratios and total column amounts of methane in the NIR. In the following section, the FTIR measurements of methane will be compared with CH_4 retrievals from low-resolution spectra from the SCIAMACHY instrument and with TM5 model simulations for Paramaribo.

4.2.1 Ground-Based and Space-Borne Measurements

Methane retrievals from SCIAMACHY are performed in a microwindow in channel 6, ranging from 5983 to 6138 cm^{-1} (1629 - 1671 nm). This spectral range covers the strong Q and R branches of the $2\nu_3$ methane band as well as numerous weaker lines, for which the quantum assignments are unknown (Frankenberg et al., 2008b). The SCIAMACHY retrievals used within this work, are described in detail by Frankenberg et al. (2008a). Individual SCIAMACHY pixels are 30 km × 60 km for channel 6. The SCIAMACHY product represents the measured total column of CH_4 normalized to the measured total column of CO_2. The measured columns of CH_4 and CO_2 are derived from neighboring spectral regions, ensuring very similar light path distributions for both species. The column averaged CH_4 mixing ratio XVMR(CH_4) is obtained by

$$\mathrm{XVMR}(CH_4) = \frac{\text{meas. column}(CH_4)}{\text{meas. column}(CO_2)} \cdot \mathrm{XVMR}_{model}(CO_2) \tag{4.1}$$

using modeled column averaged mixing ratios of CO_2 ($XVMR_{model}(CO_2)$). Carbon dioxide simulations were performed using Carbon Tracker data (CarbonTracker 2008, `http://carbontracker.noaa.gov`, Peters et al. (2007)) (for the years 2004 and 2005) and TM3-MPI3.8 model data for the years 2006 and 2007 (no Carbon Tracker data implemented in the SCIAMACHY retrieval yet). The sensitivity of SCIAMACHY retrievals as functions of altitude are described by the averaging kernels (AK). The AKs for the CH_4 and the CO_2 retrievals are close to 1.0 near the surface and in the lower troposphere, but decrease in the upper troposphere and stratosphere (Frankenberg et al., 2006).

Solar absorption spectra, recorded during seven consecutive dry seasons between September 2004 and November 2007 at the MDS in Paramaribo, Suriname, were analysed using the SFIT2 vs2.92 algorithm to retrieve volume mixing ratio profiles and total column amounts of methane. The FTIR solar absorption spectra can be analysed in the same spectroscopic regions and with the same spectroscopic linelists as used for the CH_4 retrieval from low-resolution spectra from SCIAMACHY. The SFIT2 algorithm is commonly used to retrieve profiles of atmospheric trace gases in the MIR spectral region by fitting single absorption lines in several microwindows. A lot of effort has been spend by several groups to improve the retrieval of methane volume mixing ratios in the MIR (e.g. EU-project UFTIR (`http://www..nilu.no/uftir/`), EU-project HYMN (`http://www.knmi.nl/samenw/hymn/`)), with only small success. The retrieval of methane total column amounts in the NIR spectral region by profile scaling has been used successfully in a number of cases (Warneke et al., 2006; Washenfelder et al., 2003), showing good agreement with model simulations and surface observations. In the tropics, the methane total column retrieval by profile scaling revealed problems, which we ascribe to too unrealistic apriori information for the tropical trace gases, water interference, a too restricted retrieval algorithm due to profile retrieval (no freedom to adjust the shape of the profiles) or other unknown effects. The retrieval by profile scaling showed a strong sensitivity to the apriori information as well as to different microwindows used for the retrieval. In order to solve the problem of reduced freedom due to profile scaling, we used the SFIT2 algorithm for the first time to derive volume mixing ratios and total column amounts of methane in the NIR, fitting a whole transition band instead of single lines. This resulted in a microwindow of nearly one order larger than commonly used for the profile retrieval. Since a whole transition band (consisting of several absorption lines with different temperature sensitivities) is used for the retrieval, inconsistencies of spectroscopic parameters for certain absorption lines and assumed apriori information for the pressure-temperature profiles have less impact on the results. The apriori profiles used for the FTIR retrievals are based on the a priori profiles used for tropical sites within the TCCON network (`http://www.tccon.caltech.edu/`). Profiles of pressure, temperature and relative humidity are obtained from the NOAA Climate Diagnostics Center (CDC) based on NCEP (National Centers for

Environmental Prediction) Reanalysis data (`http://www.cdc.noaa.gov/data/gridded/data.ncep.reanalysis.html`). Methane total columns are retrieved from FTIR spectra in the same spectral region as used for the SCIAMACHY retrieval. Since the SFIT2 vs2.92 limits the microwindow size to $120\,\mathrm{cm}^{-1}$, the microwindow used for the FTIR retrieval is slightly smaller than the one used for the SCIAMACHY retrieval. Figure 4.8 shows a typical fit in the microwindow used for the total column retrieval of CH_4 from FTIR measurements. The interfering species CO_2 and H_2O are also fitted in the same microwindow. The upper panel shows the residuals of the fit. The small residuals indicate a good quality of the fit. Total columns of carbon dioxide are retrieved from the same NIR spectra as methane (microwindow: 6180 - 6260 cm^{-1}) by profile scaling. The retrieved total column amounts can be converted to column averaged volume mixing ratios (XVMR) by dividing the retrieved vertical column by the total dry air mass:

$$\mathrm{XVMR}(\mathrm{CH_4}) = \frac{\mathrm{column}(\mathrm{CH_4})}{\text{total dry column}}, \tag{4.2}$$

where the total dry column is

$$\text{total dry column} = \frac{P_{obs}}{m_{dry} g(\varphi)} - \mathrm{column}(\mathrm{H_2O}) \left(\frac{m_{H_2O}}{m_{dry}} \right). \tag{4.3}$$

P_{obs} denotes the observed surface pressure, m_{dry} the mean molecular mass of dry air ($28.964\,\mathrm{g\,mol}^{-1}$), m_{H_2O} the mean molecular mass of water vapour ($18.02\,\mathrm{g\,mol}^{-1}$) and $g(\varphi)$ is the latitude dependent surface acceleration due to gravity. The total dry column can also be determined similar to the SCIAMACHY product (see Eq. (4.1)) from the retrieved CO_2 columns taking advantage of the CO_2 being constant in the atmosphere to the required degree:

$$\text{total dry column} = \frac{\mathrm{column}(\mathrm{CO_2})}{\mathrm{XVMR}(\mathrm{CO_2})} \tag{4.4}$$

$\mathrm{XVMR}(\mathrm{CO_2})$ can be either taken from models or the measured mean $\mathrm{XVMR}(\mathrm{CO_2})$ can be used. Using another retrieved gas for the calculation of the column averaged VMR minimises systematic and correlated errors present in the retrieval of both gases, such as errors in the calculated air mass and in the instrumental line shape (Yang et al., 2002).

Ground-based FTIR measurements give an instantaneous measurement of the atmosphere above the instrument (in the light path between the solar tracker and the sun) at the time of the measurement. FTIR and satellite measurements can only be performed under clear sky conditions. While FTIR measurements are at one location, satellites average over a footprint of $30\,\mathrm{km} \times 60\,\mathrm{km}$ for SCIAMACHY. SCIAMACHY has a global coverage of three days and overflies the FTIR location every three days at around the same time everyday. Due to the

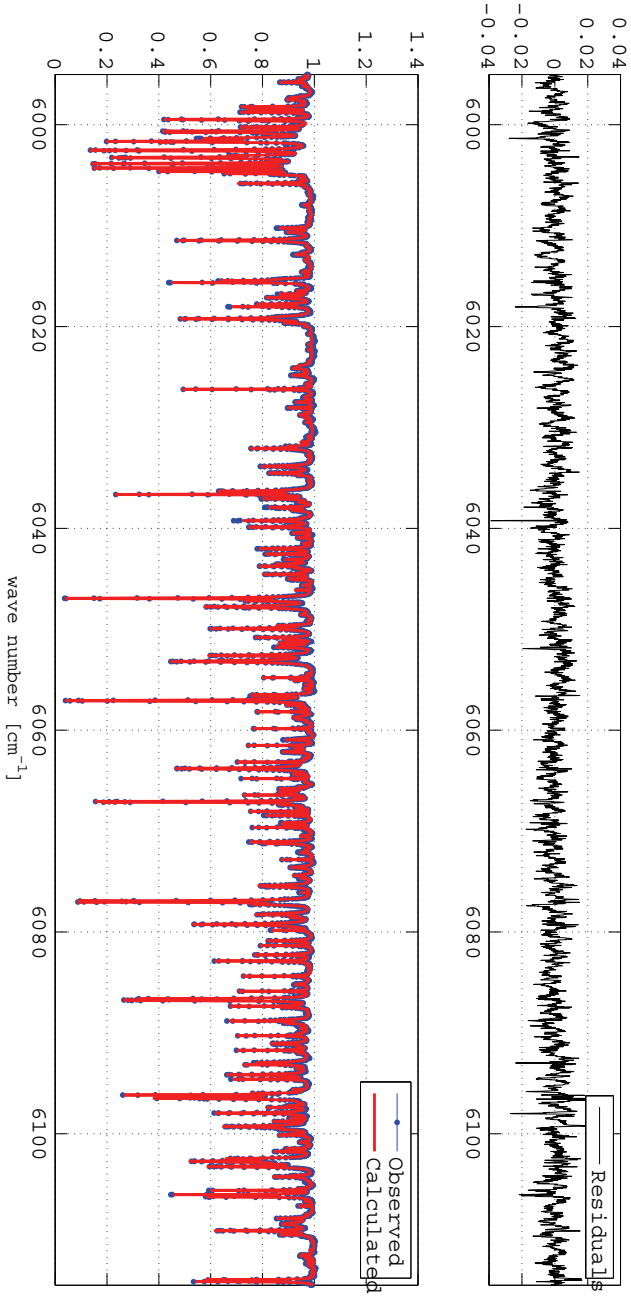

Figure 4.8: Spectral microwindow used for the total column retrieval of methane. The upper panel shows the residuals (difference between the measured and the fitted spectrum, in absolute values), indicating that the measured spectrum is well fitted. Small residuals indicate a good quality of the retrieval.

high variation/scatter of satellite measurements, the satellite measurements are often averaged over large areas and/or time spans. It is common to use a ±15 days running average over a time series of satellite measurements at a specific location.

In general, the comparison of datasets with different spacial and/or temporal resolution may reveal certain problems. The atmosphere transports and modifies the signals from the surface fluxes, giving rise to trace gas distributions, which might vary significantly on relatively small spatial and temporal scales. This variance leads to potentially large errors ("representation error") and uncertainties when point measurements like surface in situ measurements or total column measurements like FTIR measurements are compared with grid-cell averages from models (Gerbig et al., 2003a,b) or swath-averaged satellite observations. Surface in situ measurements by flask sampling are point measurements in time and space. They give information about the volume mixing ratio at the surface at the sampling location for the time of the sampling. Flask sampling measurements are very sensitive to local sources and can be highly influenced by local pollution events. Flask measurements for comparison with total columns observations or model simulations are typically taken from background sampling sites. FTIR measurements are performed at one location and give information about the vertical column above the instrument (for some trace gases information about the vertical distribution is possible) for the time of the measurement. FTIR measurements are sensitive to local and regional sources, which influence the total columns of a trace gas. Satellite observations like SCIAMACHY average over a large area. Satellite observations are well suited to reveal global trace gas distributions and trends, but are not able to detect small-scale temporal and spacial variations against the large background of methane.

For the comparison of the FTIR measurements in Paramaribo with SCIAMACHY data, the influence of the averaging process using different areas has been tested. Figure 4.9 shows the different regions of used SCIAMACHY pixels above the FTIR measurement site and above the Surinamese sea respectively. In Figure 4.10 the daily averages of the XVMR(CH_4) for the different regions are shown in different colors. Also shown are the ±15-day running mean and the standard deviations. The blue region (smallest area around the measurement site) results in the highest methane XVMRs. The green area contains only ocean pixels and results, as expected, in lower methane abundances. The red region is the largest area and contains SCIAMACHY pixels of the sea and of the Surinamese country, including areas covered with tropical rainforest. The running average of the red area data is in between the running average of the green and the blue areas (see Figure 4.10). All three data sets show in general the same variation in time. In 2004 and 2005 the methane abundances are relatively constant, while in 2006 and 2007 a clear seasonal cycle can be seen. The seasonal amplitude for Paramaribo in 2007 is slightly smaller than in 2006, in contrast to measurements from two global monitoring networks, showing a renewed growth of atmospheric

Figure 4.9: Footprints of the SCIAMACHY measurements used for the comparison with FTIR measurements at Paramaribo (blue: 5.7 - 6.2°N, 54.7 - 55.5°W, green: 6.0 - 8.0°N, 54.0 - 57.0°W, red: 4.0 - 8.0°N, 54.0 - 57.0°W).

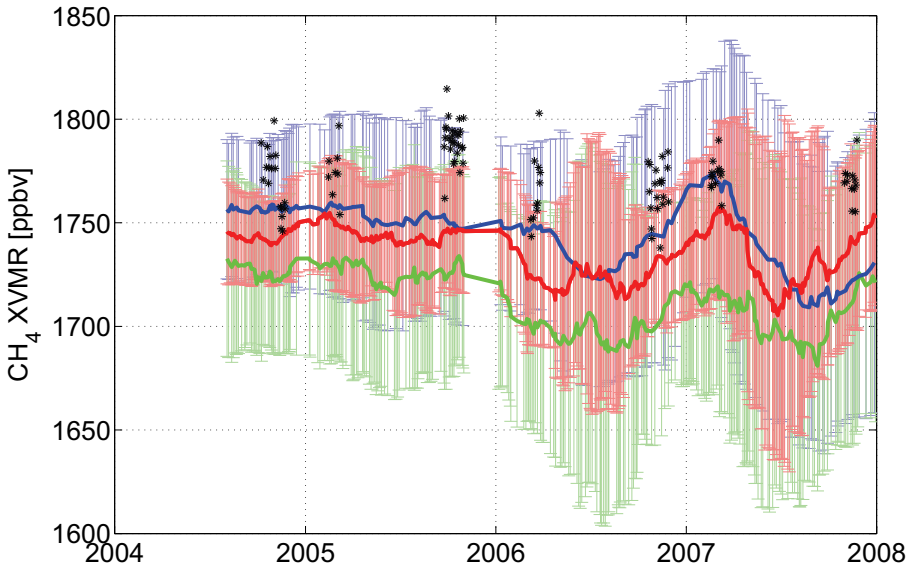

Figure 4.10: Methane XVMR retrieved from SCIAMACHY. Shown are the results for different footprints of the SCIAMACHY measurements (see above) compared with the XVMR(CH_4) retrieved from FTIR spectra in Paramaribo (black stars).

methane in 2007 as reported recently by Rigby et al. (2008).

As can be seen from the high standard deviation of the running mean in Figure 4.10, the satellite observations show in general a high variation. Within the variation, the FTIR measurements at Paramaribo agree with the satellite observations. In 2006 and 2007 the FTIR observations show the same seasonal variation as the SCIAMACHY retrievals. The enhancement observed by the FTIR during the second campaign in 2005, most likely due to biomass burning (see Section 5), cannot be seen in the SCIAMACHY observations, which can be ascribed to the fact that the satellite measurements average over a large area. The FTIR measurements are performed at one location at one point in time and thus are more sensitive to local pollution events. In general, the SCIAMACHY retrievals are relatively constant in 2004 and 2005 over Suriname and show nearly no seasonal variation during this time.

The column averaged VMR derived from FTIR total column measurements weighted with the observed surface pressure (see Eq. (4.2) and (4.3)) may introduce an error due to errors in the pressure measurement. We estimate the error on the CH_4 XVMR to be less than 0.2 % for a pressure uncertainty of 2 hPa, which we assume to be the maximal error for the pressure measurements during all campaigns. The column averaged VMR product from SCIAMACHY may introduce errors due to wrong model values for the CO_2 VMR.

Instead of comparing the column averaged CH_4 mixing ratios, the retrieval method of the FTIR allows to compare the ratios of the total columns of CH_4 and CO_2 retrieved from the FTIR spectra with those retrieved from the SCIAMACHY spectra without assuming further model information. In Figure 4.11 the ratio of CH_4 and CO_2 from FTIR measurements and SCIAMACHY retrievals are shown for the red footprint (4.0 - 8.0°N, 54.0 - 57.0°W) containing both land and ocean pixels. The ±15-day running average over the daily means of SCIAMACHY measurements is in very good agreement with the FTIR daily means. During the second campaign in 2005 (LDS 2005), the FTIR observations are slightly higher than the ±15-day running average of SCIAMACHY, but within the variation of the satellite observations. From FTIR observations of CO and other biomass burning related trace gases, model simulations and trajectory analysis (see Section 5) it is known that Paramaribo experienced air masses polluted by biomass burning during the LDS 2005. In September 2005 the CO levels peak at three specific days. During the rest of the campaign in 2005, CO levels are enhanced compared to other campaigns. Due to the larger footprint of SCIAMACHY measurements, averaging over a large area, we do not expect to observe these local effects in the SCIAMACHY measurements.

The comparison of the direct measurements of CH_4/CO_2 from both instruments allows an undisturbed analysis of both retrievals. For the comparison of the CH_4 XVMR, the high difference between FTIR and SCIAMACHY obser-

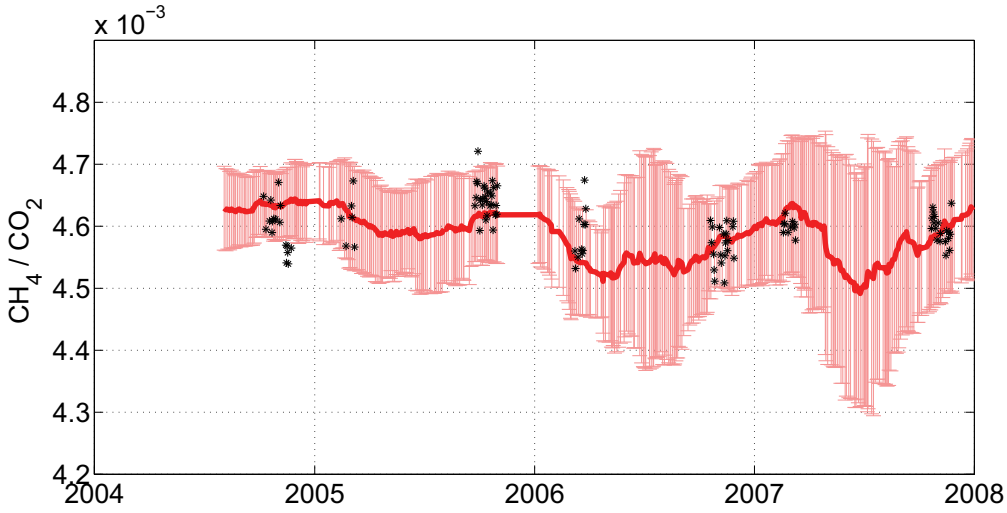

Figure 4.11: CH_4/CO_2 retrieved from FTIR and SCIAMACHY spectra for the red footprint (4.0 - 8.0°N, 54.0 - 57.0°W). Shown is the 15-days running average over daily means from SCIAMACHY retrievals (red line) and the standard deviations. The FTIR observations are daily means (black stars) .

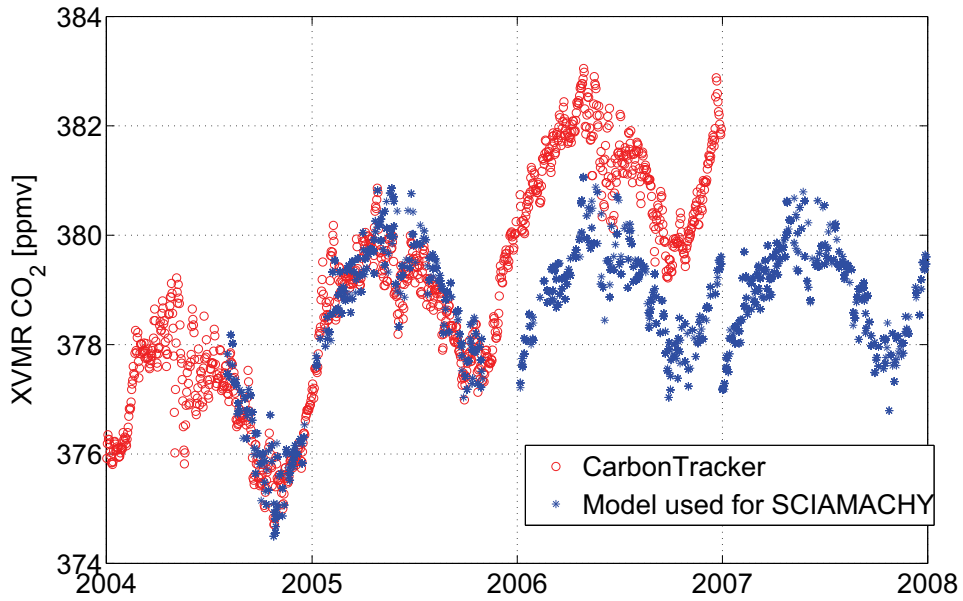

Figure 4.12: CarbonTracker (open red circles) and the CO_2 model data used for the SCIAMACHY XVMR product.

vations is caused by using unrealistic CO_2 model data Suriname to derive the XVMR(CH_4) (see Figure 4.12). For the retrieval of the years 2006 and 2007, when CarbonTracker model data was not yet available, the TM3 model has been used, resulting in a step in the timeseries. For 2007, the TM3 model data of 2006 has been used. This leads to unrealistic low methane XVMR in 2007. The potential errors in the FTIR observations due to errors in the pressure measurements are negligible compared to the natural variation.

Atmospheric chemistry and transport models (CTM) predict concentrations averaged over large grid cells with typical temporal resolution of 3 hours. Atmospheric CTMs can be used to link between local measurements and global observations with different temporal and spacial resolution. The model can be compared globally to the satellite observations and the local measurements with extractions from the model (assuming the model resolution to be high enough). Another possibility is to use the satellite observations to assimilate an inverse modeling system and compare the assimilated model with the local measurements.

4.2.2 Comparison with Model Simulations

Surface and space-borne observations of methane have been used to assimilate the TM5 model using the four-dimensional variational (4D-VAR) data assimilation system. TM5 is an offline transport model that uses meteorological fields from the ECMWF IFS model (6-hourly forecast, based on 4D-VAR analyses) (ECMWF IFS documentation, 2002 (`http://www.ecmwf.int/research/ifsdocs/`)). Chemical destruction of CH_4 by OH radicals is simulated using precalculated OH fields based on CBM-4 chemistry (Houweling et al., 1998) and optimized with methyl chloroform (Bergamaschi et al., 2005). Chemical destruction of CH_4 by OH, Cl and $O(^1D)$ radicals in the stratosphere are based on the 2-D photochemical Max-Planck-Institute (MPI) model (Bergamaschi et al., 2005; Brühl and Crutzen, 1993). For biomass burning the Global Fire Emissions Database (GFED) version 1 (van der Werf et al., 2004) was applied, using a multiannual average for the period 1997 to 2002. Details about the used emission inventories can be found in Bergamaschi et al. (2007). Methane surface observations, taken from the NOAA ESRL global cooperative air sampling network (Dlugokencky et al., 1994, 2003), have been used to optimize the two-dimensional distribution of surface emissions. Only flask measurements from marine and continental background sites have been used for the inversion.

To assess the potential implications of SCIAMACHY measurements on the distribution of global CH_4 sources, the SCIAMACHY observations together with the surface observations have been used for inversion. Global simulations at $6^\circ \times 4^\circ$ (base functions) and $3^\circ \times 2^\circ$ (final global simulations) are interpolated bi-linearly to a $1^\circ \times 1^\circ$ grid. Figure 4.13 shows the grid resolution of the TM5 model as

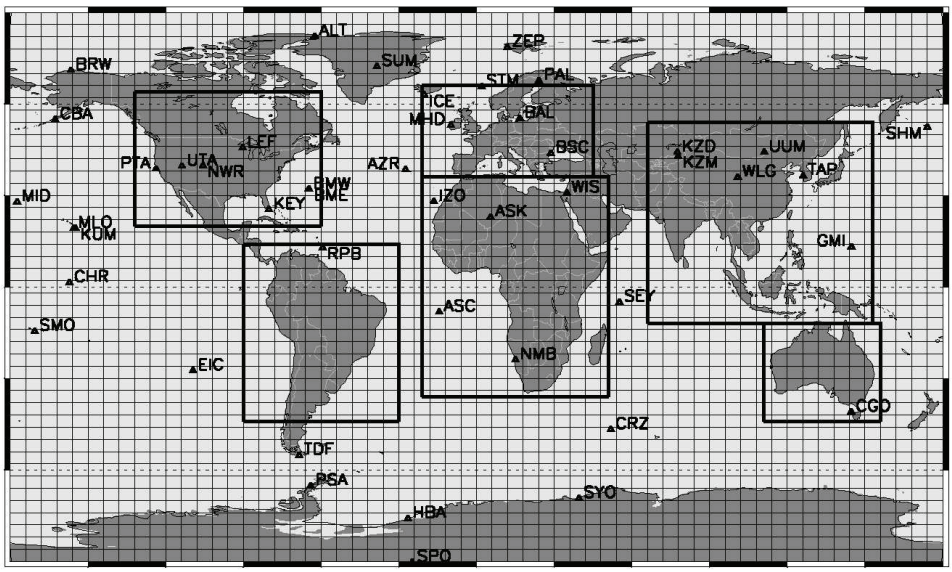

Figure 4.13: TM5 model grid with $6° \times 4°$ resolution and the surface air sampling sites from the NOAA network (Bergamaschi et al., 2007).

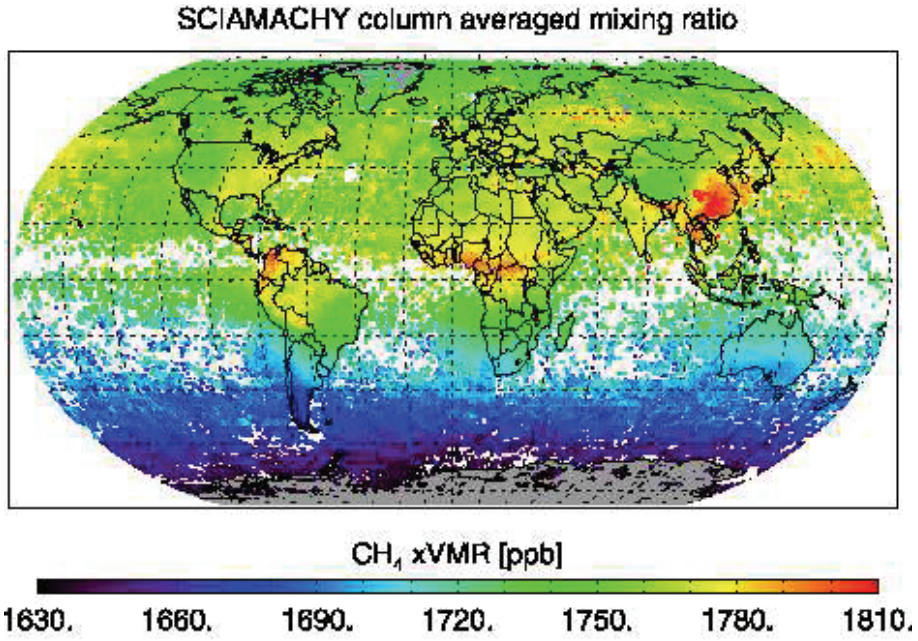

Figure 4.14: Global distributions of CH_4 retrieved from SCIAMACHY (Frankenberg et al., 2008a).

well as the surface air sampling sites from the NOAA network. The TM5 model assimilated by NOAA surface observations (here in noted as TM5 NOAA) and the SCIAMACHY together with surface data assimilated TM5 model (denoted in the following as TM5 SCIAMACHY/NOAA) will be compared with the FTIR observations performed in Paramaribo.

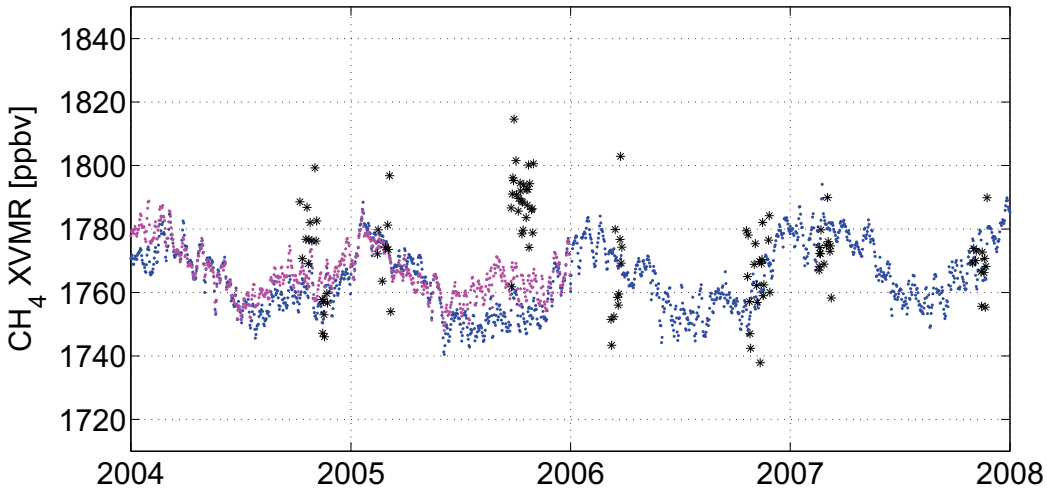

Figure 4.15: Retrieved XVMR(CH_4) from FTIR (black) compared with TM5 model simulations, assimilated with NOAA surface observations (blue) and assimilated with SCIAMACHY/NOAA observations (magenta).

In Figure 4.15 the column averaged CH_4 retrieved from FTIR spectra are compared with corresponding model output from the NOAA assimilated and the SCIAMACHY/NOAA assimilated TM5 4DVAR model for Paramaribo. The model simulations for the NOAA assimilated and the SCIAMACHY/NOAA assimilated inversions don't show a large difference for Paramaribo apart from the second part of the year where the SCIAMACHY/NOAA assimilated model is slightly higher than the one assimilated only by surface measurements. During the second campaign in 2005 (LDS 2005), the FTIR observations exceed the model simulations by far. From FTIR observations of CO and other biomass burning related trace gases, model simulations and trajectory analysis (see Section 5) it is known that Paramaribo experienced air masses polluted by biomass burning during the LDS 2005. During this time, CO is enhanced compared to other campaigns. Apart form biomass burning events in the LDS 2005 campaign, the FTIR CH_4 retrievals are in general in good agreement with the model output. The FTIR data shows higher variation than the model. For this comparison, only

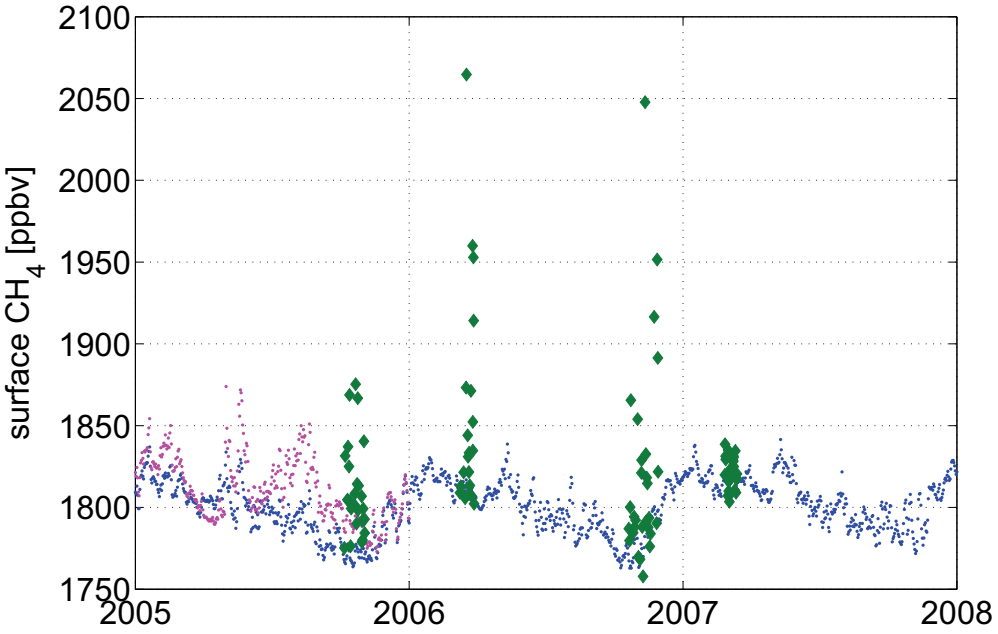

Figure 4.16: Methane surface volume mixing ratios from TM5 model simulations, assimilated with NOAA surface observations (blue) and assimilated with SCIAMACHY/NOAA observations (magenta) compared with in situ air samples taken in Paramaribo (dark green diamonds).

model data on a $6° \times 4°$ resolution grid, interpolated to a $1° \times 1°$ resolution grid, has been available. Thus the model shows an average over a large area and can not cover local variation, while the FTIR measurements are influenced by local sources. In the end of the campaign in 2004 the FTIR observations are in better agreement with the TM5 NOAA than with the TM5 SCIAMACHY/NOAA. During biomass burning periods however, the TM5 NOAA model does not reproduce the enhanced methane levels, while the TM5 SCIAMACHY/NOAA model increase slightly during the time of the year where most biomass burning is expected (dry season: August to November).

Figure 4.16 shows the surface values of the TM5 model output for Paramaribo compared with surface in situ data (dark green diamonds). The surface in situ measurements were sampled in Paramaribo and analysed by the MPI Jena by gas chromatography. The flask measurements in Paramaribo show in general a very high variation, indicating the strong influence of local sources. Assuming that the lower values for each of the campaigns are representative for air with small local pollution, it can be concluded that there is a good agreement of the "clean air" flasks with the surface model data. We assume that the high methane pollution

events are due to urban pollution from the City of Paramaribo (e.g. leaking gas tanks used for cooking purposes) or biomass burning. The used model data is at low resolution and is not able to reproduce these local effects. The magenta dots represent the surface values of the TM5 model assimilated with retrieved methane from SCIAMACHY and NOAA. The TM5 SCIAMACHY/NOAA is slightly increased compared to the TM5 NOAA model output and in better agreement with the surface observations.

4.3 Conclusion

TM5 model simulations for Paramaribo, assimilated with SCIAMACHY/NOAA, are available only for the years 2004 and 2005. For Paramaribo, the difference between the NOAA assimilated TM5 model and the SCIAMACHY/NOAA assimilated TM5 model is in general small. The largest difference between the different model simulations exists during the long dry seasons, in August to November, the season when Suriname experiences higher regional biomass burning emissions. The FTIR measurements, performed in the LDSs in 2004 and 2005 are used to quantify, which model assimilations for Paramaribo reproduces the observations better. The FTIR measurements of the LDS 2004 campaign agree well with the SCIAMACHY/NOAA assimilated TM5 model, while during the LDS 2005 campaign, the FTIR CH_4 observations are in general much higher than both model simulations, most likely due to regional biomass burning pollution. From trajectory analysis and FTIR CO observations in Paramaribo it is known that during the LDS 2005 air masses above Paramaribo were highly influenced by regional biomass burning pollution, which can be clearly seen in surface flask measurements as well as in the CH_4 FTIR observations. Apart from biomass burning events in the LDS 2005, the TM5 model simulations reproduce the methane observations from the FTIR. The FTIR CH_4 measurements show a higher variations than the model, which is expected since the TM5 model is based on a 6° x 4° resolution grid and averages over a large area, while the FTIR retrieval is more sensitive to local influences. Flask surface observations sampled in Paramaribo show in general a very high variation, indicating the high influence of local sources. However, the lower values of the surface observations, representing the "clean air" observations, agree well with the TM5 model simulations for all campaigns. In the second part of 2005, where flask measurements and both assimilated TM5 model simulations are available, the in situ measurements are in better agreement with the SCIAMACHY/NOAA assimilated TM5 model.

Within the high variation of SCIAMACHY, the FTIR measurements of the column averaged VMR CH_4 at Paramaribo agree with the satellite observations. In general, the SCIAMACHY CH_4 observations are relatively constant in 2004 and 2005 over Suriname and show nearly no seasonal variation during this time. In

2006 and 2007 the FTIR CH_4 observations show the same seasonal variation as seen from SCIAMACHY. Due to the unavailability of the most recent CO_2 model data, unrealistic CO_2 model data has been used in the SCIAMACHY retrieval, resulting in wrong timeseries. The retrieval method of the FTIR allows to compare directly the CH_4/CO_2 ratio from SCIAMACHY without relying on model assumptions. The model assumptions are used to derive column averaged volume mixing ratios. The CH_4/CO_2 ratio retrieved from FTIR spectra is in excellent agreement with the SCIAMACHY observations, apart from the LDS 2005 campaign, where the FTIR observations are influenced by regional biomass burning pollution. The comparison of the CH_4/CO_2 ratio reveals that the CarbonTracker and TM3 model assumption lead to wrong CH_4 XVMR if the CO_2 model data is not realistic.

The retrieval method of the FTIR, being very similar to the one used for satellite measurements, allows the direct comparison of the measured ratio CH_4/CO_2 without introducing potential errors due to model assumptions. Furthermore, like satellite observations, FTIR solar absorption measurements observe the whole atmospheric column and are well suited for satellite validation in contrast to surface observations, which only probe the surface air.

5 Carbon Monoxide and other Trace Gases related to Biomass Burning

Biomass burning is not restricted to the tropics, however, most burning occurs in the tropics. Satellite images have shown that the large-scale biomass burning in the tropics is strongly seasonally modulated and occurs predominantly during the dry season. In addition to this seasonal modulated, large scale burning, the burning of biomass for cooking and heating purposes has been shown to be a major source of atmospheric pollution (Ludwig et al., 2003). Among others, biomass burning releases significant amounts of carbon monoxide (CO), hydrogen cyanide (HCN), ethane (C_2H_6) and acetylene (C_2H_2). Estimates for carbon monoxide range from about 300 Tg/a to more than 700 Tg/a of CO (Bergamaschi et al. (2007); Holloway et al. (2000), IPCC: Houghton et al. (2001)). The emissions from biomass burning depend on the type of the burned biomass, meteorological conditions and the burning process itself.

In this chapter the first FTIR measurements of CO, HCN, C_2H_6 and C_2H_2 in the inner tropics over several years are presented. The FTIR observations agree well with satellite data from the MOPITT instrument and with MATCH-MPIC model simulations. The model is generally not able to reproduce the extreme enhancements seen during the specific biomass burning events by both observation instruments. The FTIR observations are used to evaluate revised MATCH-MPIC simulations with satellite-based biomass burning emissions. The revised simulations generally underestimate the observed total columns of carbon monoxide and ethane. A recently hypothesized mechanism of isoprene-OH oxidation chemistry might have an influence on the understanding of the chemical processes involved with biomass burning related trace gases. Part of this chapter is published in (Petersen et al., 2008).

CO is primarily produced from biomass burning, oxidation of methane and other biogenic hydrocarbons and fossil fuel combustion. It has a lifetime ranging from weeks to a few months and it is an effective indicator of how transport processes distribute atmospheric pollutants from biomass and fossil fuel burning on a global scale. The main sink of CO is oxidation by OH (Crutzen and Zimmermann, 1991). In contrast to CH_4, the direct radiative forcing of CO is relatively small. However, CO plays a primary role in governing OH abundances in the troposphere. CO emissions into the atmosphere may have a significant impact on climate forcing due

to chemical impact on CH_4 lifetime, and tropospheric O_3 and CO_2 photochemical production (IPCC: Houghton et al. (2001)).

Ethane is the most abundant non-methane hydrocarbon (NMHC) in the atmosphere. It is mainly produced through fossil fuel production, processing and transmission, bio-fuel use, and biomass burning. Atmospheric loss is by reaction of OH, with a mean lifetime of ∼2 month. Ethane can serve to test predictions of atmospheric transport and chemistry models and to check source strength and geographic distribution of sources of atmospheric trace gases (Rudolph, 1995).

5.1 Data Analysis

Solar absorption FTIR spectra, recorded during five consecutive dry seasons between September 2004 and November 2006 at Paramaribo, where analysed for total column amounts and volume mixing ratio (VMR) profiles of CO, C_2H_6, C_2H_2 and HCN using the algorithm SFIT2 vs2.92 (Rinsland et al., 1998). The apriori profiles used for the FTIR retrievals are based on the apriori profiles used for the MOPITT validation (Vigouroux et al., 2006). The spectral line parameters were taken from the HITRAN2004 database (Rothman et al., 1987). In Table 5.1 the microwindows used for the retrieval are shown. Interfering gases are fitted simultaneously by profile scaling. Solar lines are generally simulated in the retrieval. Global fire maps (ATSR World Fire Atlas, `http://dup.esrin.esa.int/ionia/wfa/index.asp`) were used together with back-trajectory analysis (BADC Trajectory Service, `http://badc.nerc.ac.uk`) to identify the impact of biomass burning. Data for CO from the MOPITT (Measurements Of Pollution In The Troposphere) instrument onboard the TERRA satellite were obtained from the NASA Langley Research Center Atmospheric Science Data Center (`http://eosweb.larc.nasa.gov/PRODOCS/mopitt/table\_mopitt.html`). We used MOPITT level 3 gridded daily averaged data for the comparison. Only cloud free pixels within a radius of 200 km from the FTIR measurement site were selected. The comparison of CO VMR profiles from FTIR measurements with MOPITT data has been done by Velazco et al. (2005), showing good agreement. Here we concentrate on the comparison of total columns. MATCH-MPIC, the Model of Atmospheric Transport and Chemistry, has been developed for the investigation of global tropospheric chemistry (Rasch et al., 1997; Lawrence et al., 1999, 2003; von Kuhlmann et al., 2003). It is an offline model that reads in gridded time-dependent values for the basic meteorological parameters, e.g. temperature, surface pressure, and horizontal winds. It then uses these parameters to calculate further meteorological parameters like cloud fields and convective mass fluxes that are required for atmospheric chemistry simulations. MATCH-MPIC employs monthly-mean biomass burning emissions, which do not vary from year to year. The MATCH-MPIC model, in the forecast and analysis configuration (Lawrence

et al., 2003), has been used to calculate VMR profiles of CO and C_2H_6 for Paramaribo for the same time periods as the measurement campaigns. The model is simulated at global resolution of 6° × 4°. The mixing ratios for Paramaribo are calculated from the model output by interpolation from the 4 surrounding grid points, due to the location of Paramaribo in the edge of one model grid cell.

	Microwindow $[cm^{-1}]$	Interfering Gases
CO	2057.70 - 2057.95	H_2O, N_2O, O_3, OCS
	2069.55 - 2069.72	H_2O, N_2O, O_3, OCS
	2157.30 - 2159.92	H_2O, N_2O, O_3
HCN	3268.18 - 3268.30	H_2O
	3286.60 - 3288.00	H_2O
	3305.30 - 3305.60	H_2O, CO_2
C_2H_2	3250.43 - 3250.77	H_2O
	3304.78 - 3305.12	CO_2, N_2O, HCN, H_2O
C_2H_6	2976.62 - 2976.92	H_2O, CH_4, O_3

Table 5.1: Microwindows and Interfering Gases for CO, HCN, C_2H_6 and C_2H_2

5.2 Ground-Based and Space-Borne Measurements

Total columns of CO, C_2H_6, C_2H_2 and HCN retrieved from ground based solar absorption measurements in Paramaribo, Suriname, are shown in Figure 5.1. The CO total column averaged over all of the campaigns is $2.0 \pm 0.3 \times 10^{18}$ molec/cm^2. During the LDS campaign in 2005 it is about 11.4 % higher than the average. The LDS campaigns (SH) are more strongly impacted by biomass burning emissions than the SDS campaigns (NH). Variability is also much higher during LDS than during SDS campaigns. This is especially so during the LDS 2005, when very high total column amounts of CO were observed. Statistics on the fire counts during the LDS 2004 and 2005 give no evidence for enhanced biomass burning during the LDS 2005, neither in Africa nor in South America. However, back-trajectories indicate that during the LDS of 2005, a higher percentage of air masses are coming from South America compared to the same season in the years 2004 and 2006, presumably resulting in greater levels of regional biomass burning pollution.

CO total columns from MOPITT measurements are plotted together with the FTIR observations in Figure 5.1 (upper panel). There is a very good agreement between the FTIR and MOPITT data, especially for the significant enhancements during 18-20 October 2004 and 27-29 September 2005, which are observed by the FTIR as well as by the MOPITT instrument. The back-trajectory analysis shows that the enhancements most likely resulting from biomass burning events in South America (see Figure 5.2). CO total columns of the MATCH-MPIC

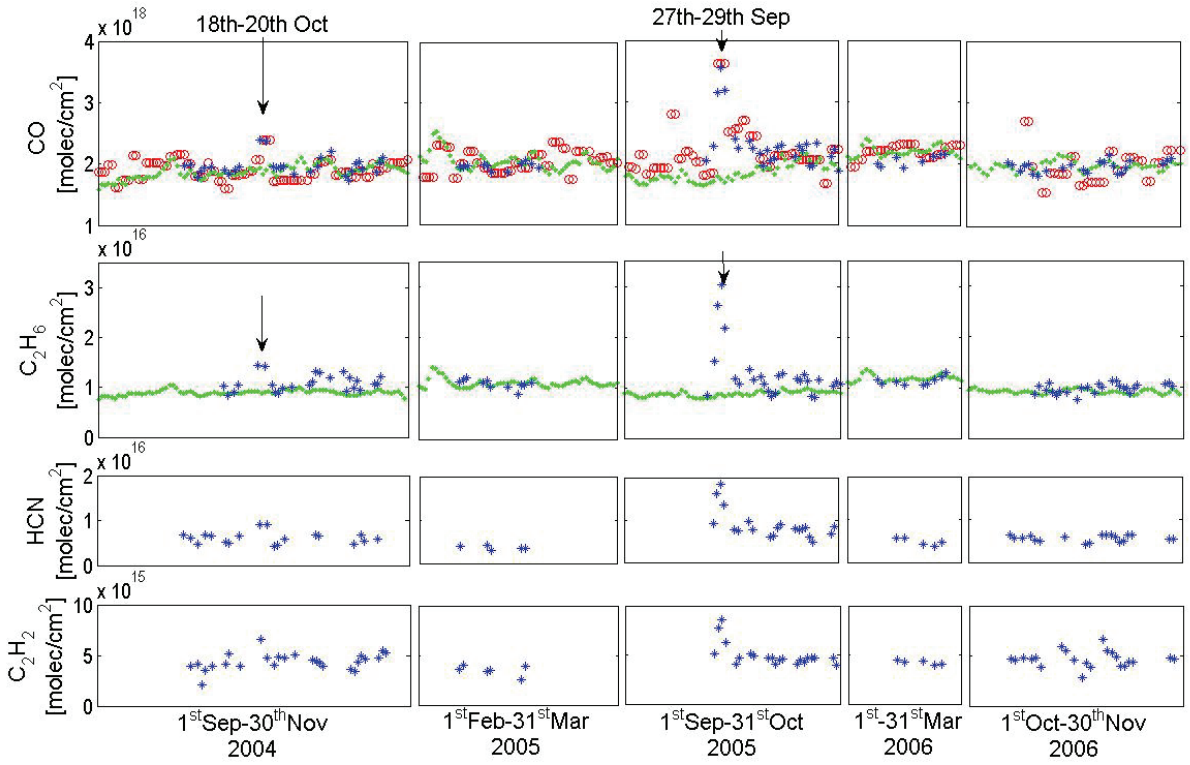

Figure 5.1: Total columns of CO, C_2H_6, HCN and C_2H_2 retrieved from FTIR measurements (blue stars). The upper most panel shows the comparison of CO total columns from FTIR measurements with cloud free data from the MOPITT instrument (open red circles) within a radius of 200 km around the FTIR measurement site. Also shown are the CO total columns of the MATCH-MPIC model runs for Paramaribo (green dots).The middle panel shows the comparison of C_2H_6 total columns from FTIR measurements with total columns of the MATCH-MPIC model runs (green dots) for Paramaribo. The two lower most panels show the retrieved total columns of HCN and C_2H_2 from FTIR measurements.

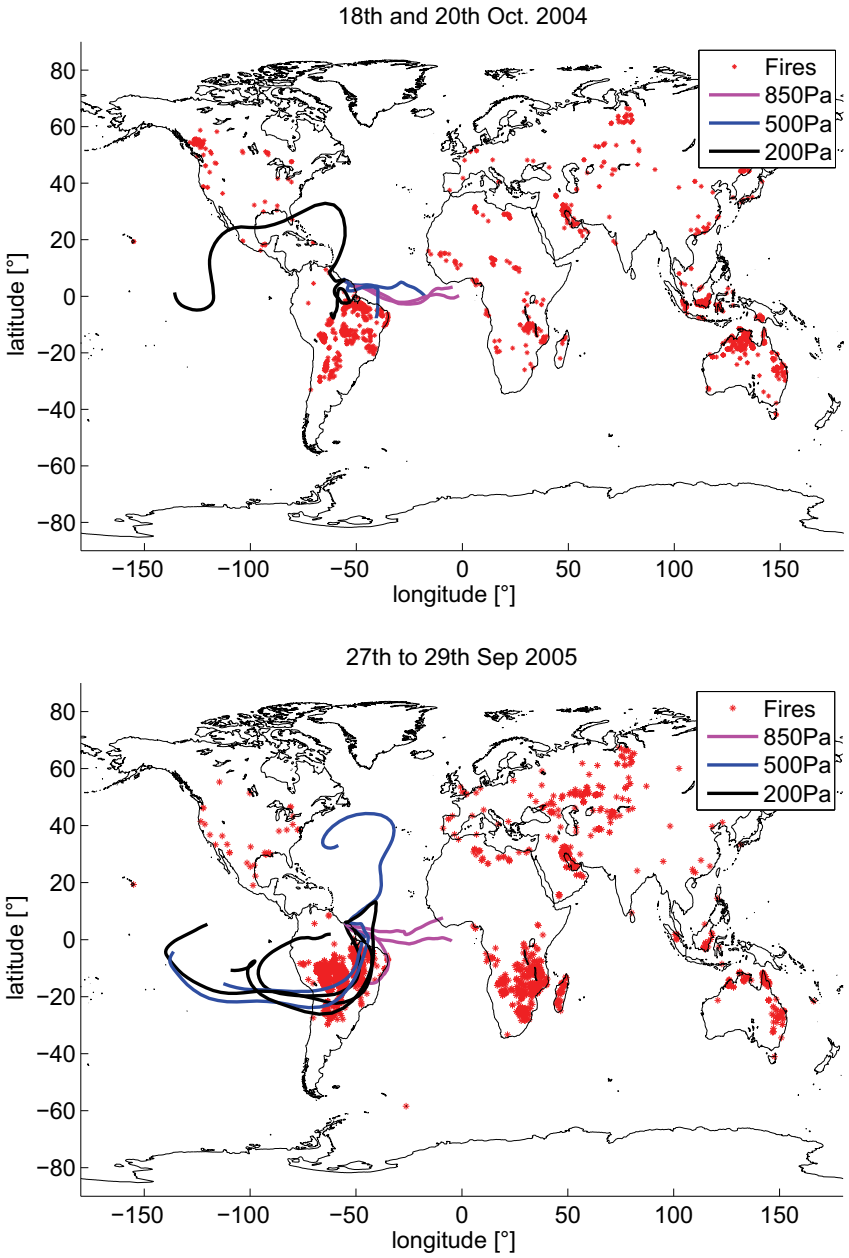

Figure 5.2: Kinematic 10-day back-trajectories of the air masses reaching the 200, 500 and 850 hPa levels above Paramaribo were calculated by the BADC (British Atmospheric Data Centre) Trajectory Service (`http://badc.nerc.ac.uk`) for the measurement days. Global fire maps generated using ATSR-2 (Along Track Scanning Radiometer onboard the ERS-2 satellite) night time data in the ATSR World Fire Atlas (`http://dup.esrin.esa.int/ionia/wfa/index.asp`) were used together with the trajectory analysis to identify the impact of biomass burning.

model for Paramaribo are also plotted. Apart from the LDS 2005, the CO total columns of the model are in good agreement with both the FTIR and the MOPITT observations. A detailed discussion is done in Section 5.3. The second panel of Figure 5.1 shows the C_2H_6 total columns from FTIR measurements and the MATCH-MPIC model, having an excellent agreement, apart from the biomass burning events. Differences between the NH and SH are seen for both the HCN and C_2H_2 total columns, showing that the sources of these two gases in the NH are not as abundant as in the SH. The HCN and C_2H_2 total columns are on average about $7.0 \pm 2.7 \times 10^{15}$ molec/cm^2 and $4.6 \pm 1.0 \times 10^{15}$ molec/cm^2, respectively, during the LDS (SH) campaigns. During the SDS (NH) campaigns they are about 40% and 17.4% lower than during the LDS campaigns (averaging $4.2 \pm 0.9 \times 10^{15}$ and $3.8 \pm 0.5 \times 10^{15}$ molec/cm^2, respectively). As for CO, especially in the LDS 2005 campaign, high HCN and C_2H_2 total columns were observed. Further, the variation during LDS campaigns is larger than during the SDS measurement periods. These two differences are also seen for the C_2H_6 measurements, though the hemispheric differences are not as clear.

5.3 Comparison of Model Simulations with FTIR Measurements

CO mixing ratio profiles for Paramaribo have been calculated from MATCH-MPIC output by interpolation from the 4 surrounding grid points. Figure 5.3 shows the corresponding FTIR measurements and model output for all campaigns. The profiles from MATCH-MPIC have a higher vertical resolution compared to the FTIR profiles. To make allowance for characteristics of the observing remote sensing instrument, it is necessary to take the averaging kernels into account when intercomparing the observations with model simulations (Rodgers and Connor, 2003; Palm et al., 2005). Owing to the nature of the retrieval problem being underdetermined, the FTIR averaging kernels tell us that the retrievals at each designated atmospheric layer have contributions from neighboring layers. In the middle panel of Figure 5.3, the model smoothed by the averaging kernels is shown. Details on similar profiles and averaging kernels are given by Velazco et al. (2005). The middle panel shows what would be seen by FTIR spectrometry if the MATCH-MPIC profiles represented the true CO profile. For visual clarity, FTIR measurements are interpolated in this plot for days without measurements if the gaps do not exceed three days. Gaps in the measurements are due to unsuitable weather or solar viewing conditions, and to various logistical problems.

As can be seen by comparing the upper with the middle panel of Figure 5.3, the model generally reproduces the vertical structure with a peak in the middle to upper troposphere. This is well illustrated in the mean vertical profiles for each

season (see Figure 5.5). The model tends to overestimate the observed mixing ratios, generally by about 10-30%, and has a broader pollution peak in the upper troposphere, presumably due to smearing out of plumes by numerical diffusion, which is inherent in the transport algorithms used in the model. The overall seasonal differences are also reproduced, with greater CO mixing ratios throughout the troposphere during LDS versus SDS, and more frequent intense pollution events during LDS. However, the very high near-surface CO mixing ratios during SDS are not simulated, nor are the anomalously large CO mixing ratios in the middle troposphere during the LDS 2005. Furthermore, the model fails to reproduce most of the individual observed pollution events, for example, the two periods with enhanced CO levels due to pollution by South American biomass burning discussed in Section 5.2. This is in contrast to several previous studies (e.g. Lawrence et al., 2003; Velazco et al., 2005), which often showed very good correspondences between observed and modeled pollution plumes, indicating, in particular, a reasonable representation of the outflow meteorology by the model. A likely candidate for the discrepancy here is that climatological monthly mean biomass burning emissions are used, whereas in reality the location of fires varies on a year-to-year basis. Yearly-varying emissions have been used with MATCH-MPIC now in a few specific test cases, showing substantial improvements for comparison to other data sets with observations influenced by biomass burning. Very recently, yearly-varying emissions have been implemented into the operational forecast and analysis system, and have been used for a revised comparison with our tropical FTIR data set. A detailed discussion can be found in Section 5.5. Nevertheless, the overall good agreement with the statistical characteristics of the observations allows the model output based on climatological biomass burning emissions to be used for further analysis of regional CO.

The contributions of CO tracers from various regions and sources (e.g. biomass burning, fossil fuel combustion, and oxidation of methane and NMHCs) were also calculated by the model and are shown in Figure 5.4. The results show that methane oxidation provides a large background source of CO while biomass burning and other sources largely account for the variability in CO. During the SDS campaigns with the main wind direction from the northeast, the model indicates that biomass burning from the African continent is the main source for enhancements in the simulated CO, whereas biomass burning in South America does not contribute significantly. During the LDS campaigns, with the main wind direction from the southeast, the biomass burning sources from both South America and Africa are largely responsible for variation in the CO concentrations. The oxidation of NMHCs is also a large and variable source, corresponding frequently to the biomass burning CO enhancements, indicating the further importance of biomass burning as an indirect source of CO to the troposphere over Paramaribo.

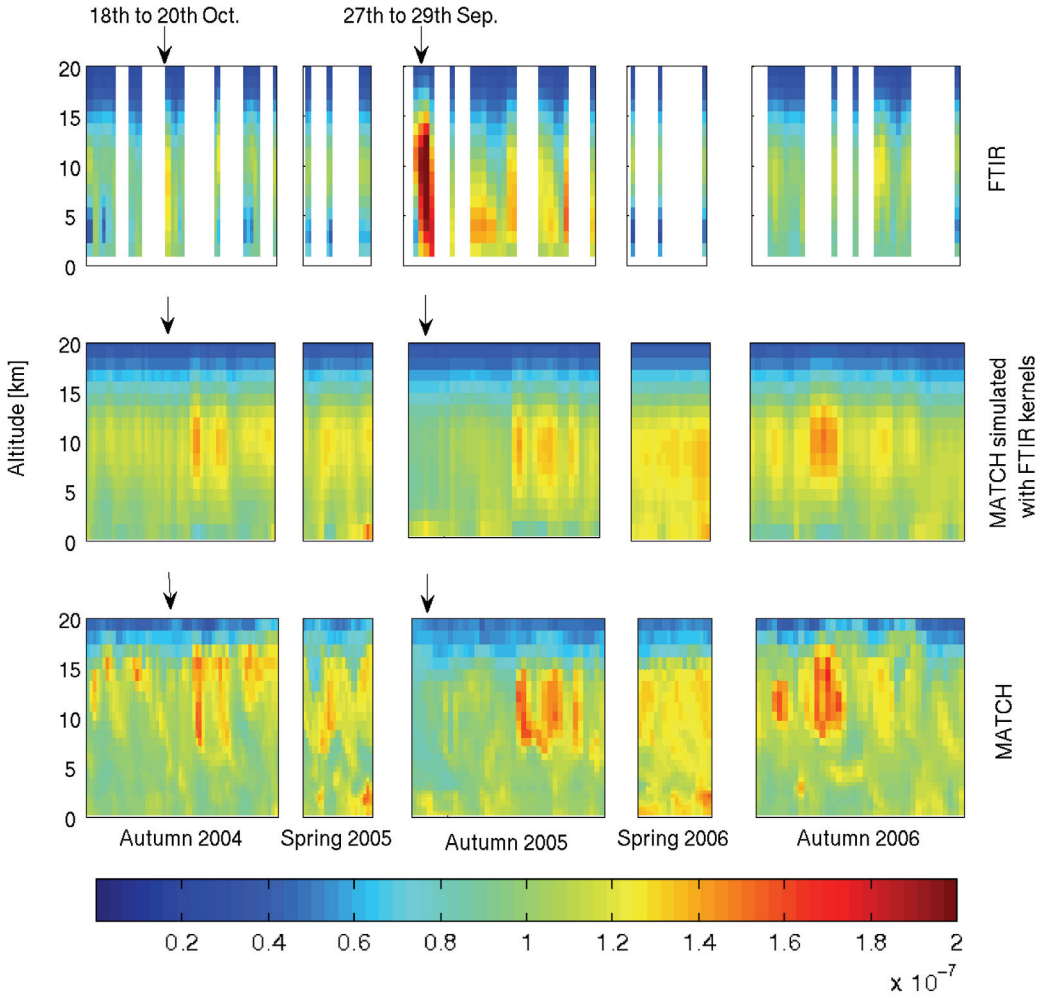

Figure 5.3: CO volume mixing ratio data from MATCH-MPIC (lowest row) and the FTIR in Paramaribo (upper row) for five consecutive measurement campaigns between September 2004 and November 2006. The time axis is scaled on the time periods of the FTIR measurements. In the row in the middle, CO profiles from MATCH smoothed by FTIR averaging kernels are shown.

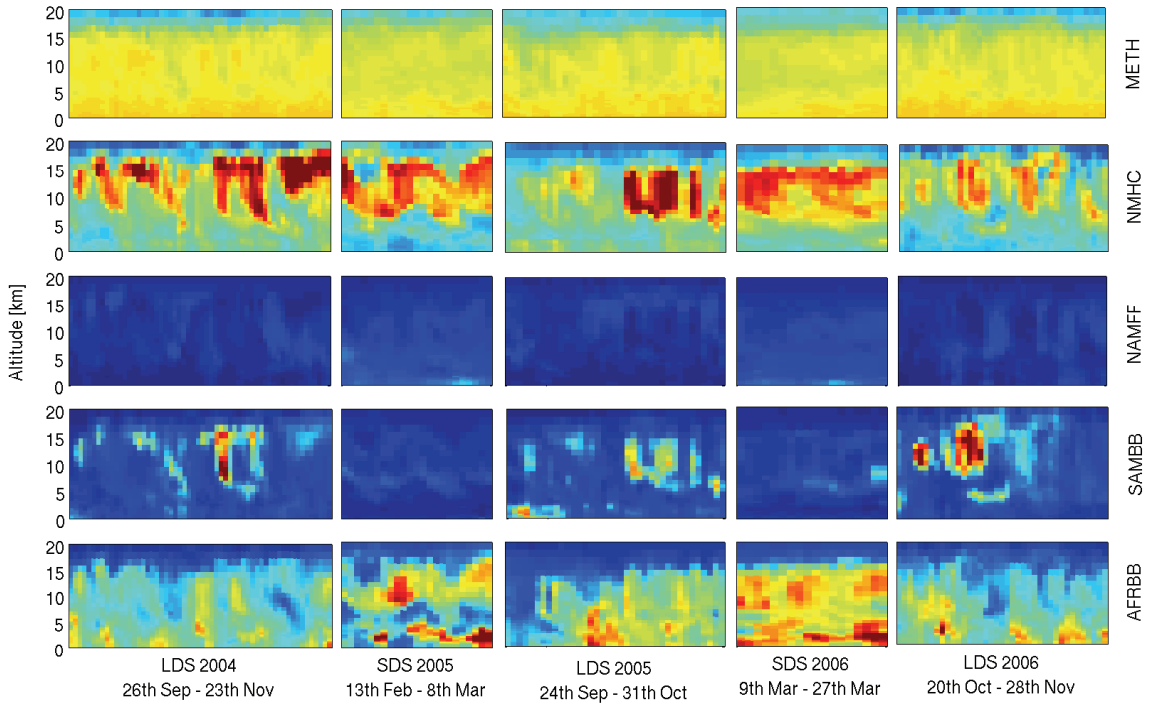

Figure 5.4: Absolute contributions of some regional tracer fields to the CO budget for Paramaribo from MATCH-MPIC (in ppb) for the same time periods as in Figure 5.3. The CO tracer fields are: North American Fossil Fuel (NAMFF), South American Biomass Burning (SAMBB), African Biomass Burning (AFRBB), and methane oxidation (METH). NMHC is the CO source from the chemical oxidation of NMHCs, which originally comes from various sources like biomass or fossil fuel burning, plus the surrogate CO that should result from higher NMHCs, such as monoterpenes, which are not represented explicitly in the model.

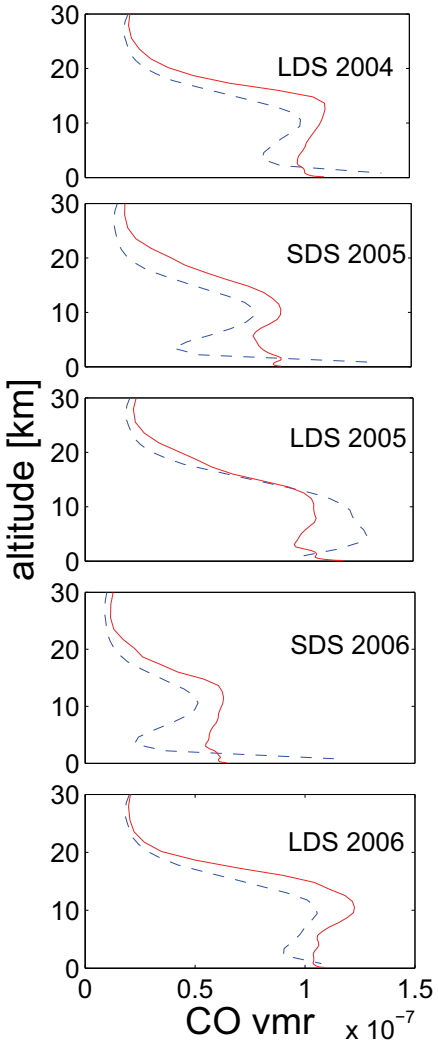

Figure 5.5: Mean CO volume mixing ratio profiles from MATCH-MPIC (red line) and the FTIR (blue dashed line) in Paramaribo for five consecutive measurement campaigns between September 2004 and November 2006
.

5.4 Correlations of HCN, C_2H_2 and C_2H_6 with CO

The correlations coefficients between daily mean values of the CO, HCN, C_2H_2 and C_2H_6 total columns for the five measurement campaigns between September 2004 and December 2006 were obtained by linear least square fits to the data, and are shown in Figure 5.6. For the LDS campaigns, when Paramaribo belongs to the meteorological Southern Hemisphere, the gases show very high correlations with CO when biomass burning pollution is experienced. Correlation coefficients of 0.87, 0.97 and 0.5 between CO and HCN, of 0.41, 0.90 and 0.3 between CO and C_2H_2 and of 0.44, 0.93 and 0.63 between CO and C_2H_6 can be found during the LDS campaigns. The relatively low correlations for the last LDS in 2006 are ascribed to relatively low concentrations of these trace gases and no biomass burning pollution events. These high correlations indicate that in the Southern Hemisphere these four molecules underly similar production and dilution processes. During the SDS, when Paramaribo belongs to the meteorological Northern Hemisphere, very low correlations or even anticorrelations are observed for all C_2H_2, C_2H_6 and HCN to CO (0.41 and -0.46 for CO-HCN, -0.11 and -0.37 for CO-C_2H_2). The correlation coefficient between CO and C_2H_6 is relatively high for the SDS 2005 (0.74 in 2005 and 0.04 in Spring 2006), but it should be noticed that for the SDS campaigns only a few days of measurements exist due to bad weather conditions, so the correlations are statistically not meaningful. Kasai et al. (2005) report slopes of CO-HCN plots between 0.3×10^{-3} and 7.3×10^{-3} for different seasons at Poker Flat, Alaska, which is in good agreement with our results. They found the highest correlations, when biomass burning emissions occur. Zhao et al. (2002) report a slope of 2.02×10^{-3} for northern Japan. Zhao et al. (2002) report a slope for the C_2H_2 versus CO plot for Northern Japan about 2.85×10^{-3} for a correlation coefficient r=0.67, which fits very well with our results. For the C_2H_6 versus CO plot they report a slope of 13.2×10^{-3}, which is nearly twice of our result. The migration of the ITCZ has no effects on the total columns of CO. This could be accounted for by the different sources of CO (e.g. biomass burning and fossil fuel combustion), which are present in both hemispheres. However, HCN total columns showed a slight decrease after the migration of the ITCZ, showing that the HCN source in the northern hemisphere is not as abundant as in the southern hemisphere. Another fact is the non correlation of HCN and CO for the northern hemisphere, which indicates different sources of HCN and CO during this time.

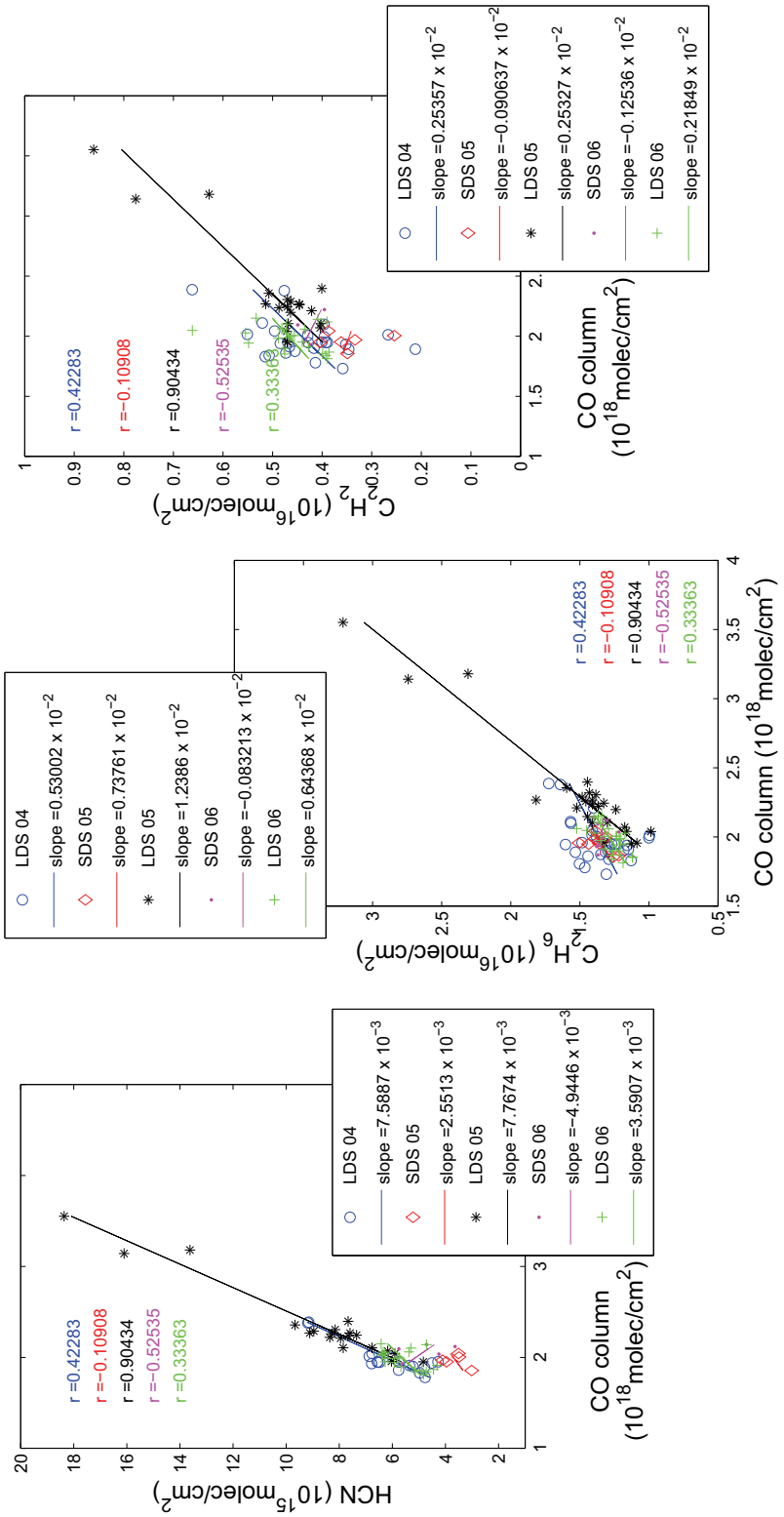

Figure 5.6: Correlations between CO and HCN, C2H2, C2H6

5.5 Model Simulations with Improved Biomass Burning Emissions

Yearly-varying biomass burning emissions have been used with MATCH-MPIC now in a few specific test cases, showing substantial improvements for comparison to observational data sets with biomass burning influences. Very recently, yearly-varying satellite-based emissions have been implemented into the MATCH-MPIC operational forecast and analysis system, used in the previous Section. In this Section, the revised model simulations are discussed and compared with FTIR measurements performed in Suriname. The biomass burning emissions have been changed from monthly varying climatological Galanter emissions, based on a multiannual average over several years (Galanter et al., 2000) to yearly and monthly varying satellite-based biomass burning emissions from the Global Fire Emissions Database (GFED) (van der Werf et al., 2004). The new, satellite-based biomass burning emissions should be more realistic. In the new simulations, the highest CO levels are more concentrated into the biomass burning regions, which can be seen in Figure 5.7, demonstrating the new (top panel) and old (bottom panel) simulations of global surface level carbon monoxide. Shown are the surface level concentrations, which are more closely connected to the emissions. In the new simulation the highest CO concentrations are concentrated in the regions where biomass burning occurs.

In Figure 5.8 the tracer field of South American biomass burning CO can be seen, in the upper panel the new MATCH-MPIC simulations, in the bottom panel the old simulations. In the old simulations, the biomass burning emissions are spread out over the continent, including in Suriname, due to the biomass burning emission scenario based on fire statistics (monthly varying, but based on an average over several years), compared the new runs, where the biomass burning emissions are more realistically concentrated to the central Amazon based on the satellite-based GFED data.

Figure 5.10 shows the CO total columns derived from FTIR and MOPITT measurements and from the previous and the revised MATCH-MPIC model simulations. The revised model runs generally underestimate the measured CO total columns by far (around 25 % or 0.5 molec/cm^2 too low). The panels below show the CO volume mixing ratio profiles from corresponding FTIR measurements and model output for all campaigns. As in Section 5.3, in the third panel of Figure 5.10, the model smoothed by the averaging kernels is shown. As the previous simulations, the model generally reproduces the vertical structure with the peak in the middle to upper troposphere, but is in general to low. This is well illustrated in the mean vertical profiles for each season (see Figure 5.14). The revised model doesn't tend to overestimate the observed mixing ratio profiles in the upper troposphere any more. There is a better agreement in the upper troposphere, while

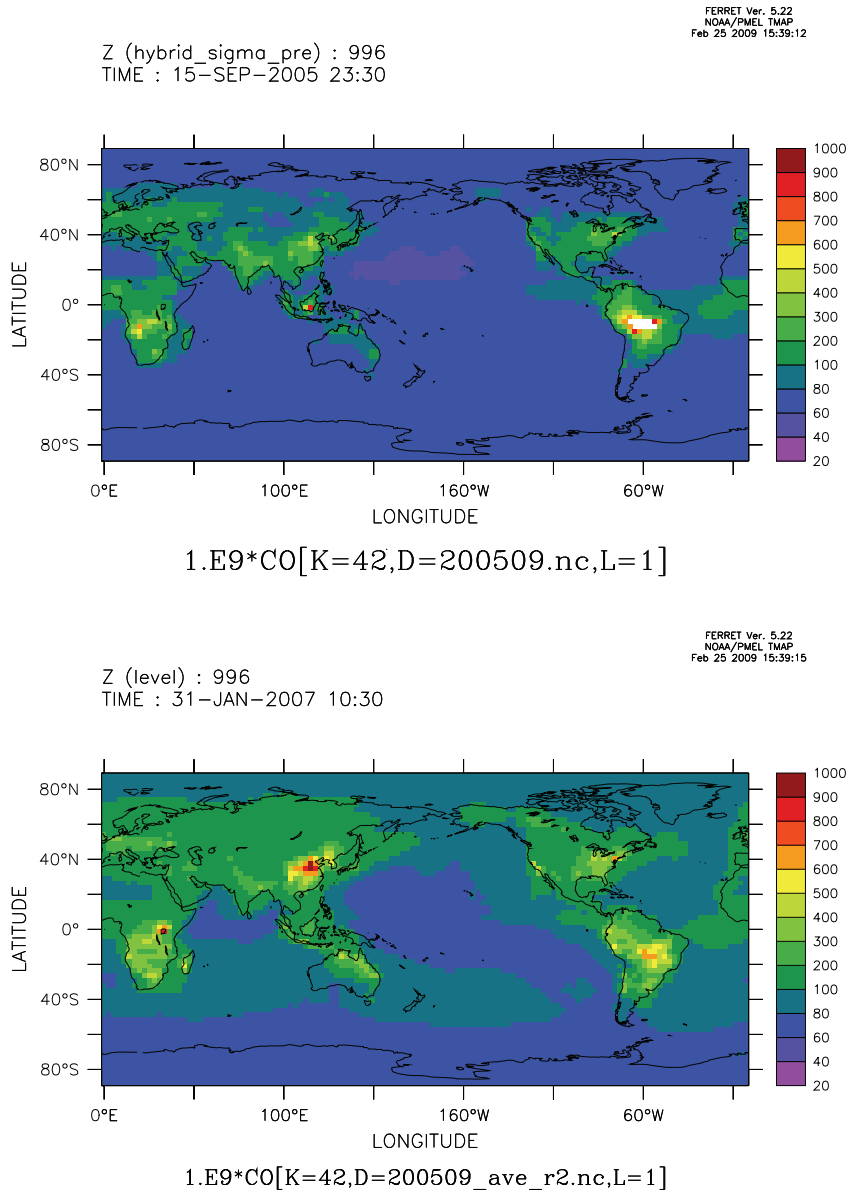

Figure 5.7: Simulated global surface level concentrations of carbon monoxide. The top panel shows the revised MATCH model simulation with GFED satellite-based biomass burning emissions, the bottom panel the old simulations (Galanter climatological BB emissions).
Provided by M. G. Lawrence.

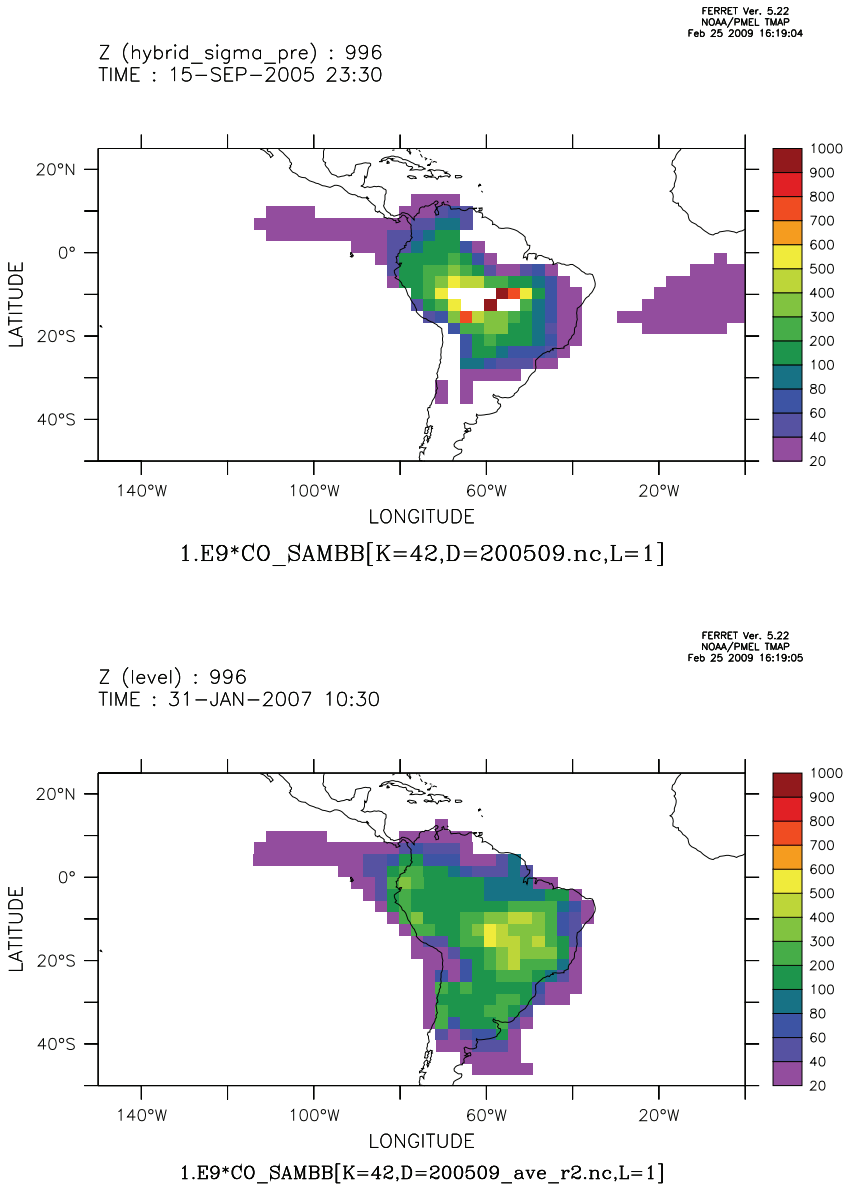

Figure 5.8: Tracer field of the South American biomass burning CO. The top panel shows the the South American biomass burning CO tracer for the new MATCH model simulation with satellite-based biomass burning emissions, the bottom panel this for the old simulations (Galanter climatological BB emissions).
Provided by M. G. Lawrence.

in the boundary layer and lower troposphere the revised model underestimates the FTIR measurements. Since the column is more determined by the denser boundary layer, this results in underestimated total columns as demonstrated in the upper most panel. The revised model still fails to reproduce most of the individual observed pollution events, for example, the two periods with enhanced CO levels due to pollution by South American biomass burning discussed in Section 5.2. Figure 5.13 shows the C_2H_6 total columns derived from FTIR measurements and from the previous and the revised MATCH-MPIC model simulations. As CO, ethane is also underestimated by the revised model. However, the model underestimates the measurements only by around 10 % of the total column (compared to around 25 % for carbon monoxide).

Figure 5.11 shows the contribution of CO tracers from various regions and sources as calculated by the model. As predicted by Figure 5.8, the impact of South American biomass burning CO is reduced over Suriname, especially during the LDS, where the previous (old) simulations revealed that biomass burning in South America is responsible for the variation in the CO concentrations. The African biomass burning is significantly reduced during all measurement periods, resulting in significantly decreased CO concentrations compared to the previous simulations, which were in better agreement with the observations. Furthermore, the reduced biomass burning source effects the NMHC concentrations (as biomass burning is a source of NMHCs), resulting in a decreased CO source from NMHC oxidation compared to the previous model simulations.

Current generation atmospheric chemistry models like the MATCH-MPIC underestimate OH is the tropical region. To compensate for this part, isoprene emissions are set too low in most models. An airborne field measurement campaign, conducted over the Guyanas in October 2005, revealed unexpected high concentrations of the hydroxyl radical (OH) compared to current generation atmospheric chemistry models (Lelieveld et al., 2008). Based on the hypothesis that this missing OH is due to an as-yet undiscovered mechanism for recycling OH during the oxidation chain of isoprene, Butler et al. (2008) determined that an OH recycling of about 40-50 % (compared with 5-10 % in current generation isoprene oxidation mechanisms) is necessary for approaching the observed OH concentrations. Such a large amount of OH in the model leads to unrealistically low mixing ratios of isoprene. In order for the modeled isoprene VMRs to match those observed during the measurement campaign, Butler et al. (2008) reduced the effective rate constant for the reaction of isoprene with OH by about 50 % compared with the lower bound of range recommended by IUPAC (International Union of Pure and Applied Chemistry). They explain this lower effective rate constant by segregation of isoprene and OH in the mixed layer due to unefficient mixing. The modeling results are consistent with a global, annual isoprene source of about 500 $\mathrm{Tg(C)yr^{-1}}$.

This hitherto unknown mechanism might have a great impact on the under-

standing of the distribution of carbon monoxide and ethane in the tropics where high emissions of isoprene from tropical forest occur. Since oxidation by OH is the main sink of these trace gases, changes in the oxidation capacity of the atmosphere have a direct effect on the CO and C_2H_6 concentrations. The CO concentrations are in addition impacted by VOCs like isoprene, being one of the major sources.

Current generation atmospheric chemistry models underestimate OH is the tropical region. To compensate for this part, isoprene emissions are set too low in most models. It is speculated that, if a mechanism like e.g. isoprene recycling would be included in current models, and the isoprene emissions are set realistically, it would result in a powerful CO source in the boundary layer over Suriname from the isoprene oxidation. The CO oxidation rate would also increase due to higher OH concentrations. Because of the complex chemistry and transport processes, it is difficult to predict the exact changes without having done the simulations.

These observations are valuable for evaluating revised emission scenarios and the model resolution and meteorology, to determine which are critical for simulating plumes more accurately in this region. It is planned to compare the observations to high resolution simulations to quantify the impact of model resolution on the simulations. Furthermore, detailed comparison of satellite observations with the revised MATCH-MPIC for source regions of the CO in Suriname (South America and Africa) is planned. This might help to understand the impact of the revised biomass burning emissions and of transport processes for this region. In oder to better understand the complex VOC-OH chemistry, further field campaigns with in situ measurements and more laboratory work is needed.

5.6 Conclusion and Outlook

Measurements and analysis of CO, HCN, C_2H_2 and C_2H_6 were successfully carried out at the tropical site Paramaribo during five consecutive dry seasons. Results of VMR profiles for CO and total columns for CO, HCN, C_2H_2 and C_2H_6 have been presented. The results of CO have been compared with space-borne data from the MOPITT instrument and with output from the MATCH-MPIC model. Two significant distinct enhancements in the total column concentrations of all four trace gases occurred on 18-20 October 2004 and on 27-29 September 2005. They are clearly caused by emissions from fires on the South American continent confirmed by back-trajectory analysis and fire counts from satellite measurements. There is a very good agreement between the FTIR and the MOPITT total columns of CO for all of the measurement campaigns; in particular, the enhancements due to biomass burning events are seen by both instruments. The MATCH-MPIC model has been used to calculate VMR profiles for Paramaribo for the same time periods as the measurement campaigns. The model reproduces the mean vertical structure of the FTIR observations, but is generally not able to reproduce the extreme enhancement seen during the biomass burning events in October, 2004, and September, 2005, as well as enhanced CO levels during the first part of the campaign during the LDS in 2005. The model indicates that methane oxidation provides a large background source of CO, while biomass burning and other sources largely account for the variability in CO. During the spring campaigns CO emissions from biomass burning transported from Africa is important, while biomass burning in South America makes no significant contribution. During the LDS campaigns with the main wind direction from the southeast, biomass burning from the African and South American continents are responsible for variation in the CO concentrations. The revised MATCH-MPIC model with yearly-varying satellite-based biomass burning emissions generally underestimates the observed concentrations of carbon monoxide and ethane. The revised model is in better agreement with the observations in the upper troposphere, while in the boundary layer and lower troposphere the revised model underestimates the FTIR measurements and results in underestimated total columns. Current generation atmospheric chemistry models underestimate OH is the tropical region. To compensate for this part, isoprene emissions are set too low in most models. It is speculated that, if a mechanism like e.g. isoprene recycling would be included in current models, and the isoprene emissions are set realistically, it would result in a powerful CO source in the boundary layer over Suriname from the isoprene oxidation. The CO oxidation rate would also increase due to higher OH concentrations. Because of the complex chemistry and transport processes, it is difficult to predict the exact changes without having done the simulations. The revised model still fails to reproduce most of the individual observed pollution events, for example, the two periods with enhanced CO levels due to pollution by South

American biomass burning.

These observations are valuable for evaluating revised emission scenarios and the model resolution and meteorology, to determine which are critical for simulating plumes more accurately in this region. It is planned to compare the observations to high resolution simulations to quantify the impact of model resolution on the simulations. Furthermore, detailed comparison of satellite observations with the revised MATCH-MPIC for source regions of the CO in Suriname (South America and Africa) is planned. This might help to understand the impact of the revised biomass burning emissions and of transport processes for this region. In oder to better understand the complex VOC-OH chemistry, further field campaigns with in situ measurements and more laboratory work is needed.

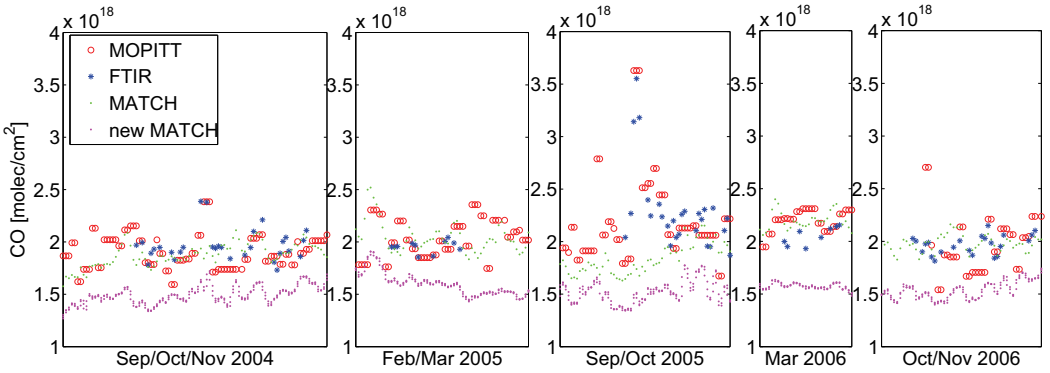

Figure 5.9: CO total columns from the different model runs and from the FTIR and MOPITT measurements for Paramaribo.

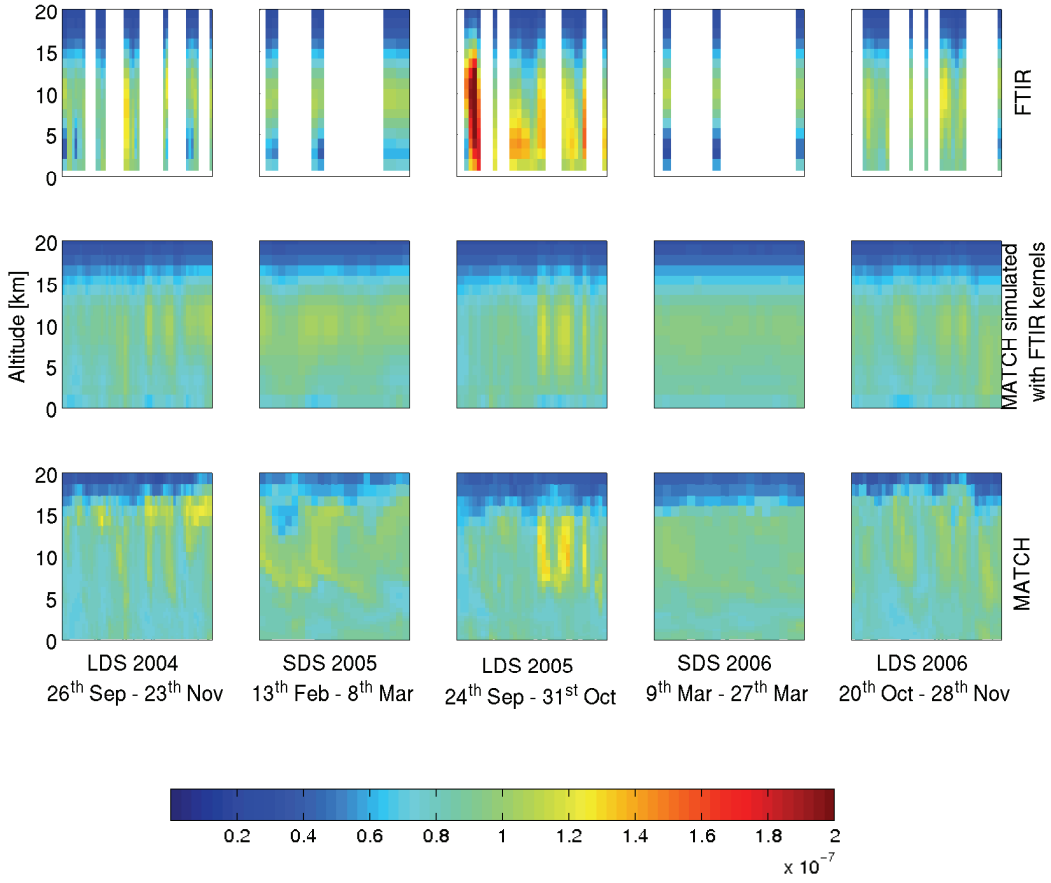

Figure 5.10: CO volume mixing ratio data from the revised MATCH-MPIC (lowest panel) and the FTIR in Paramaribo (first panel) for five consecutive measurement campaigns between September 2004 and November 2006. The time axis is scaled on the time periods of the FTIR measurements. In the middle panel, CO profiles from MATCH smoothed by FTIR averaging kernels are shown.

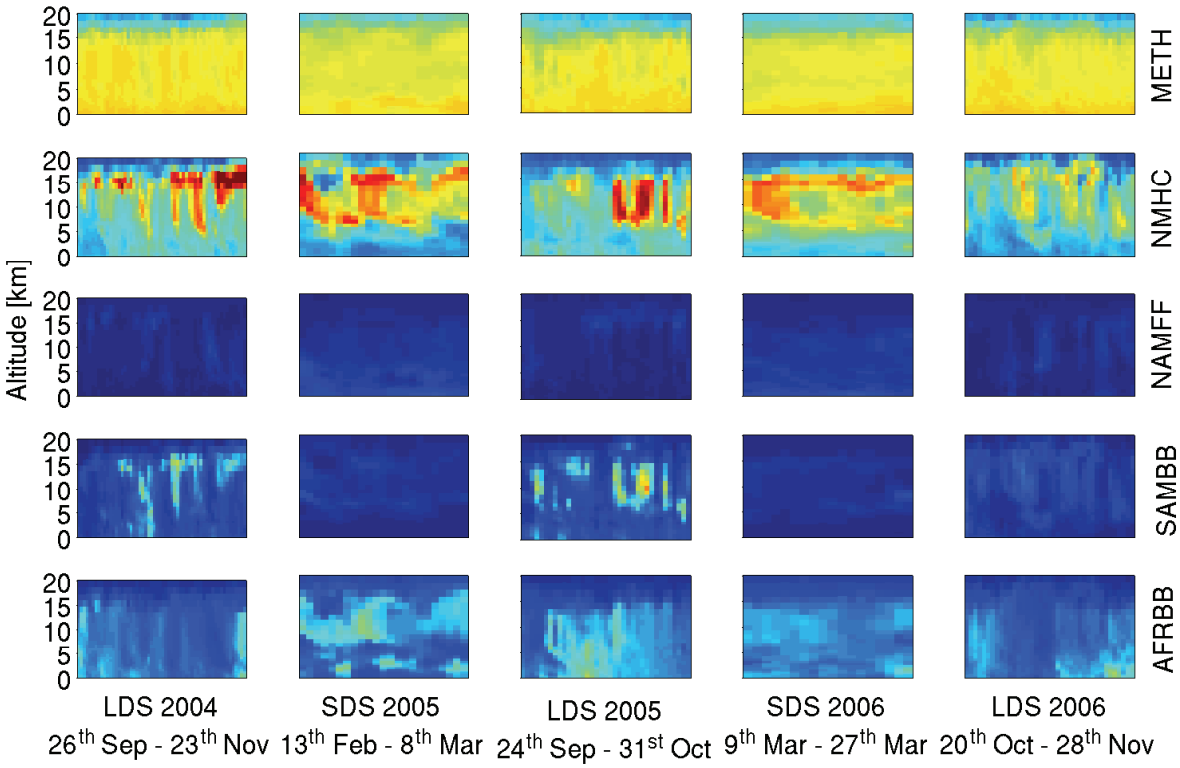

Figure 5.11: Absolute contributions of some regional tracer fields to the CO budget for Paramaribo from the revised MATCH-MPIC (in ppb) for the same time periods as in Figure 5.10. The CO tracer fields are: North American Fossil Fuel (NAMFF), South American Biomass Burning (SAMBB), African Biomass Burning (AFRBB), and methane oxidation (METH). NMHC is the CO source from the chemical oxidation of NMHCs, which originally comes from various sources like biomass or fossil fuel burning, plus the surrogate CO that should result from higher NMHCs, such as monoterpenes, which are not represented explicitly in the model.

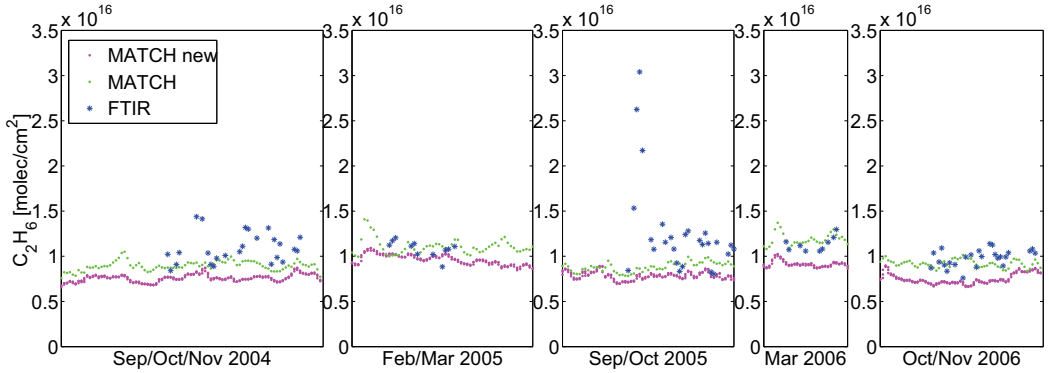

Figure 5.12: C_2H_6 total columns from the different model runs and from the FTIR measurements.

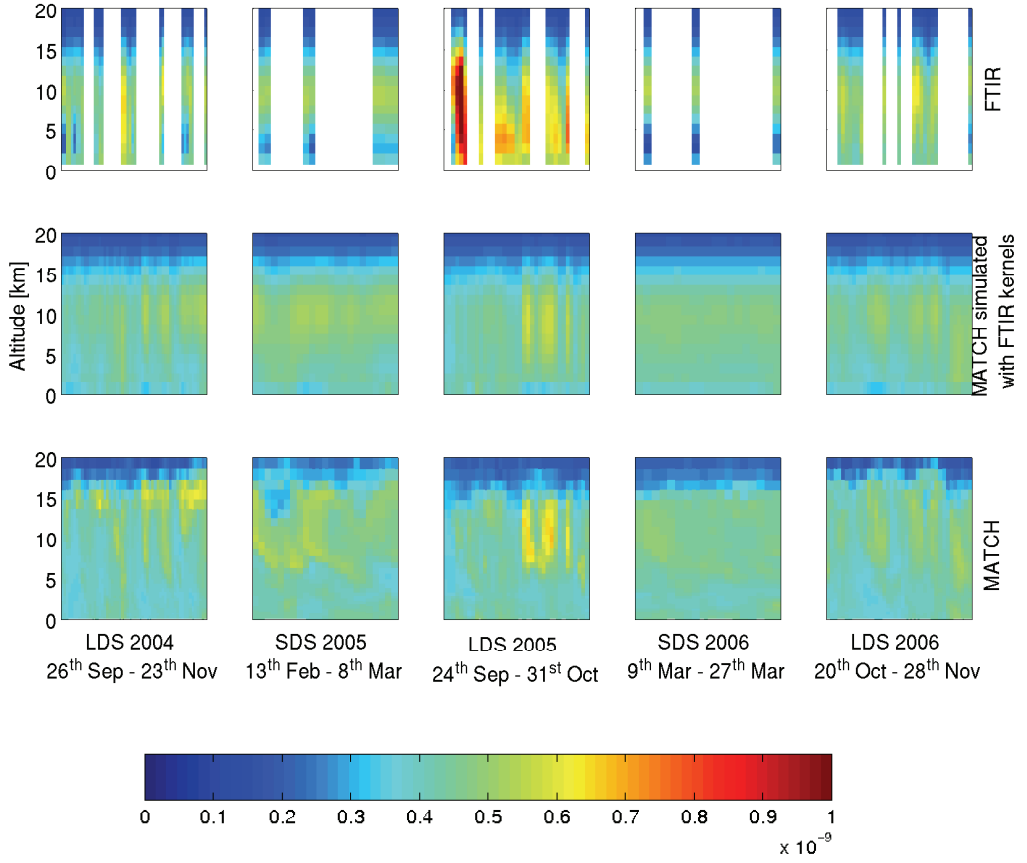

Figure 5.13: C_2H_6 volume mixing ratio data from the revised MATCH-MPIC (lowest row) and the FTIR in Paramaribo (first row) for five consecutive measurement campaigns between September 2004 and November 2006. The time axis is scaled on the time periods of the FTIR measurements. In the middle panel, C_2H_6 profiles from MATCH smoothed by FTIR averaging kernels are shown.

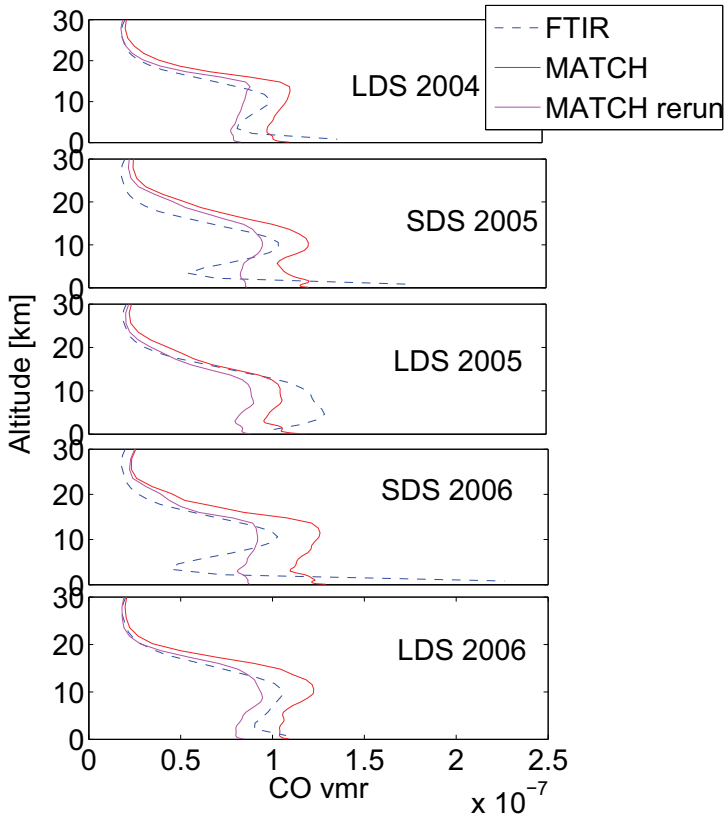

Figure 5.14: Mean CO volume mixing ratio profiles from the old MATCH-MPIC (red line), the new MATCH-MPIC simulations (magenta line) and the FTIR (blue dashed line) in Paramaribo for five consecutive measurement campaigns between September 2004 and November 2006.

Part III

Flux Measurements

6 Micrometeorological Flux Measurements

The exchange of trace gases between the biosphere and the atmosphere affects the atmospheric concentrations of gases such as methane, carbon dioxide, carbon monoxide, ammonia, volatile organic compounds, nitrogen dioxide and others. The quantification of the exchange between a biogenic system and the atmosphere is necessary for the evaluation of the impact of these interactions. This is of special interest for agricultural systems which can be sources or sinks of trace gases, and the measurement of the fluxes is necessary when evaluating both the environmental impact of agricultural activities and the impact of atmospheric pollution on agricultural production and sustainability.

The flow and mixing of trace gases by turbulence in the surface layer results in rapidly varying trace gas concentrations in time and small concentration gradients with height. Difficulties in micrometeorological flux measurements of trace gases arise due to slow time response sensors/instruments and need for detection of small concentration differences or fluctuations against a large background concentration.

In general, there are two different types of flux measurements, those which interfere with the transport process and those that minimise the interference of transport processes. Flux measurements can be made by enclosure, micrometeorological and tracer techniques. Enclosure or chamber methods are often used because they are simple and have a lower sensitivity requirement for measuring gas concentrations. However, they interfere highly with the exchange process by changing the radiation, energy balance, evaporation rate, temperature, wind speed, dew formation and others. For tracer methods, stable isotopes (e.g. ^{15}N for the measurement of NH_3 loss) or tracer gases are used to study exchange processes. One major problem are high biases compared to other flux measurement methods.

Micrometeorological flux measurements are noninterference methods because they do not disturb the soil, plant, water system or environmental processes that may influence the exchange processes. There are several different micrometeorological methods, they will be presented in the following section.

6.1 Micrometeorological Methods

Different techniques have been invented to measure surface fluxes of trace gases and volatile organic compounds. The most direct methods without perturbing the nature of the surface are the micrometeorological techniques: the eddy covariance, the flux gradient, the conditional sampling or eddy accumulation and the relaxed eddy accumulation technique.

6.1.1 Eddy Covariance Method

The eddy covariance (EC) method provides a direct measure of the vertical turbulent flux across the mean horizontal streamlines. Fast response sensors for the wind vector and the scalar entity of interest (temperature, concentration of water vapour or gas) are needed. The vertical turbulent flux is the covariance of a time series of the vertical wind velocity and the value of a scalar entity over some time period. The averaging interval should be long enough to capture all flux contributing eddy motions (30 to 60 min periods) (Lenschow et al., 1993; Foken, 2006).

The general equation for the eddy covariance flux is given by Eq. (6.1). The instantaneous values of s (the entity of unit mass) and w (vertical wind velocity) can be written as the sum of the mean values $\overline{s}$ or $\overline{w}$ and the corresponding deviations from the mean s' and w':

$$F = \overline{\rho w s} = \overline{(\rho\overline{w} + \rho w')(\overline{s} + s')} = \overline{\rho w' s'} \tag{6.1}$$

where ρ denotes the density, w the the mean velocity in z direction and s the entity per unit mass of air.

$\overline{s'}$ and $\overline{w'}$ are zero by definition and $\overline{w}$ is assumed to be zero near the ground when the averaging period is long enough compared to the lifetime of the largest eddy. This relation provides the eddy covariance method of measuring vertical fluxes.

When fluxes of an atmospheric constituent are measured it is sometimes necessary to take into account the simultaneous fluxes of heat and water vapour (Webb et al., 1980). Water vapour or heat fluxes affect the density of the constituents in air. Correction is not necessary if the flux is evaluated from measurements of the dry air mixing ratio of the constituent (mass of constituent per unit mass of dry air) at constant temperature.

The measurement of fluxes with the EC method requires fast response vertical wind velocity and trace gas sensors (Businger and Delany, 1990). The necessary response time of the sensors depends on the range of eddy sizes that carry the flux. Eddy sizes grow with height over the surface and increase with increasing surface roughness and wind speed. In general, sensors with a frequency of 10-20 Hz are required (Foken, 2006).

6.1.2 Flux Gradient Method

The flux gradient (FG) method relies on the existence of relation between flux and gradient. It is based on Fick's first law, which relates the diffusive flux to the concentration field, by postulating that the flux goes from regions of high concentration to regions of low concentration, with a magnitude that is proportional to the concentration gradient (spatial derivative). In one (spatial) dimension the diffusion flux F is given by

$$F = -D\frac{\partial C}{\partial x} \tag{6.2}$$

where D is the diffusion coefficient, C the concentration and x the position (e.g. height). The flux gradient method allows an estimation of the flux F from mean concentration gradients in the vertical direction z in a relatively simple manner:

$$F = \frac{u_* k}{\Phi(z/L)}\frac{\partial C}{\partial \ln z} \tag{6.3}$$

where u_* denotes the friction velocity (which can be derived in the experiment from the momentum flux, calculated from the correlation between the horizontal and vertical velocities u and w respectively), $k = 0.4$ is the von Karman constant, $\partial C/\partial \ln z$ is the change of concentration C with the logarithm of height z, and $\Phi(z/L)$ is the Monin-Obukhov stability function. The stability function account for the effect of atmospheric stability on the scalar concentration profiles (Paulson, 1970; Kaimal and Finningan, 1994). The Monin-Obukhov stability length scale L is given by $L = -\rho c_p u_*^3 \bar{T}/(kg\bar{H})$, in which g is the acceleration due to gravity, $\bar{T}$ the mean air temperature, $\bar{H}$ the sensible heat flux, ρ the density of air and c_p the specific heat of air at constant pressure.

6.1.3 Eddy Accumulation Method

The eddy accumulation method was first proposed by Desjardin (1972). Hicks and McMillen (1984) verified the suitability of this method for the measurement of pollutant fluxes. It is commonly used for flux measurements of atmospheric trace gases (e.g. Beverland, 1994; Pattey et al., 1993; Nie et al., 1995). This technique overcomes the need for fast-response gas sensors. It relies on the conditional sampling of air into two reservoirs at a flow rate proportional to the vertical wind velocity; the entity of interest is measured later, after a statistically meaningful sample has been obtained. The vertical velocity w is used to determine the conditional sampling by opening a valve to a reservoir when the vertical velocity w is positive and another valve to another reservoir when w is negative. These valves are adjusted so that the amount of air sampled is proportional to the magnitude of w. After a sufficiently long sampling period, the positive and negative reservoirs

contain air samples which are proportional to $\overline{w^+c}$ and $\overline{w^-c}$. Adding these two quantities gives the flux:

$$\begin{aligned}\overline{w^+c} + \overline{w^-c} &= (\overline{w^+} + \overline{w^-})\bar{c} + \overline{w^+c'} + \overline{w^-c'} \\ &= \overline{w^+c'} + \overline{w^-c'} \\ &= \overline{w'c'} = F \end{aligned} \tag{6.4}$$

since $\overline{w^+} + \overline{w^-} = \overline{w} = 0$. The eddy flux has to be corrected for fluctuations in c due to fluctuations in water vapour concentrations and temperature, when latent heat or sensible heat fluxes are non-zero (Webb et al., 1980). These corrections are not necessary when mean dry air mixing ratios are used to calculate the eddy flux.

Since both $\overline{w^+c}$ and $\overline{w^-c}$ are much larger in magnitude than the flux itself, they have to be measured with great accuracy.

6.1.4 Relaxed Eddy Accumulation Method

The operation of valves to assure a sampling proportional to the wind velocity is technically very difficult. Businger and Oncley (1990) suggested a conditional sampling which is easier to implement under field conditions: the relaxed eddy accumulation (REA) method. The flow rate through the sample valves is constant, which is technically easier and more accurate. High frequency is required only for the anemometer. The conditional sampling is only determined by positive or negative velocity. The measurements are simply the average concentration for the reservoir with $w > 0$, $\overline{c^+}$ and for the reservoir with $w < 0$, $\overline{c^-}$. The flux is obtained by assuming:

$$\overline{w'c'} = \beta\sigma_w(\overline{c^+} - \overline{c^-}) \tag{6.5}$$

where σ_w is the standard deviation of the vertical wind speed, β is a coefficient for the correlation between the vertical wind speed and the gas mixing ratio and which has to be determined.

Since this method is based on the eddy covariance method, it needs to operate fast enough to sample all flux carrying eddies, ideally requiring a vertical wind sensor and sampling valve assembly with a time response of at least 0.1 s. The fast responding gas sensor is eliminated by accumulation process which permits high precision determination of the mixing ratio differences off-line in the field or lab.

To derive the flux of a scalar with REA technique, the coefficient β has to be determined. This can be done by either (1) using the theoretically derived value of 0.627 (Baker et al., 1992; Wyngaard and Moeng, 1992), (2) calculating β_w from the vertical wind data (Pattey et al., 1993; Oncley et al., 1993) or from

high frequency temperature or humidity measurements (Oncley et al., 1993), or (3) using a published empirical derived value for similar stability and surface conditions (e.g. Nie et al., 1995; Pattey et al., 1993; Ammann and Meixner, 2002).

7 Combined FTIR-Micrometeorological Technique for Continuous Flux Measurements

With the exception of CO_2, micrometeorological measurements of the fluxes of greenhouse gases are still mostly possible only in campaign mode due to the complexity and logistical requirements of the existing techniques. This limitation precludes studies of fluxes which run for longer periods, for example over full seasonal or growing cycles for both animal- and crop-based agriculture.

Together with the Centre for Atmospheric Chemistry, University of Wollongong, Australia and the National Institute for Water and Atmospheric Research (NIWA), Wellington, New Zealand, we have developed an instrument system for long-term flux measurements through a combination of micrometeorological flux measurement techniques (relaxed eddy accumulation (REA) and flux gradient (FG)) with FTIR spectroscopy. The combined technique is potentially capable of simultaneous flux measurements of N_2O, CH_4 and CO_2 at paddock to regional scales continuously, over longer terms (months, seasonal cycles, years). It is described in Section 7.1. The system was tested on a 3 week field campaign. The flux of the atmospheric CO_2 was measured by relaxed eddy accumulation, flux gradient, and eddy covariance. We used a conventional LICOR 7500 for the measurement of CO_2 eddy covariance fluxes.
Simultaneously, fluxes of CH_4 and N_2O were measured by REA and FG technique. Results are presented in Section 7.2.

7.1 Development of a Combined Technique for Continuous Long-Term Flux Measurements

The technique of relaxed eddy accumulation relies on conditional sampling. The conditional sampling is only determined by positive or negative vertical wind velocity, air is sampled at a constant flow rate. This technique overcomes the need for fast-response gas sensors. The entity of interest is measured later offline, after a statistically meaningful sample has been obtained.

The combination of the REA flux measurement technique with the high preci-

sion multi-species analysis capabilities of FTIR spectroscopy offers the capacity to measure a range of gases simultaneously under field conditions and makes this flux measurement technique suitable for long-term implementation with minimal routine maintenance and operator intervention.

The combined technique consists of a REA system for the conditional sampling, a lung system to store the air samples and to maintain continuous measurements, and a cell-based FTIR spectrometer for the simultaneous analysis of gases including methane, carbon dioxide, nitrous oxide, carbon monoxide and others. These different components are described in the following.

7.1.1 REA System

The REA sampling system was developed at the National Institute of Water and Atmospheric Research (NIWA), New Zealand. Air from upward and downward moving eddies is sampled into separate gas lines leading to the lung-system using two fast switching solenoid valves (ETO-3 12VDC, Clippard Instrument Laboratory) and pumps to maintain a constant air flow. The inlet valves have to be installed in close proximity to the sensing path of the sonic anemometer to achieve maximal correlation between the vertical wind velocity and the concentration of the scalar entity. The digital output of the sonic anemometer is used as input to a portable PC. REA-Software, developed at NIWA in QBasic, drives the switching of the valves, depending on the direction of the vertical wind. Both the sonic anemometer and the valve switching are operated at 20 Hz. The software calculates averages for the vertical wind speed, the standard deviation of the vertical wind speed (σ_ω), the eddy covariance heat flux (H_{EC}), and the empirical REA parameter β for the REA averaging period (for our experimental setup: 30 min) from the 20 Hz data of the sonic anemometer wind speed and temperature. The empirical REA parameter β is calculated from the eddy covariance heat flux H_{EC} and the sonic anemometer temperature and wind speed by following equation:

$$\beta = \frac{H_{EC}}{\sigma_\omega(\overline{T^+} - \overline{T^-})} \tag{7.1}$$

The sonic data (including data from a conventional LICOR 7500) are also stored by the data logger at 20 Hz and for 15 min average periods. For our experimental setup the sonic anemometer and the inlet for the REA analyser and the LICOR 7500 were installed at a height of 2.5 m above ground.

7.1.2 Lung System

To maintain continuous air sampling and analysis, we developed and constructed a lung system. The lung consists of two pairs of sampling reservoirs; one pair

is composed of one up- and one down-reservoir. While one pair of reservoirs is being filled during one averaging period, the other pair, filled during the previous period, is being analysed by the FTIR spectrometer (see Figure 7.1). After the analysis, the analysed pair is evacuated before it gets filled in the next averaging period, while the previously filled pair is then analysed. Details can be found in the following.

The systems consists of three three-way solenoid valves (Bürkert No. 6014) for each inlet line to sample the air into reservoir bags and two two-way solenoid valves (Bürkert No. 6013) for the evacuation of the reservoir bags of each sample line (see Figure 7.2). 5 L Barrier Bag-Water (Scholle Industries, Product Code 800342) were used for sampling bags. For the duration of one averaging period, air is sampled into reservoir bags A-up and A-down; after this period, the valves are switched to sample the air in reservoir bags B-up and B-down, while the reservoir bags A-up and A-down are analysed one after the other by the FTIR analyser, and the residual sample is then evacuated. Figure 7.2 shows the schematic diagram of the REA-lung-FTIR system, the real manifold is shown in Figure 7.3. Details for the different steps of the measurement cycle are shown in the Appendix C.

For our experimental setup, the averaging period was 30 min. Since the analysis of one pair of bags did not require the whole filling time and in order to have another comparison to the REA flux measurements, the lung system was constructed to enable FG measurements. During the last 15 min of the 30 min averaging period, the valves No. 3 (one for the updraft-line, one for the downdraft-line, see Figure 7.2) of the lung system opened to inlet lines at $z_1 = 0.5$ m and at $z_2 = 1.5$ m respectively, installed at the met-station. The FG air samples were analysed instantaneously (no buffer-volume), the delay between z_1 and z_2 was 7.5 min. The analysis of the two samples was finished within 15 min. Table 7.1 shows the cycle for an averaging period of 30 min for the combined REA and FG measurements.

Time [min]	Bag A up	Bag A down	Bag B up	Bag B down	FG z_1	FG z_2
0 - 7.5	Analysis	–	Filling	Filling	–	–
7.5 - 15	–	Analysis	Filling	Filling	–	–
15 - 22.5	Evacuation	Evacuation	Filling	Filling	Analysis	–
22.5 - 30	Evacuation	Evacuation	Filling	Filling	–	Analysis
30 - 37.5	Filling	Filling	Analysis	–	–	–
37.5 - 45	Filling	Filling	–	Analysis	–	–
45 - 52.5	Filling	Filling	Evacuation	Evacuation	Analysis	–
52.5 - 60	Filling	Filling	Evacuation	Evacuation	–	Analysis

Table 7.1: Measurement cycle (for a 30 min averaging period) for combined REA and FG measurements

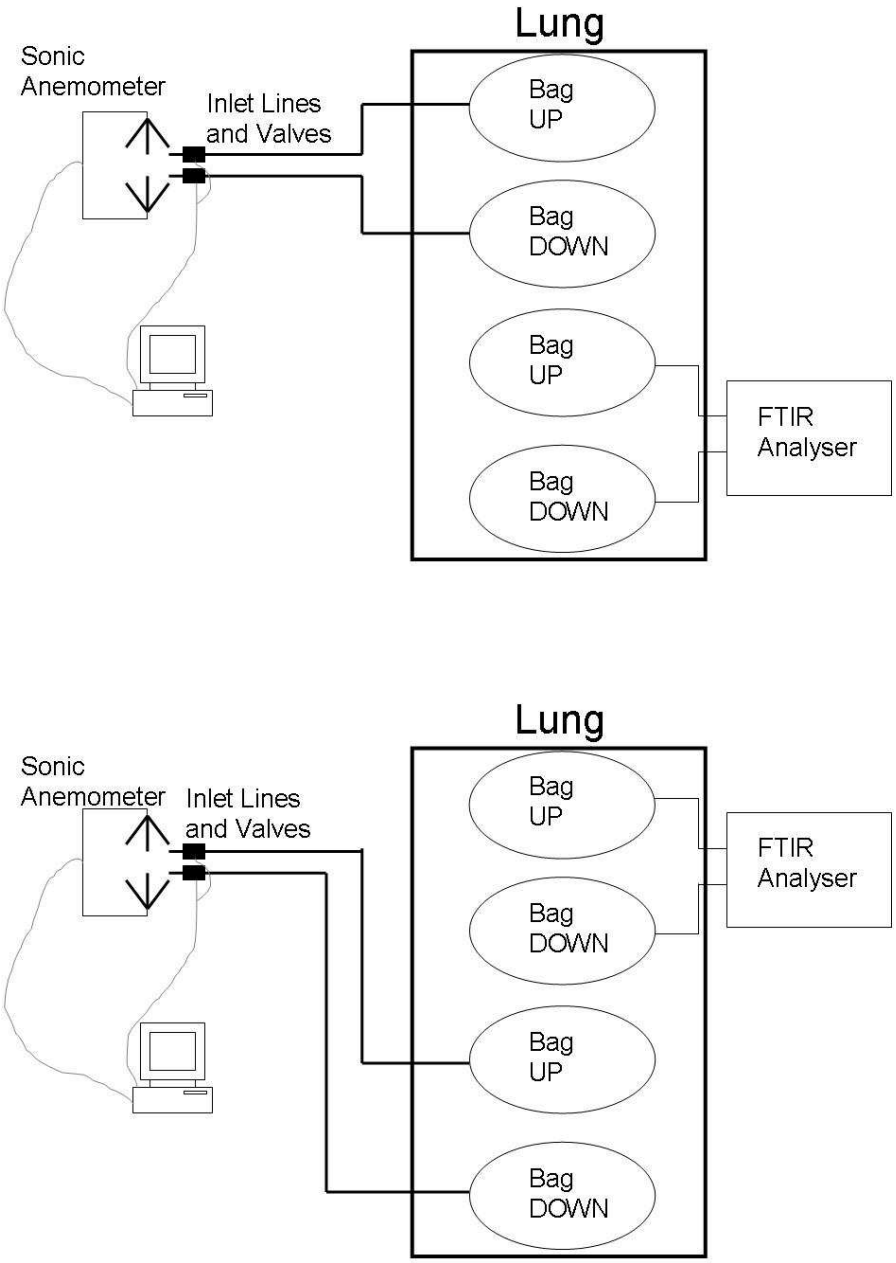

Figure 7.1: The principle of the REA-lung-FTIR system: One pair of bags is being filled, while the other pair is being analysed by the FTIR spectrometer. After one averaging period, the full bags are being analysed, the other pair is being filled. After each analysis the bags are evacuated.

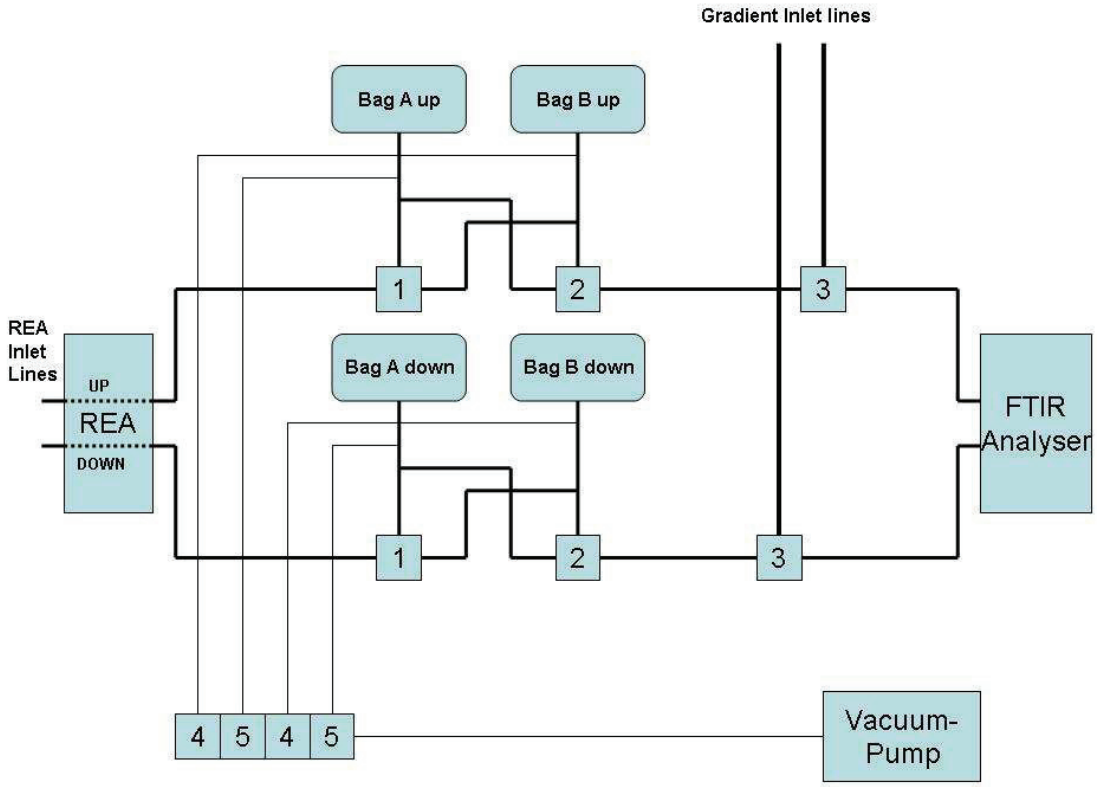

Figure 7.2: Schematic design of the REA-lung-FTIR system.

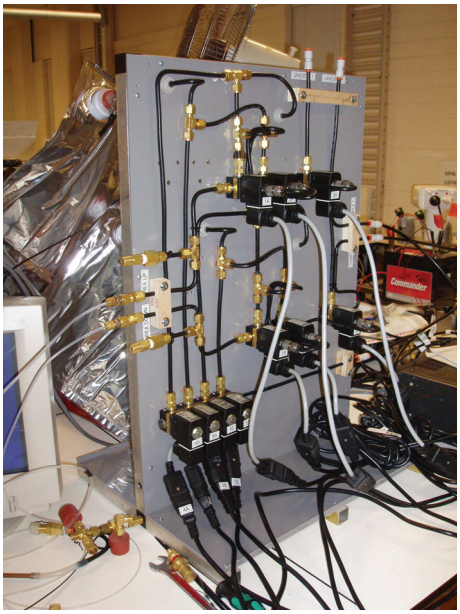

Figure 7.3: Picture of the manifold of the REA-lung-FTIR system.

7.1.3 FTIR Analyser

The air samples in the reservoir bags were analysed with a cell-based FTIR spectrometer. The FTIR spectra were recorded from 1500 to 7800 cm^{-1} at 1 cm^{-1} resolution with a Bruker Matrix-M IRCube FTIR spectrometer with a thermoelectrically cooled MCT detector and a 20 m multi-pass White cell (volume $\sim$ 2 L, Infrared Analysis) to enhance the IR absorption. The spectrometer and cell were thermostated to 25°C to ensure stability and avoid temperature-dependent calibration fluctuations. The IR beam path through the spectrometer and outside the sample cell was purged with nitrogen to remove interference from CO_2 and water vapour. The sampled air has been dried by flowing through a nafion dryer and magnesium perchlorate, before it is filled in the cell for analysis. The spectrometer and sampling system operated continuously and automatically. The analysis of one reservoir bag took 7.5 min (4.5 min for collecting spectra and 3 min for flushing and filling of the cell), so one pair of bags was analysed in 15 min. After the analysis the bags were evacuated. For the analysis of each reservoir, 541 spectra at 1 cm^{-1} were averaged. A signal to noise ratio greater than 8000 was achieved. Spectra were analysed by a non-linear least squares fitting technique, in which the measured FTIR spectrum is fitted with an iteratively-calculated spectrum until a least squares best fit is obtained (Griffith, 2006, 1996). In the spectral region 1500 to 7800 cm^{-1}, CO_2, CO and N_2O were fitted from 2150 to 2320 cm^{-1}, CH_4 and H_2O from 3001 to 3150 cm^{-1},and CO_2 and H_2O from 3520 to 3775 cm^{-1}. CO_2_1 and CO_2_2 are the main isotopologues of CO_2 ($^{12}CO_2$ and $^{13}CO_2$) scaled by the

natural abundances. δ^{13}C is calculated from CO_2_1 and CO_2_2 by $\delta^{13}C = (CO_2\_2 / CO_2\_1 - 1)*1000$.

The least squares fitting procedure used for quantitative spectrum analysis is based on tabulated spectral data (HITRAN 2004) and requires no calibration gases. For more accurate absolute calibration, measurements can be compared to independently calibrated reference gases.

To avoid biases between the two inlet lines, the whole set up was constructed highly symmetrically. The system was tested for biases by opening both REA switching valves for a period of 1 hour (4×15 min periods) in order to sample the same air in both bags. The variation of the bag differences relative to the mean concentrations of the bags was around 0.01 % for CO_2 and below 0.1 % for N_2O and CH_4. Another test for biases was the switch between the inlet lines to the lung-system. For 17 hours during our field campaign the line updraft was sampled in the bags connected with the sample inlet 2 of the FTIR analyser, and the line downdraft was sampled in the bags connected with the sample inlet 1. No bias was observed for these flux measurements.

7.2 Initial Investigation of the Combined Technique in the Field

The flux of atmospheric CO_2 was measured with three different micrometeorological techniques: relaxed eddy accumulation (REA), flux gradient (FG), and eddy covariance (EC). Since both the REA and the FG techniques used an FTIR spectrometer to analyse the air samples, CH_4, N_2O, CO, H_2O and δ^{13}C were also measured at the same time. The flux measurements were made near Nowra, in NSW Australia at 34.82°S, 150.67°E, elevation 1 m asl on a flat, homogeneous circular grass paddock (diameter 1 km) periodically spray irrigated by a circular pivot irrigator. During the entire measurement period, approximately 200 cows were present on the paddock. Relaxed eddy accumulation (REA) flux and flux gradient (FG) measurements were carried out continuously from 18:00 on 28th August 2008 until 05:30 on 18th September 2008 (all times Australian Eastern Standard Time, UT+10). In parallel to the FTIR measurements, a LICOR 7500 open path CO_2 analyser was used for conventional CO_2 eddy covariance flux measurements.

7.2.1 Experimental Setup

The combined system of REA and lung system and FTIR analyser was installed in a caravan in the middle of a flat, homogeneous circular grass paddock (diameter 1 km) (see Figure 7.4). A CSAT3 Campbell Scientific weather station was set up

including a sonic anemometer and a LICOR 7500. The inlet lines for the REA were installed at 15 cm distance to the sensing path of the sonic anemometer to assure the correlation between the sampled eddies and the wind direction (see Figure 7.5). The sonic anemometer and the inlet for the REA analyser and the LICOR 7500 were installed at a height of 2.5 m above the ground.

The inlet lines for the FG measurements were located at the weather station at heights $z_1 = 0.5$ m and $z_2 = 1.5$ m. The averaging interval for the REA was 30 min to capture all flux contributing eddy motions. Both the sonic anemometer and the REA switching valves were operated at 20 Hz. The software calculated averages for the vertical wind speed, the standard deviation of the vertical wind speed, the REA heat flux and the Eddy covariance heat flux for the REA averaging period (30 min) from the 20 Hz data of the sonic anemometer. The empirical REA parameter β has been calculated from the heat flow by both Eddy covariance and REA methods following Eq. (7.1). During the field campaign, the measurement setup operated automatically. Every five days, the tank of N_2 for flushing the spectrometer had to be changed manually. The data download and the supervision of the whole setup was done via remote desktop (internet connection, modem + mobile simcard). Calibration measurements were performed daily with a standard tank of air calibrated by CSIRO Gas lab against standards traceable to the WMO scale. The calibration drifts for CO_2, N_2O and CH_4 over the 3 week duration of the campaign were around 0.1 %. Calibration drifts and factors are listed in table 7.2.

7.3 Results

7.3.1 CO_2 Flux

CO_2 is the most important anthropogenic greenhouse gas. However, the contribution from various sources and especially sinks is uncertain due to the lack of accurate field measurements of gas exchange. Such information is needed to develop process-based models and to obtain regional and global flux estimates (Andreae and Schimel, 1989).
Figure 7.6 shows the flux of CO_2 obtained with the REA technique and from the LICOR EC technique for the measurement campaign near Nowra, NSW. The CO_2 flux shows a clear daily cycle over the whole measurement period with a build up of CO_2 during nighttime and CO_2 uptake (negative fluxes) during day time. As can be seen in Fig. 7.7, the CO_2 flux obtained with the REA technique is well correlated with the LICOR EC measurements ($R = 0.6$). Since the EC LICOR data were averaged over periods of 15 min, while the REA fluxes are an average over 30 min periods, the mean of two LICOR data points is used for the comparison with the REA measurements. During days with a lot of rain, the CSAT did not

Figure 7.4: Picture of the measurement setup during the field campaign

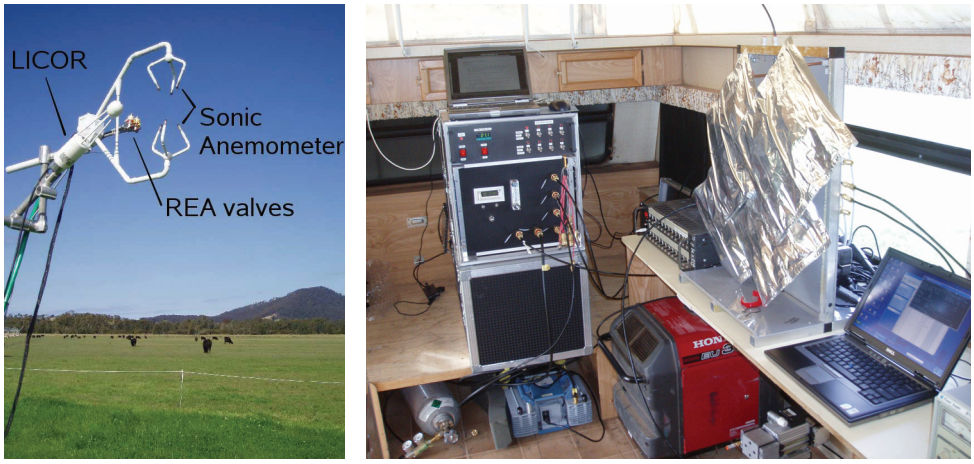

Figure 7.5: Pictures of the sonic anemometer, the LICOR 7500 and the REA inlet valves (left) and the REA-lung-FTIR system inside the caravan (right) during the field campaign.

	CO_2_2 [ppmv]	N_2O [ppbv]	CO [ppbv]	CH_4 [ppbv]	CO_2 [ppmv]	CO_2_1 [ppmv]
Calibration tank	376.2	319.9	60.8	1709.8	376.2	376.2
CalFac	1.0553	0.9956	1.2166	1.0344	1.0308	1.0110
StDev	0.08%	0.09%	1.19%	0.04%	0.10%	0.11%

Table 7.2: Calibration measurements for the three weeks field campaign. The first column ('Calibration tank') gives the absolute calibrated values for the gas concentrations in the calibration tank. The second column ('CalFac') gives the calibration factor for the measured concentrations for each gas, derived from daily analysis of the calibration gas tank during the whole campaign at Nowra. The third column ('StDev') shows the standard deviations for the daily calibration measurements during the whole test campaign, and gives an idea about the stability of the measurements. The data was checked for drifts in the calibration. It is possible to correct for drifts by using daily calibration factors. During this test campaign, the calibration measurements have been very stable, this is indicated in the low standard deviations.

work reliably, these data are removed. Only measurements at wind speed greater than $1\,\mathrm{m\,s^{-1}}$ are taken into account. The REA data are filtered for unrealistic values of β (only $0.3 < \beta < 0.8$ are taken into account).

Figure 7.8 shows the flux of CO_2 obtained with the FG as well as with the REA technique. The flux of CO_2 obtained with the FG technique is well correlated with the REA measurements (R = 0.58, see Figure 7.9). The FG data is filtered for $0.1 < u^* < 0.4$. The FG CO_2 fluxes show high variation compared to those obtained with the REA technique. It must be taken into account that the FG measurements are instantaneous measurements obtained by using the differences between two concentration measurements which are 7.5 min apart from each other, since our experimental setup does not contain a buffer volume. The REA fluxes are mean fluxes over 30 min periods. For this setup, the REA technique compares better with the EC LICOR measurements than the FG technique for measuring CO_2 fluxes.

7.3.2 N_2O Flux

The global atmospheric N_2O concentration increased from a pre-industrial value of about 270 ppb to 319 ppb in 2005, primarily due to agriculture, driven by increased use of nitrogen fertilizers and higher livestock numbers (IPCC: Forster et al. (2007)). Due to the high input of nitrogen into the soil from animal excreta and nitrogen fertilizer, irrigated, grazed pastures are expected to be a major source of N_2O emissions (IPCC: Forster et al. (2007), Phillips et al. (2007)).

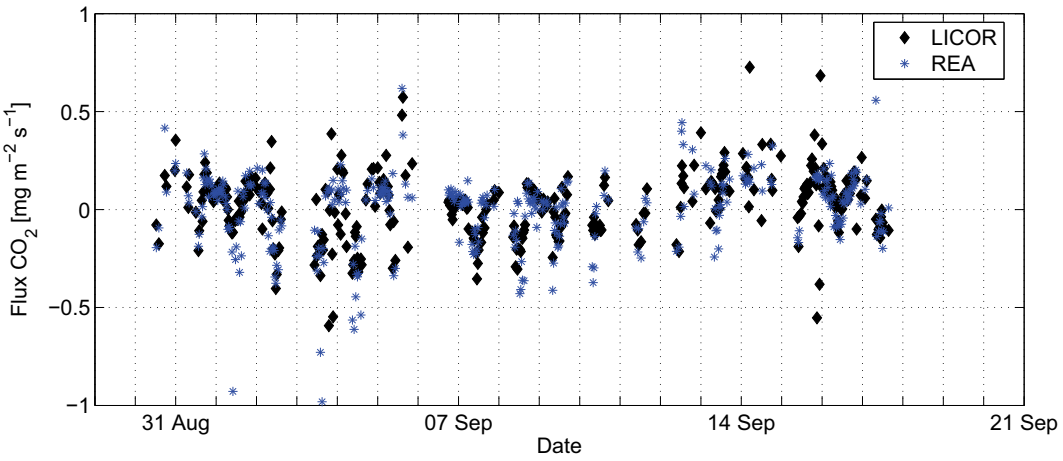

Figure 7.6: Flux of CO_2 measured with the REA and EC method

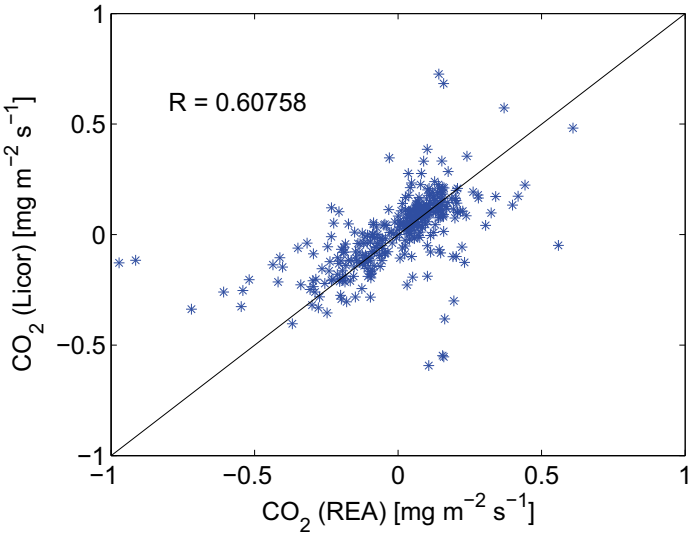

Figure 7.7: Correlation of the CO_2 flux measured with the REA and EC method

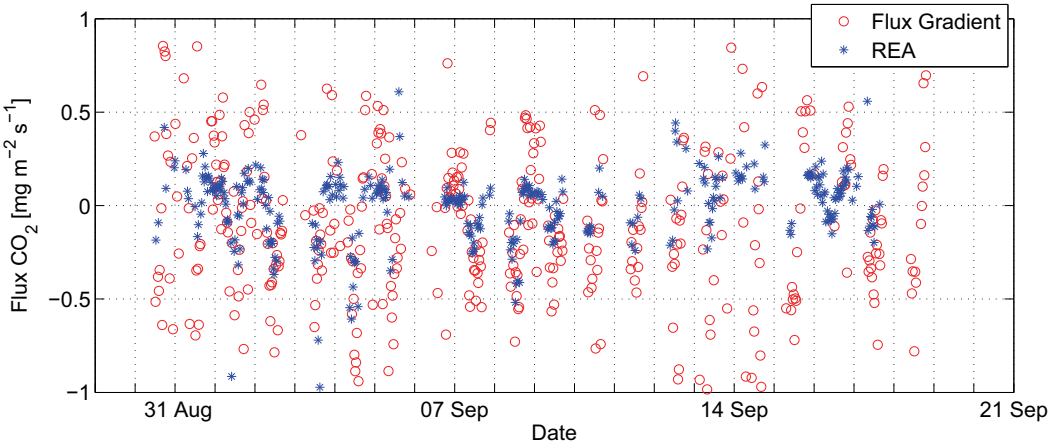

Figure 7.8: Flux of CO_2 measured with the REA and flux gradient method

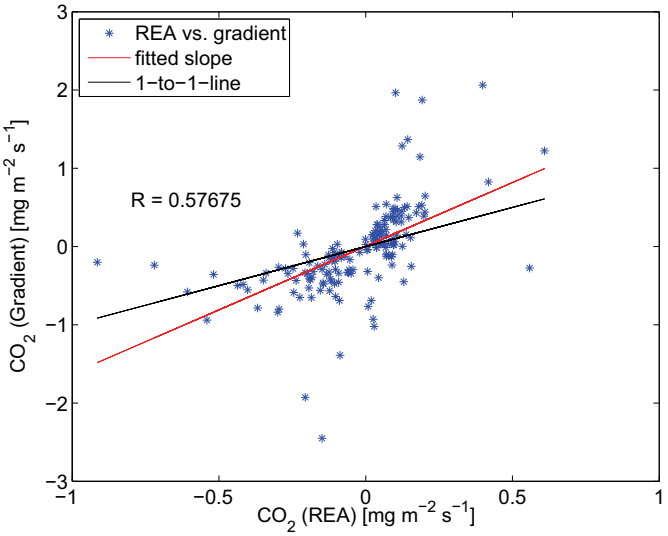

Figure 7.9: Correlation of the CO_2 flux measured with the REA and flux gradient method

Figure 7.10 shows the N_2O flux for the measurement campaign at Nowra using both the REA and the FG technique. The mean of the N_2O fluxes for the whole measurement period was close to zero with a standard deviation of $\sim 20\,\mathrm{ng\,m^{-2}\,s^{-1}}$. From the 13th September to the end of the campaign the N_2O fluxes are increasing and show a higher variation. The reason for this might be the warming of the soil after some rainy days, resulting in higher N_2O emissions from the drying soil. We estimate to be able to measure minimum fluxes of about $50\,\mathrm{ng\,m^{-2}\,s^{-1}}$ with this technique.

Figure 7.11 shows the N_2O concentrations versus the CO_2 concentrations during the measurement campaign. During night time there is a build up in both CO_2 and N_2O. They are highly correlated (R = 0.87). CO_2 and N_2O fluxes are often found to be correlated (Xu et al., 2008). Even it is still not clear weather the fluxes of these two greenhouse gases are correlated at the ecosystem scale (Xu et al., 2008), the correlation can be used to scale N_2O emissions in atmospheric chemistry and transport models (R. Wania, personal communication, April 2009). Since we can measure the CO_2 flux during these periods, we can get a crude estimate of the mean N_2O emissions assuming that the loss from the boundary layer is the same for CO_2 and N_2O and both have the same source footprint (which can be assumed in this case since both CO_2 and N_2O are mainly emitted from soil/surface for this specific setup). The CO_2 flux during night time is approximately $0.2\,\mathrm{mg\,CO_2\,m^{-2}\,s^{-1}}$. The observed correlation slope of 0.09 yields about $10\,\mathrm{ngN\ m^{-2}\,s^{-1}}$, so we do not expect to measure any N_2O emissions with the REA technique during the measurement campaign.

The uncertainty of the slope can be estimated to $\sim$0.25; with the assumption of similar footprints for CO_2 and N_2O and the same losses through the boundary height, we estimate to be able to measure N_2O fluxes of $2\,\mathrm{ng\,m^{-2}\,s^{-1}}$ using the correlation of CO_2 and N_2O.

7.3.3 CH_4 Flux

The total global CH_4 source is relatively well known but the strength of each source component and their trends are not. The sources are mostly biogenic and include wetlands, rice agriculture, biomass burning and ruminant animals (IPCC: Forster et al. (2007)). Ruminant livestock can produce 250 to 500 L of methane per day (Johnson and Johnson, 1995; Griffith et al., 2008) and are responsible for about 85 Tg of the 550 Tg CH_4 released annually (McGinn et al., 2006). Eddy correlation, eddy accumulation, and gradient methods can be used to measure methane emissions from cattle (Lenschow and Hicks, 1987; Andreae and Schimel, 1989; Griffith et al., 2008) and other ruminants.
Figure 7.12 shows the CH_4 flux for the measurement campaign near Nowra using the REA technique. During the whole campaign, approximately 200 beef cattle were grazing on the 1 km diameter grass paddock. As for all meteorological

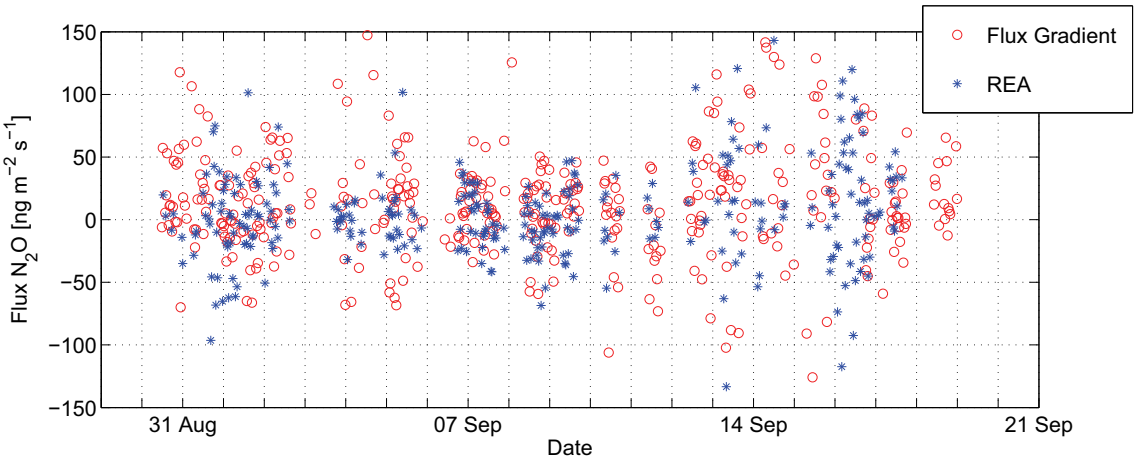

Figure 7.10: Flux of N_2O measured with the REA and flux gradient method

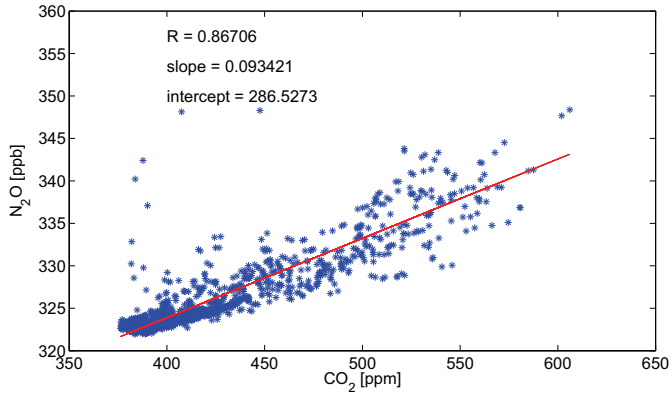

Figure 7.11: N_2O versus CO_2 concentrations

methods, it is required that the plume emanating from the grazing cattle is included in the footprint of the measurement tower. The cattle are usually not randomly distributed and to make an estimate of the CH_4 emission per cow, the distribution (locations of the cows) with time need to be known to backtrack the measured CH_4 with a micrometeorological model. A micrometeorological tracer model can be used to backtrack the measured concentrations (e.g. windtrax (`http://www.thunderbeachscientific.com/windtrax.html`)). The distribution of the cattle can be influenced by limiting the pasture size for the time of the measurements, for long term measurements the location of the cattle can be traced either by photography or GPS systems. The purpose of our field campaign was the test of the new technique under real conditions. We did not concentrate on methane emissions and were limited in expenses and effort. It can be seen that the CH_4 REA fluxes are generally positive and quite variable, as is expected, since both the location and number of the cattle and the back trajectories are varying in time and strength. The order of magnitude is reasonable, assuming emissions of $\sim 165\,\mathrm{gCH_4\,d^{-1}\,cow^{-1}}$ for beef cattle (Houghton et al., 1996; McGinn et al., 2006). For the initial investigation of the new flux measurement technique, the performed measurements with the REA technique are satisfying. In Figure 7.13 the CH_4 fluxes measured with the REA and with the FG technique are shown. The CH_4 fluxes measured with the FG technique are not satisfying in variation and sign (positive and negative fluxes). One problem of measuring the CH_4 fluxes with the gradient technique in this specific case, is the height of the inlet lines with respect to the altitude where the emissions occur. For emissions from the soil, the height of 1.5 m and 0.5 m above the ground is sufficient, while the emissions from cattle occur in higher altitudes (size of the cattle). In order to measure these fluxes correctly, the heights of the inlet lines have to be taken appropriately. Since the FG measurements are instantaneous measurements obtained by using the differences between two concentration measurements which are 7.5 min apart from each other (experimental setup does not contain a buffer volume), variation of the sources (moving cattle, different wind direction) in time and strength have a higher impact on these measurements than for example on N_2O, where the sources are equally distributed.

7.4 Conclusion and Outlook

We successfully combined two highly sophisticated techniques, the REA technique with a FTIR analyser, and developed a lung system to be able to perform automated and continuous flux measurements. The combination of the REA technique with the FTIR analyser was tested successfully in the lab and during a three weeks field campaign. The advantage of simultaneous multi-species analysis of a FTIR spectrometer made it possible to study emissions of carbon dioxide, nitrous oxide

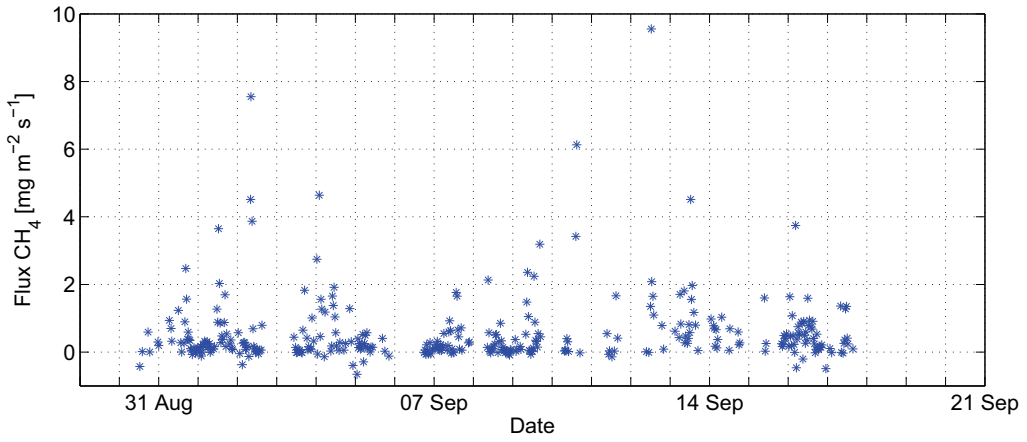

Figure 7.12: Flux of CH_4 measured with the REA method

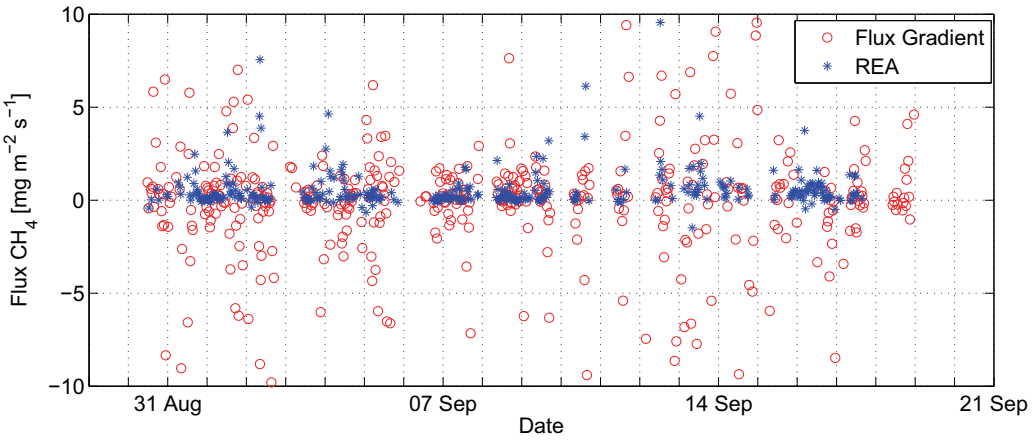

Figure 7.13: Flux of CH_4 measured with the REA and flux gradient method

and methane at the same time without any further effort. Especially the REA measurements of CO_2 fluxes are in nice agreement with those from EC (LICOR) measurements. The emissions of N_2O during the field campaign were very small and below the measurement limit of the REA technique. For further investigation, flux measurement with higher N_2O emissions are of interest. The newly combined technique can be used to study CH_4 emissions from dairy or beef cattle but require further preparation. During the field campaign, the measurement setup was working automatically. The combined REA-FTIR technique can be used for continuous long-term measurements of greenhouse gas fluxes with minimal operator maintenance. The system was working reliable apart from periods with heavy rain. In general, micrometeorological methods, relaying on a sonic anemometer, are not able to measure during heavy rainfall.

The combined FTIR-REA-technique introduced here has several advantages. The whole measurement setup was working automatically and was controllable from remote, which allows operation with minimal maintenance. With the exception of CO_2, micrometeorological flux measurements of greenhouse gases have been mostly possible only in campaign mode due to the complexity and logistical requirements of the existing techniques. The automated FTIR-REA setup allows to measure atmospheric trace gas fluxes continuously over longer time periods. This is of special interest for agricultural systems, which can be sources or sinks of atmospheric trace gases. The new technique is in no competition with the conventional LICOR technique for CO_2 flux measurements regarding costs and operator maintenance, but can be a suitable method for the observation of CH_4 and potentially N_2O fluxes and allows to measure fluxes from different species simultaneously, including CO_2. The FTIR-REA technique enables studies of fluxes which run for longer periods, for example over full seasonal or growing cycles for both animal- and crop-based agriculture. The high precision multi-species analysis capabilities of FTIR spectroscopy offers the capacity to measure a range of gases simultaneously under field conditions and makes this flux measurement technique preferable for long-term monitoring of greenhouse gas fluxes.

Summary

Within this work, Fourier Transform Infrared (FTIR) spectrometry has been used for ground-based solar absorption, laboratory and flux measurements, to study the atmospheric composition, as well as physical and chemical processes in the atmosphere.

Ground-based solar absorption FTIR spectra have been successfully recorded at the tropical site Paramaribo, Suriname between September 2004 and November 2007 and represent the first remote sensing measurements in the inner tropics over several years. These measurements are of great importance for a better understanding of global climate and physical and chemical processes of the tropical atmosphere as well as for satellite validations.

Vertical profiles and total column concentrations of carbon monoxide and other short-living trace gases related to biomass burning have been retrieved. These observations have been compared with satellite observations and model simulations and contribute substantially to the understanding of atmospheric chemistry transport processes. The observations are valuable for evaluating revised emission scenarios and the model resolution and meteorology, to determine which are critical for simulating plumes more accurately in the tropics.

The vertical distribution and total columns of methane can be retrieved from solar absorption FTIR spectra. The quality of the methane retrieval was limited by the available spectroscopic data. In cooperation with the Forschungszentrum Karlsruhe, laboratory cell-measurements have been performed to correct the methane spectroscopy in the infrared spectral region, which significantly improved the retrieval of methane from SCIAMACHY and FTIR spectra. Total column concentrations of methane have been retrieved for the first time from FTIR spectra recorded in Paramaribo. The retrieval of methane profiles from near-infrared FTIR spectra by optimal estimation significantly improved the results. The methane FTIR observations have been compared with TM5 model simulations and satellite observations from SCIAMACHY, and were the first validation of the SCIAMACHY retrieval in the tropics using remote sensing techniques. The ratio CH_4/CO_2, which can be measured directly from SCIAMACHY and FTIR, compared very good, while the column averaged volume mixing ratio (XVMR(CH_4)) of SCIAMACHY did not agree with the FTIR observations. Model assumptions are used in the SCIAMACHY retrieval to derive the XVMR(CH_4) from the directly measured CH_4/CO_2 ratio. The worse agreement of SCIAMACHY XVMR(CH_4) with FTIR compared to the SCIAMACHY CH_4/CO_2 ratio with FTIR could be

attributed to unrealistic model assumptions used in the SCIAMACHY retrieval that led to wrong time series of the column averaged CH_4 VMR. A good agreement of the FTIR XVMR(CH_4) was found with the TM5 model.

During my research project in Australia, we successfully combined two highly sophisticated techniques, the REA technique with a FTIR analyzer, and advanced these techniques to be able to perform automated and continuous flux measurements. The combination of the REA technique with the FTIR analyzer was tested successfully in the lab and during a three weeks field campaign. The FTIR-REA technique offers the capacity to measure a range of gases simultaneously under field conditions and enables long-term measurements and monitoring of atmospheric greenhouse gas fluxes.

Cell-based FTIR analyser are highly valuable for high precision measurements of greenhouse gases and can be used for the improvement of spectroscopic linelists, indispensable for the retrieval from satellites and FTIR spectra. In summary, it was shown that the ground-based FTIR remote sensing measurements have been performed successfully in the tropics and provide an indispensable dataset for the validation of satellite observations and for the testing of atmospheric transport and chemistry models.

Part IV

Appendix

A Tropospheric Chemistry Relevant for This Work

The content of this section is largely adopted from the lecture 'Tropospheric Chemistry' held by Veronika Eyring in October/November 2005 and standard textbooks. Due to the complexity of the involved tropospheric chemistry, this chapter doesn't claim completeness and only gives a short overview about the most important chemical processes relevant for this work. Further details can be found in Jacob (1999); Finnlayson-Pitts and Pitts (2000).

OH Radicals - Cleansing agent of the Atmosphere

The most important chemical cleaning agent of the atmosphere is the hydroxyl radical OH. It determines the oxidizing power of the atmosphere, and thereby controls the removal of nearly all gaseous atmospheric pollutants. Because it is so reactive, the average lifetime of an OH molecule in the atmosphere is only $\sim$1 s. The atmospheric supply of OH is limited, however, and could be overcome by consumption due to increasing pollution and climate change (Rohrer and Berresheim, 2006). Since it is strongly correlated with ultra-violet solar radiation (Rohrer and Berresheim, 2006), the OH production is strongest in the tropics. Hydroxyl radicals are produced when solar UV radiation decomposes O_3 into molecular oxygen and energetically excited oxygen atoms (O^*)

$$O_3 + h\nu \quad (\lambda < 330\,\text{nm}) \quad \rightarrow \quad O^* + O_2 \qquad \text{(R1)}$$

Most of the excited atomic oxygen atoms produced by (R1) dissipate their excess energy as heat and eventually recombine with O_2 to form O_3, which is, together with (R1) a null cycle (no chemical net effect).

$$\begin{aligned} O^* + M &\rightarrow O + M \qquad \text{(R2)} \\ O + O_2 &\rightarrow O_3 \end{aligned}$$

However, a small fraction ($\sim$1 %) of the O^* atoms reacts with water vapor to produce two molecules of OH:

$$O^* + H_2O \rightarrow 2\ OH \quad (R3)$$

Reaction (R3) is the main free tropospheric source of hydroxyl radicals. In the lower troposphere, it has a rate coefficient 10 times larger than the quenching reaction (R2). In the upper troposphere, H_2O is scarce, and other reactions may be more important sources of OH. The OH radical is unreactive toward oxygen and survives to react with most atmospheric trace species. Through the formation of OH, O_3 ultimately maintains the chemical composition of the troposphere. The dominant sinks for OH in the global troposphere are the oxidation of CO and CH_4. Over the continents, reactions with nonmethane hydrocarbon (NMHC) can be strong local sinks for OH. In forests, the dominant reactant with OH is often isoprene (C_5H_8), which is emitted by deciduous trees.

CO oxidation

The simplest example of OH recycling is given by oxidation of CO, quickly forming the stable end product CO_2 and the reactive hydrogen atom:

$$CO + OH \rightarrow CO_2 + H$$

The H-atom rapidly combines with O_2 to form the hydroperoxy radical:

$$H + O_2 + M \rightarrow HO_2 + M$$

The addition of an H atom to O_2 weakens the bond in the O_2 molecule, leading to a greater reactivity. In particular, HO_2 reacts with NO:

$$NO + HO_2 \rightarrow NO_2 + OH$$

When the concentration of NO exceeds about 100 ppt (as over most of Europe during daytime), the NO + HO_2 path is by far the fastest reaction of HO_2. The OH consumed in the oxidation of CO is regenerated.

Methane Oxidation

Following the initial attack of OH on CH_4 the prevailing concentration of nitrogen oxides determines which oxidation pathways dominate. In NO-rich regions, rapid formation of O_3 and HCHO occurs with OH, HO_2, NO and NO_2 serving as

catalysts:

$$
\begin{array}{lcl}
CH_4 + OH & \rightarrow & CH_3 + H_2O \\
CH_3 + O_2 + M & \rightarrow & CH_3O_2 + M \\
CH_3O_2 + NO & \rightarrow & CH_3O + NO_2 \\
CH_3O + O_2 & \rightarrow & CH_2O + HO_2 \\
HO_2 + NO & \rightarrow & NO_2 + OH \\
2(NO_2 + h\nu) & \rightarrow & 2(NO + O) \\
2(O + O_2 + M) & \rightarrow & 2(O_3 + M) \\
\hline
\text{net: } CH_4 + 4\,O_2 + h\nu & \rightarrow & CH_2O + H_2O + 2\,O_3 \qquad \text{(R4)}
\end{array}
$$

In NO-poor environments, the methylperoxy radical (CH_3OO) reacts with HO_2 instead, providing one of the following reaction chains:

$$
\begin{array}{lcl}
CH_4 + OH & \rightarrow & CH_3 + H_2O \\
CH_3 + O_2 + M & \rightarrow & CH_3O_2 + M \\
CH_3O_2 + HO_2 & \rightarrow & CH_3OOH + O_2 \\
CH_3OOH + h\nu & \rightarrow & CH_3O + OH \\
CH_3O + O_2 & \rightarrow & HCHO + HO_2 \\
\hline
\text{net: } CH_4 + O_2 & \rightarrow & HCHO + H_2O \qquad \text{(R5)}
\end{array}
$$

$$
\begin{array}{lcl}
CH_4 + OH & \rightarrow & CH_3 + H_2O \\
CH_3 + O_2 + M & \rightarrow & CH_3O_2 + M \\
CH_3O_2 + HO_2 & \rightarrow & CH_3OOH + O_2 \\
CH_3OOH + OH & \rightarrow & HCHO + H_2O + OH \\
\hline
\text{net: } CH_4 + OH + HO_2 & \rightarrow & HCHO + 2\,H_2O \qquad \text{(R6)}
\end{array}
$$

The hydroxyl radical is the major component in the methane oxidation process. Hydroxyl radicals are involved and consumed in many other trace species reactions, so increasing pollution of the atmosphere by other trace species might lead to a reduced methane oxidation rate.

Methane oxidation plays an important role for the production of atmospheric carbon monoxide. Most of the CO further oxidizes to CO_2. In the presence of NO_x, the oxidation of CO to CO_2 can also produce ozone.

$$
\begin{array}{lcll}
\mathrm{CO} + \mathrm{OH} & \rightarrow & \mathrm{CO_2} + \mathrm{H} & \\
\mathrm{H} + \mathrm{O_2} + \mathrm{M} & \rightarrow & \mathrm{HO_2} + \mathrm{M} & \\
\mathrm{HO_2} + \mathrm{NO} & \rightarrow & \mathrm{NO_2} + \mathrm{OH} & \\
\mathrm{NO_2} + \mathrm{h}\nu & \rightarrow & \mathrm{NO} + \mathrm{O} & \\
\mathrm{O} + \mathrm{O_2} + \mathrm{M} & \rightarrow & \mathrm{O_3} + \mathrm{M} & \\
\hline
\text{net: } \mathrm{CO} + 2\,\mathrm{O_2} + \mathrm{h}\nu & \rightarrow & \mathrm{CO_2} + \mathrm{O_3} & \text{(R7)}
\end{array}
$$

Neither OH nor HO_2 is consumed, so these reactions describe the catalytic oxidation of CO and CO_2. Net formation of O_3 occurs, because the conversion of NO to NO_2 is accomplished by the HO_2 radical than by ozone itself. The chain is terminated by all reactions removing the participant molecules.

$$
\begin{array}{lcll}
\mathrm{CO} + \mathrm{OH} & \rightarrow & \mathrm{CO_2} + \mathrm{H} & \\
\mathrm{H} + \mathrm{O_2} + \mathrm{M} & \rightarrow & \mathrm{HO_2} + \mathrm{M} & \\
\mathrm{HO_2} + \mathrm{O_3} & \rightarrow & \mathrm{OH} + 2\,\mathrm{O_2} & \\
\hline
\text{net: } \mathrm{CO} + \mathrm{O_3} & \rightarrow & \mathrm{CO_2} + \mathrm{O_2} & \text{(R8)}
\end{array}
$$

The oxidation of CO in a NO_x-free atmosphere would lead to the destruction of ozone, whereas it led to a production while NO_x was present.

B Pressure-Temperature Profiles

Figure B.1 to B.3 show the differences between the pT-profiles over height for Paramaribo (5.81°N, 55.21°W, Fig. B.1), Bremen (53.11°N, 8.85°E, Fig. B.2) and Spitsbergen (78.92°N, 11.92°E, Fig. B.3). At higher latitudes (Bremen, Spitsbergen) the pT-profiles from ECMWF and NCEP agree in the troposphere and stratosphere, but tend to show higher deviations above ∼35 km. Especially in Bremen, ECMWF profiles show higher temperatures above 40 km relative to NCEP. In the tropics (Paramaribo) the differences between ECMWF and NCEP are larger than at higher latitudes. Especially in tropopause region (∼17 km) and above 35 km the differences are larger than the standard deviation.

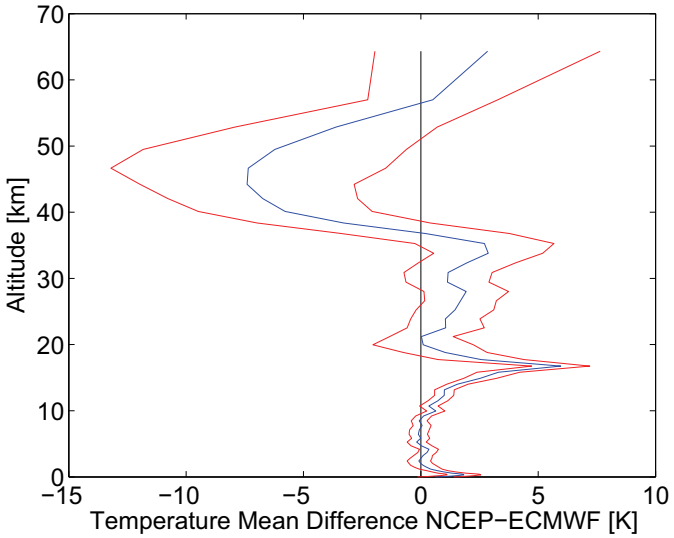

Figure B.1: Temperature mean differences between NCEP- and ECMWF-pT-profiles from 2004 for Paramaribo. Also shown are the standard deviations.

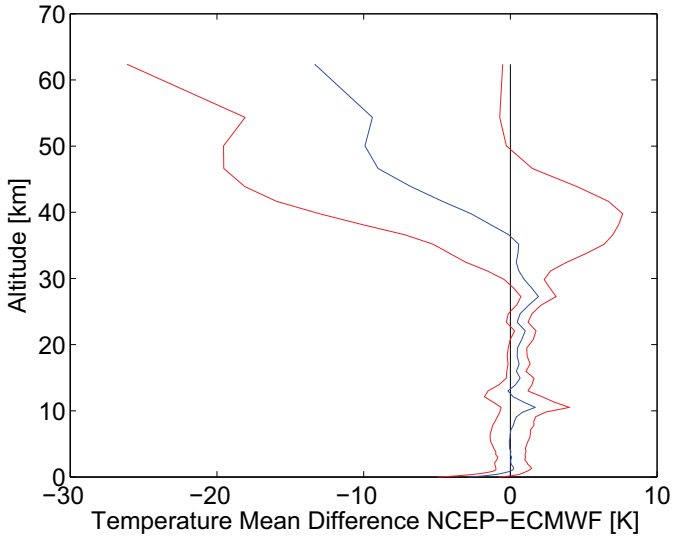

Figure B.2: Temperature mean differences between NCEP- and ECMWF-pT-profiles from 2004 for Bremen. Also shown are the standard deviations.

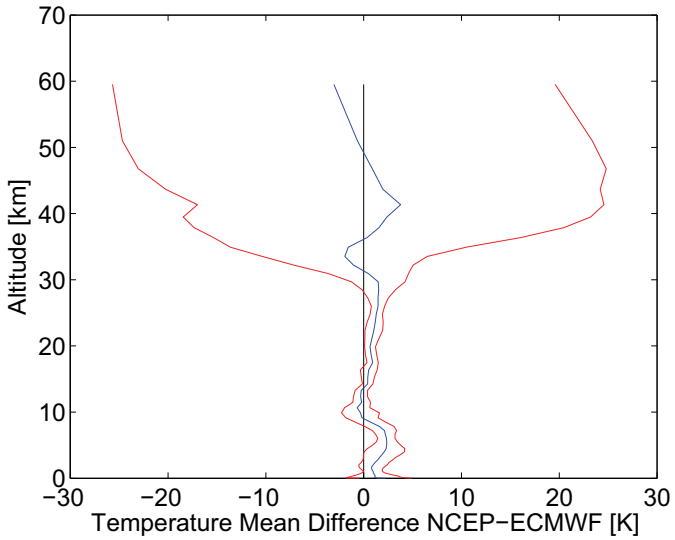

Figure B.3: Temperature mean differences between NCEP- and ECMWF-pT-profiles from 2004 for Spitsbergen. Also shown are the standard deviations.

C Details of the REA-Lung-FTIR System

The lung consists of two pairs of sampling reservoirs; one pair is composed of one up- and one down-reservoir. While one pair of reservoirs is being filled during one averaging period, the other pair, filled during the previous period, is being analysed by the FTIR spectrometer. After the analysis, the analysed pair is evacuated before it gets filled in the next averaging period, while the previously filled pair is then analysed. The systems consists of three three-way solenoid valves (Bürkert No. 6014) for each inlet line to sample the air into reservoir bags and two two-way solenoid valves (Bürkert No. 6013) for the evacuation of the reservoir bags of each sample line (see Figure 7.2). 5 L Barrier Bag-Water (Scholle Industries, Product Code 800342) were used for sampling bags. For the duration of one averaging period (30 min in this setup), air is sampled into reservoir bags A-up and A-down; after this period, the valves are switched to sample the air in reservoir bags B-up and B-down, while the reservoir bags A-up and A-down are analysed one after the other by the FTIR analyser, and the residual sample is then evacuated. Since the analysis of one pair of bags did not require the whole filling time and in order to have another comparison to the REA flux measurements, the lung system was constructed to enable FG measurements. During the last 15 min of the 30 min averaging period, the valves No. 3 (one for the updraft-line, one for the downdraft-line) of the lung system opened to inlet lines at $z_1 = 0.5\,\mathrm{m}$ and at $z_2 = 1.5\,\mathrm{m}$ respectively, installed at the met-station. The FG air samples were analysed instantaneously (no buffer-volume), the delay between z_1 and z_2 was 7.5 min. The analysis of the two samples was finished within 15 min. Figure C.1 to C.4 show the different states of the valves during the measurement cycle of the combined REA-lung-FTIR system.

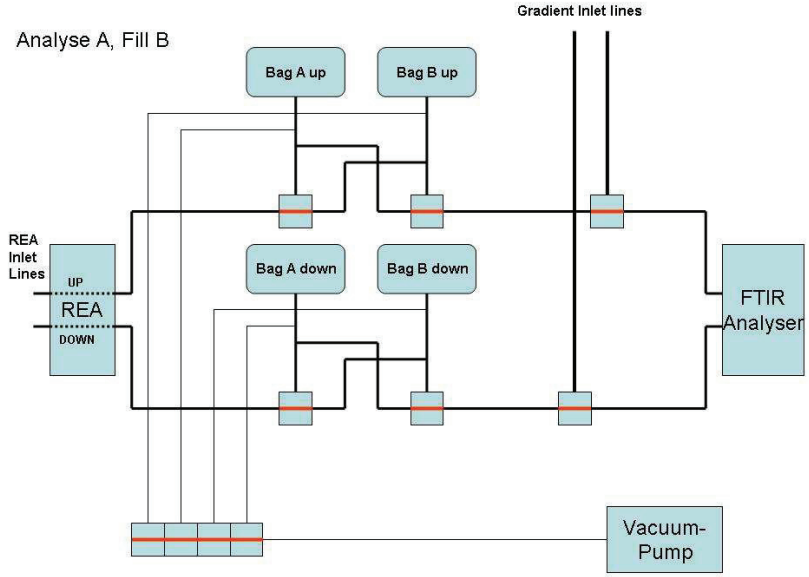

Figure C.1: Schematic design of the REA-lung-FTIR system. While the reservoir bags A are being analysed by the FTIR spectrometer, the reservoir bags B are being filled. (First quarter of one measurement cycle)

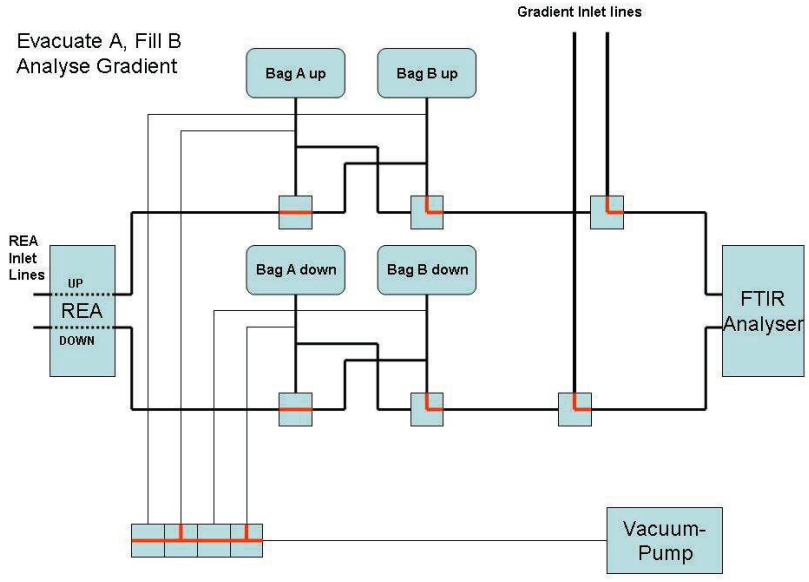

Figure C.2: Schematic design of the REA-lung-FTIR system. The reservoir bags B are still being filled, while the air samples of the FG inlet lines are analysed. At the same time, the bags A get evacuated. (Second quarter of one measurement cycle)

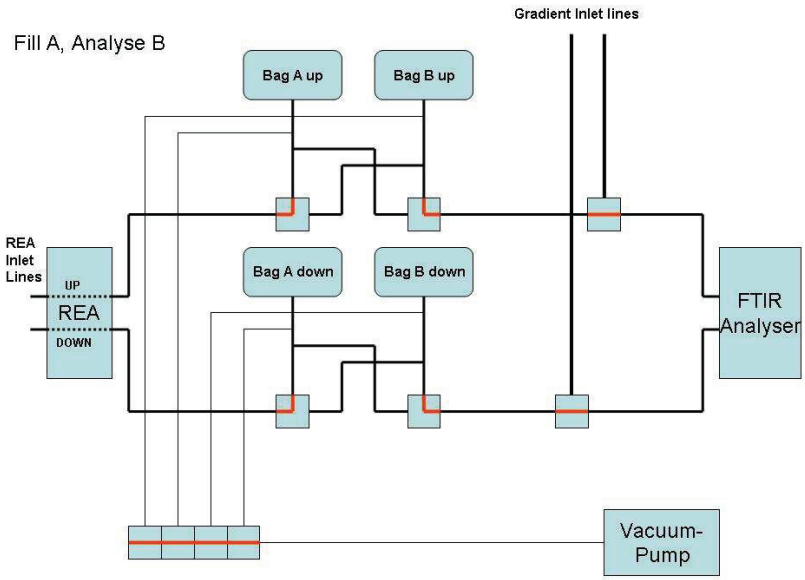

Figure C.3: Schematic design of the REA-lung-FTIR system. While the reservoir bags B are being analysed by the FTIR spectrometer, the reservoir bags A are being filled. (Third quarter of one measurement cycle)

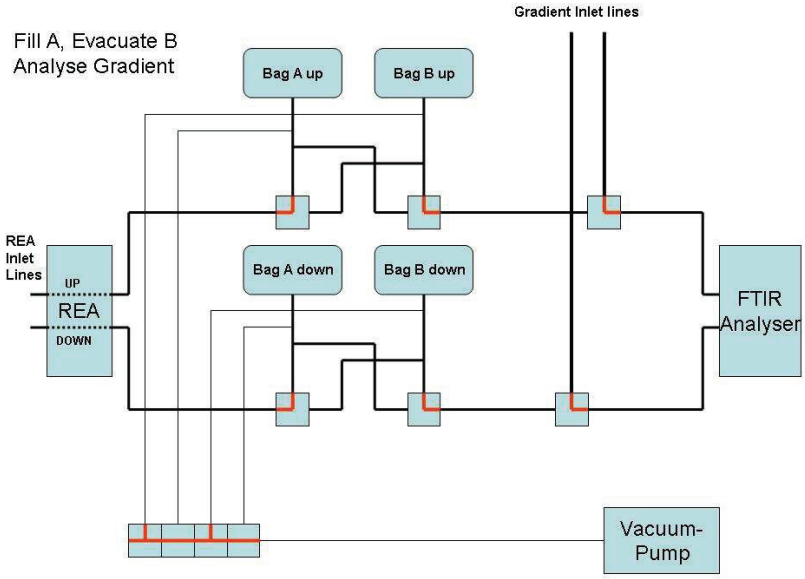

Figure C.4: Schematic design of the REA-lung-FTIR system. The reservoir bags A are still being filled, while the air samples of the FG inlet lines are analysed. At the same time, the bags B get evacuated. (Forth quarter of one measurement cycle)

List of Figures

List of Tables

Bibliography

Ammann, C. and Meixner, F.: Stability dependence of the relaxed eddy accumulation coefficient for various scalar quantities, J. Geophys. Res., 107, 2002.

Andreae, M. O. and Merlet, P.: Emission of trace gases and aerosols from biomass burning, Global Biogeochem. Cycles, 15, 955–966, 2001.

Andreae, M. O. and Schimel, D. S., eds.: Exchange of Trace Gases between Terrestrial Ecosystems and the Atmosphere, John Wiley and Sons, New York, 1989.

Baker, J., Norman, J., and Bland, W.: Field-scale application of flux measurement by conditional sampling, Agr. For. Meteorol., 62, 31–52, 1992.

Bergamaschi, P., Krol, M., Dentener, F., Vermeulen, A., Meinhardt, F., Graul, R., Ramonet, M., Peters, W., and Dlugokencky, E. J.: Inverse modelling of national and European CH_4 emissions using the atmospheric zoom model TM5, Atmos. Chem. Phys., 5, 2431–2460, 2005.

Bergamaschi, P., Frankenberg, C., Meirink, J., Krol, M., Dentener, F., Wagner, T., Platt, U., Kaplan, J., Körner, S., Heimann, M., and Goede, A.: Satellite cartography of atmospheric methane from SCIAMACHY on board ENVISAT: II. Evaluation based on inverse model simulations, J. Geophys. Res., 112, doi:10.1029/2006JD007268, 2007.

Beverland, I. J.: Design, construction and operation of flux measurement systems using the conditional sampling technique, Submission to Atmospheric Environment, 1994.

Brasseur, G. P. and Solomon, S.: Aeronomy of the Middle Atmosphere, D. Reidel Publishing Company, 1984.

Brühl, C. and Crutzen, P. J.: The MPIC 2D model, NASA Ref. Publ., 1292, 103–104, 1993.

Buchwitz, M., de Beek, R., Noël, S., Burrows, J. P., Bovensmann, H., Schneising, O., Khlystova, I., Bruns, M., Bremer, H., Bergamaschi, P., Körner, S., and Heimann, M.: Atmospheric carbon gases retrieved from SCIAMACHY by

WFM-DOAS: Version 0.5 CO and CH_4 and impact of calibration improvements on CO_2 retrieval, Atmos. Chem. Phys., 6, 2727–2751, 2006.

Businger, J. and Delany, A.: Chemical Sensor Resolution Required for Measuring Surface Fluxes by Three Common Micrometeorological Techniques, J. Atmos. Chem., pp. 10:399–410, 1990.

Businger, J. and Oncley, S.: Flux Measurement with Conditional Sampling, J. Atmos. Ocean. Tech., 7, 1990.

Butler, T. M., Taraborrelli, D., Brühl, C., Fischer, H., Harder, H., Martinez, M., Williams, J., Lawrence, M. G., and Lelieveld, J.: Improved simulation of isoprene oxidation chemistry with the ECHAM5/MESSy chemistry-climate model: lessons from the GABRIEL airborne field campaign, Atmos. Chem. Phys., 8, 4529–4546, 2008.

Crutzen, P. and Andreae, M. O.: Biomass burning in the tropics: Impact on atmospheric chemistry and biogeochemical cycles, Science, 250, 1669–1678, 1990.

Crutzen, P. and Zimmermann, P. H.: The changing photochemistry in the troposphere, Tellus, 43, 136–151, 1991.

Davis, S. P., Abrams, M. C., and Brault, J. W.: Fourier Transform Spectrometry, Academic Press, 2001.

Desjardin, R. L.: A Study of Carbon Dioxide and Sensible Heat Fluxes Using the Eddy Correlation Technique, Ph.D. dissertation, Cornell University, 1972.

Dlugokencky, E. J., Steele, L. P., Lang, P. M., and Masarie, K. A.: The growth rate and distribution of atmospheric methane, J. Geophys. Res., 99, 17 021–17 043, 1994.

Dlugokencky, E. J., Houweling, S., Bruhwiler, L., Masarie, K. A., Lang, P. M., Miller, J. B., and Tans, P. P.: Atmospheric methane levels off: Temporary pause or a new steady state?, Geophys. Res. Lett., 30, doi:10.1029/2003GL018126, 2003.

Finnlayson-Pitts, B. J. and Pitts, J. N.: Chemistry of the upper and lower atmosphere, Academic Press, 2000.

Foken, T.: Angewandte Meteorologie: Mikrometeorologische Methoden, Springer Verlag, 2 edn., 2006.

Forster, P., Ramaswamy, V., Artaxo, P., Berntsen, T., Betts, R., Fahey, D., Haywood, J., Lean, J., Lowe, D., Myhre, G., Nganga, J., R. Prinn, G. Raga, M. S., and Dorland, R. V.: Changes in Atmospheric Constituents and in Radiative

Forcing, Climate Change 2007: The Physical Science Basis. Contribution of Working Group I to the Fourth Assessment Report of the Intergovernmental Panel on Climate Change (IPCC), 2007.

Fortuin, J., Becker, C., Fujiwara, M., Immler, F., Kelder, H. M., Scheele, M. P., Schrems, O., , and Verver, G. H. L.: Origin and transport of tropical cirrus clouds observed over Paramaribo, Suriname (5.8°N, 55.2°W), J. Geophys. Res., 112, doi:10.1029/2005JD006420, 2007.

Frankenberg, C., Meirink, J. F., van Weele, M., Platt, U., and Wagner, T.: Assessing methane emissions from global space-borne observations, Science, 308, 1010–1014, doi:10.1126/science.1106644, 2005.

Frankenberg, C., Meirink, J. F., Bergamaschi, P., Goede, A. P. H., Heimann, M., Körner, S., Platt, U., van Weele, M., and Wagner, T.: Satellite chartography of atmospheric methane from SCIAMACHY on board ENVISAT: Analysis of the years 2003 and 2004, J. Geophys. Res., 111, doi:10.1029/2005JD006235, 2006.

Frankenberg, C., Bergamaschi, P., Butz, A., Houweling, S., Meirink, J.-F., Notholt, J., Petersen, A. K., Schrijver, H., Warneke, T., and Aben, I.: Tropical methane emissions: A revised view from SCIAMACHY onboard ENVISAT, Geophys. Res. Lett., doi:10.1029/2008GL034300, 2008a.

Frankenberg, C., Warneke, T., Butz, A., Brown, L., Hase, F., Spietz, P., and Aben, I.: Pressure broadening in the $2\nu_3$ band of methane and its implication on atmospheric retrievals, Atmos. Chem. Phys., 8, 5061–5075, 2008b.

Galanter, M., Levy, H., and Carmichael, G. R.: Impacts of biomass burning on tropospheric CO, NOx, and O_3, J. Geophys. Res., 105, 6633–6653, 2000.

Gerbig, C., Lin, J. C., Wofsy, S. C., Daube, B. C., Andrews, A. E., Stephens, B. B., Bakwin, P. S., and Grainger, C. A.: Toward constraining regional-scale fluxes of CO_2 with atmospheric observations over a continent: 1. Observed spatial variability from airborne platforms, J. Geophys.Res., 108, doi:10.1029/2002JD003018, 2003a.

Gerbig, C., Lin, J. C., Wofsy, S. C., Daube, B. C., Andrews, A. E., Stephens, B. B., Bakwin, P. S., and Grainger, C. A.: Toward constraining regional-scale fluxes of CO_2 with atmospheric observations over a continent: 2. Analysis of COBRA data using a receptor-oriented framework, J. Geophys.Res., 108, doi:10.1029/2003JD003770, 2003b.

Griffith, D. W. T.: Synthetic calibration and quantitative analysis of gas phase infrared spectra, Applied Spectroscopy, 50, 59–70, 1996.

Griffith, D. W. T.: MALT5 User Guide, University of Wollongong, Wollongong, Australia, version 5.2 edn., 2006.

Griffith, D. W. T., Bryant, G. R., Hsu, D., and Reisinger, A. R.: Methane emissions from free-ranging cattle: Comparison of tracer and integrated horizontal flux techniques, J. Environ.Qual., 37, 582–591, doi:10.2134/jeq2006.0426, 2008.

Haken, H. and Wolf, H. C.: Molekülphysik und Quantenchemie: Einfürung in die experimentellen und theoretischen Grundlagen, Springer Verlag, 2006.

Hase, F., Blumenstock, T., and Paton-Walsh, C.: Analysis of the instrumental line shape of high-resolution Fourier IR spectrometers with gas cell measurement and new retrieval software, Applied Optics, 38, 1999.

Hicks, B. B. and McMillen, R. T.: A simulation of the eddy accumulation method for measuring pollutant fluxes, J. Climate and Appl. Meteorology, 23, 637–643, 1984.

Holloway, T., Levy, H., and Kasibhatla, P.: Global distribution of carbon monoxide, J. Geophys. Res., 105(D10), 12,123–12,147, 2000.

Holton, J. R.: The tropical tropopause layer, the quasibiennial oscillation, and stratospheric dehydration, Destinguished lecture series, University of Washington, 2002.

Holton, J. R., Haynes, P. H., McIntyre, M. E., Douglass, A. R., Rood, R., and Pfister, L.: Stratosphere-Troposphere Exchange, Reviews of Geophysics, 33, 403–439, 1995.

Houghton, J., Ding, Y., Griggs, D., Noguer, M., van der Linden, P., Dai, X., Maskell, K., and Johnson, C.: IPCC, 2001: Climate change 2001: The scientific basis. contributions of working group I to the third assessement Report of the Intergovermental Panel on Climate Change, Cambridge University Press, 2001.

Houghton, J. T., Filho, L. G. M., Lim, B., Treanton, K., Mamaty, I., Bonduki, Y., Griggs, D. J., and Callander, B. A.: Greenhouse gas inventory manual, vol. 3 (Agriculture), Intergovernmental Panel on Climate Change, revised 1996 IPCC guidelines for national greenhouse gas inventories edn., 1996.

Houweling, S., Dentener, F., and Lelieveld, J.: The impact of nonmethane hydrocarbon compounds on tropospheric photochemistry, J.Geophys. Res., 103, 10 673–10 696, 1998.

Houweling, S., Röckmann, T., Aben, I., Keppler, F., Krol, M., Meirink, J., Dlugokencky, E., and Frankenberg, C.: Atmospheric constraints on global emissions

of methane from plants, Geophys. Res. Lett., 33, doi:10.1029/2006GL026162, 2006.

Immler, F., Krüger, K., Tegtmeier, S., Fujiwara, M., Fortuin, P., Verver, G., and Schrems, O.: Cirrus clouds, humidity, and dehydration in the tropical tropopause layer observed at Paramaribo, Suriname (5.8°N, 55.2°W), J. Geophys. Res., 112, doi:10.1029/2006JD007440, 2007.

I.Vigano, van Weelden, H., Holzinger, R., Keppler, F., and Röckmann, T.: Effect of UV radiation and temperature on the emission of methane from plant biomass and structural components, Biogeosciences Disc., 5(1), 243–270, 2008.

Jacob, D. J.: Introduction to Atmospheric Chemistry, Princeton University Press, 1999.

Jenouvrier, A., Daumont, L., Régalia-Jarlot, L., Tyuterev, V. G., Carleer, M., Vandaele, A. C., Mikhailenko, S., and Fally, S.: Fourier transform measurements of water vapor line parameters in the 4200-6600 cm^{-1} region, J. Quant. Spectrosc. Radiat. Transfer, 105, 326–355, 2007.

Johnson, K. A. and Johnson, D. E.: Methane emissions from cattle, Journal of Animal Science, 73, 2483–2492, 1995.

Kaimal, J. C. and Finningan, J. J.: Atmospheric Boundary Layer Flows: Their Structure and Measurement, Oxford University Press, 1994.

Kasai, Y. J., Kagawa, A., Jones, N., Fujiwara, A., Seki, K., Murayama, Y., and Murcray, F.: Seasonal variations of CO and HCN in the troposphere measured by solar absorption spectroscopy over Poker Flat, Alaska, Geophys. Res. Lett., 32, doi:10.1029/2005GL022826, 2005.

Keppler, F., Hamilton, J. T. G., Braß, M., and Rockmann, T.: Methane emissions from terrestrial plants under aerobic conditions, Nature, 439, 187–191, doi:10.1038/nature04420, 2006.

Keppler, F., Hamilton, J. T. G., McRoberts, W. C., Vigano, I., Braß, M., and Röckmann, T.: Methoxyl groups of plant pectin as a precursor of atmospheric methane: Evidence from deuterium labelling studies, New Phytol., 178(4), 808–814, doi:10.1111/j.1469-8137.2008.02411.x, 2008.

Lawrence, M. G., Crutzen, P. J., Rasch, P. J., Eaton, B. E., and Mahowald, N. M.: A model for studies of tropospheric photochemistry: Description, global distributions, and evalution, J. Geophys. Res., 104, 26,245–26,278, 1999.

Lawrence, M. G., Rasch, P. J., von Kuhlmann, R., Williams, J., Fischer, H., de Reus, M., Lelieveld, J., Crutzen, P. J., Schultz, M., Stier, P., Huntrieser, H., Heland, J., Stohl, A., Forster, C., Elbern, H., Jakobs, H., and Dickerson, R. R.: Global chemical weather forecasts for field campaign planning: Predictions and observations of large-scale features during MINOS, CONTRACE, and INDOEX, Atmos. Chem. Phys., 3, 267–289, `http://www.atmos-chem-phys.net/3/267/2003/`, 2003.

Lelieveld, J., Butler, T. M., Crowley, J. N., Dillon, T. J., Fischer, H., Ganzeveld, L., Harder, H., Lawrence, M. G., Martinez, M., Taraborrelli, D., and Williams, J.: Atmospheric oxidation capacity sustained by a tropical forest, Nature, 452, 737–740, 2008.

Lenschow, D. H. and Hicks, B. B., eds.: Global Tropespheric Chemistry: Chemical Fluxes in the Global Atmosphere, National Center for Atmospheric Research, Boulder, CO, 1987.

Lenschow, D. H., Mann, J., and Kristensen, L.: How long is long enough when measuring fluxes and other turbulence statistics, J. Atmos. Ocean. Tech., 11, 661–673, 1993.

Ludwig, J., Marufu, L. T., Huber, B., Andreae, M. O., and Helas, G.: Domestic combustion of biomass fuels in developing countries: A major source of atmospheric pollutants, J. Atmos. Chem., 44, 23–37, 2003.

Maiss, M. and Levin, I.: Global increase of SF_6 observed in the atmosphere, Geophys. Res. Lett., 21, 569–572, 1994.

McGinn, S. M., Flesch, T. K., Harper, L. A., and Beauchemin, K. A.: An approach for measuring methane emissions from whole farms, J. Environ.Qual., 35, 14–20, doi:10.2134/jeq2005.0250, 2006.

Meirink, J., Bergamaschi, P., Frankenberg, C., d'Amelio, M., Dlugokencky, E., Gatti, L., Houweling, S., Miller, J., Roeckmann, T., Villani, M., and Krol, M.: Four-dimensional variational data assimilation for inverse modeling of atmospheric methane emissions: Analysis of SCIAMACHY observations, J. Geophys. Res., 113, doi:10.1029/2007JD009740, 2008.

Miller, J., Gatti, L., d'Amelio, M., Crotwell, A., Dlugokencky, E., Bakwin, P., Artaxo, P., and Tans, P.: Airborne measurements indicate large methane emissions from the eastern amazon basin, Geophys. Res. Lett., 34, doi:10.1029/2006GL029213, 2007.

Nie, D., T.E.Kleindienst, R.R.Arnts, and J.E.Sickles: The design and testing of a relaxed eddy accumulation system, J. Geophys. Res., 100, 11,415–11,423, 1995.

Notholt, J., Kuang, Z., Rinsland, C., Toon, G., Rex, M., Jones, N., Albrecht, T., Deckelmann, H., Krieg, J., Weinzierl, C., Bingemer, H., Weller, R., and Schrems, O.: Enhanced upper tropical tropospheric COS: Impact on the stratospheric aerosol layer, Science, 300, 307–310, 2003.

Oncley, S., Delany, A., and Horst, T.: Verification of Flux Measurement using Relaxed Eddy Accumulation, Atmospheric Environment, 27A, pp.2417–2426, 1993.

Palm, M., Savigny, C. V., Warneke, T., Velazco, V., Notholt, J., Künzi, K., Burrows, J., and Schrems, O.: Intercomparison of O_3 profiles observed by SCIAMACHY, ground based microwave and FTIR instruments, Atmos. Chem. Phys. Discuss., 5, 911–936, 2005.

Pattey, E., Desjardins, R., and P.Rochette: Accuracy of the relaxed eddy-accumulation technique, evaluated using CO_2 flux measurements, Boundary-Layer Meteorol., 66, 341–355, 1993.

Paulson, C. A.: The mathematical representation of wind speed and temperature profiles in the unstable atmospheric surface layer, J. Appl. Meteorol., 9, 857–861, 1970.

Peters, W., Krol, M. C., Fortuin, J. P. F., Kelder, H. M., Thompson, A. M., Becker, C. R., Lelieveld, J., and Crutzen, P. J.: Tropospheric ozone over a tropical atlantic station in the northern hemisphere: Paramaribo, Surinam (6°N, 55°W), Tellus, B 56 1, 21–34, 2004.

Peters, W., Jacobson, A. R., Sweeney, C., Andrews, A. E., Conway, T. J., Masarie, K., Miller, J. B., Bruhwiler, L. M. P., tron, G. P., Hirsch, A. I., Worthy, D. E. J., van der Werf, G. R., annd Paul O. Wennberg, J. T. R., Krol, M. C., and Tans, P. P.: An atmospheric perspective on North American carbon dioxide exchange: CarbonTracker, PNAS, 104, 18 925–18 930, 2007.

Petersen, A. K., Warneke, T., Lawrence, M. G., Notholt, J., and Schrems, O.: First ground-based FTIR observations of the seasonal variation of carbon monoxide in the tropics, Geophys. Res. Lett., 35, doi:10.1029/2007GL031393, 2008.

Phillips, F. A., Leuning, R., Baigent, R., Kelly, K. B., and Denmead, O. T.: Nitrous oxide flux measurements from an intensively managed irrigated pasture using micrometeorological techniques, Agr. For. Meteorol., 143, 92–105, 2007.

Rasch, P., Mahowald, N. M., and Eaton, B. E.: Representations of transport, convection, and the hydrologic cycle in chemical transport models: Implications

for the modelling of short-lived and soluble species, J. Geophys. Res., 102, 28,127–28,138, 1997.

Rigby, M., Prinn, R. G., Fraser, P. J., Simmonds, P. G., Langenfelds, R. L., Huang, J., Cunnold, D. M., Steele, L. P., Krummel, P. B., Weiss, R. F., O'Doherty, S., Salameh, P. K., Wang, H. J., Harth, C. M., Mühle, J., and Porter, L. W.: Renewed growth of atmospheric methane, J. Geophys. Res., 35, doi:10.1029/2008GL036037, 2008.

Rinsland, C. P., Jones, N. B., Connor, B. J., Logan, J. A., Pougatchev, N. S., Goldman, A., Murcray, F. J., Stephen, T. M., Pine, A. S., Zander, R., Mahieu, E., and Demoulin, P.: Northern and Southern hemisphere ground-based infrared spectroscopic measurements of tropospheric carbon monoxide and ethane, J. Geophys. Res., 103, 28,197–28,217, 1998.

Rodgers, C. and Connor, B.: Intercomparison of remote sounding instruments, J. Geophys. Res., 108 (D3), doi:10.1029/2002JD002299, 2003.

Rohrer, F. and Berresheim, H.: Strong correlation between levels of tropospheric hydroxyl radicals and solar ultraviolet radiation, Nature, 442(7099), 2006.

Rothman, L. S., Gamache, R., Goldman, A., Brown, L., Toth, R., Pickett, H., Poynter, R., Flaud, J.-M., Camy-Peyret, C., Barbe, A., Husson, N., Rinsland, C., and Smith, M.: The HITRAN database: 1986 Edition, Applied Optics, 26, 4058–4097, 1987.

Rudolph, J.: The tropospheric distribution and budget of ethane, J. Geophys. Res., 100 (D6), 11,369–11,381, 1995.

Toon, G., Farmer, C., Schaper, P., Lowes, L., and Norton, R.: Composition measurements of the 1989 arctic winter stratosphere by airborne infrared solar absorption spectroscopy, J. Geophys. Res., 97, 7939–7961, 1992.

van der Werf, G. R., Randerson, J. T., Collatz, G. J., Giglio, L., Kasibhatla, P. S., Jr., A. F. A., Olsen, S. C., and Kasischke, E. S.: Continental-scale partitioning of fire emissions during the 1997 to 2001 El Nino/LaNina period, Science, pp. 73–76, 2004.

Velazco, V., Notholt, J., Warneke, T., Lawrence, M., Bremer, H., Drummond, J., Schulz, A., and Krieg, J.: Latitude and altitude variability of carbon monoxide measured from fourier transform spectrometry on ship cruises in the atlantic: Comparisons with model and satellite data, J. Geophys. Res., 110, doi:10.1029/2004JD005351, 2005.

Verver, G., Fujiwara, M., Dolmans, P., Becker, C., Fortuin, P., and Miloshevich, L.: Performance of the Vaisala RS80 A/H and RS90 Humicap sensors and the Meteolabor Snow White chilled-mirror hygrometer in Paramaribo, Suriname, J. Atmos. Oceanic Technol., 23, 1506–1518, 2006.

Vigouroux, C., Mazière, M. D., Errera, Q., Mahieu, E., Duchatelet, P., Wood, S., Smale, D., Mikuteit, S., Blumenstock, T., Hase, F., and Jones, N.: Comparison between ground-based ftir and mipas N_2O and HNO_3 profiles before and after assimilation in BASCOE, Atmos. Chem. Phys. Discuss., 6, 8335–8382, 2006.

von Kuhlmann, R., Lawrence, M. G., Crutzen, P., and Rasch, P. J.: A model for studies of tropospheric ozone and non-methane hydrocarbons: Model description and ozone results, J. Geophys. Res., 108, 4294, doi:10.1029/2002JD002893, 2003.

Wallace, J. M. and Hobbs, P. V.: Atmospheric Sicence, An introductory survey, Academic Press, second edition edn., 2006.

Warneke, T., Meirink, J. F., Bergamaschi, P., Grooß, J. U., Notholt, J., Toon, G. C., Velazco, V., Goede, A. P. H., and Schrems, O.: Seasonal and latitudinal variation of atmospheric methane: A ground-based and ship-borne solar IR spectroscopic study, Geophys. Res. Lett., 33, doi:10.1029/2006GL025874, 2006.

Washenfelder, R. A., Wennberg, P. O., and Toon, G. C.: Tropospheric methane retrieved from ground-based near-IR solar absorption spectra, Geophys. Res. Lett., 30(23), doi:10.1029/2003GL017969, 2003.

Washenfelder, R. A., Toon, G. C., Blavier, J.-F., Yang, Z., Allen, N. T., Wennberg, P. O., Vay, S. A., Matross, D. M., and Daube, B. C.: Carbon dioxide column abundances at the Wisconsin Tall Tower site, J. Geophys. Res., 111, doi:10.1029/2006JD007154, 2006.

Webb, E. K., Pearmann, G. I., and Leuning, R.: Correction of flux measurements for density effects due to heat and water vapour transfer, Quart. J. R. Met. Soc., 106, 85–100, 1980.

Wyngaard, J. and Moeng, C.: Parameterizing turbulent diffusion through the joint probability, Boundary-Layer Meteorol., 60, 1–13, 1992.

Xu, X., Tian, H., and Hui, D.: Convergence in the relationship of CO_2 and N_2O exchanges between soil and atmosphere within terrestrial ecosystems, Global Change Biology, 14, 1651–1660, doi:10.1111/j.1365-2486.2008.01595.x, 2008.

Yang, Z., Washenfelder, R. A., Keppel-Aleks, G., Wennberg, P. O., Krakauer, N. Y., Randerson, J. T., Tans, P. P., and Sweeney, C.: New constraints on Northern Hemisphere grewing season net flux, J. Geophys. Res., 34, 2002.

Zhao, Y., Strong, K., Kondo, Y., Koike, M., Matsumi, Y., Irie, H., Rinsland, C. P., Jones, N. B., Suzuki, K., Nakajima, H., Nakane, H., and Murata, I.: Spectroscopic measurements of tropospheric CO, C_2H_6, C_2H_2 and HCN in northern Japan, J. Geophys. Res., 107(D18), doi:10.1029/2001JD000748, 2002.

Acknowledgment

I would like to thank Prof. Dr. Justus Notholt for supervising and mentoring my PhD studies. He was always available to answer my questions or give advices, but also gave me the freedom for own ideas. I enjoyed his humorous and relaxed attitude during work and leisure, but if necessary he always gives support and stands up for his students. Thanks for the soldering-lessons on top of the Paramaribo-container roof!

Many thanks to Thorsten Warneke for sharing his enthusiasm and optimism, especially during many measurement campaigns in Paramaribo. I am grateful for his dedicated support, advices and encouragements during my PhD studies.

I wish to thank Prof. Dr. David Griffith for providing me the chance to experience the Australian way of life and work and the warm welcome in his group at the University of Wollongong. I appreciate his willingness to share his experience of FTIR spectrometers and the fruitful discussions about flux measurement techniques. I enjoyed the opportunities to gain a deep insight into the research projects of his group during many field trips. Thanks for being my Australian supervisor and for the enthusiastic support with the FTIR-REA project, especially during the field trip!

I thank all my colleagues and members of the Institute of Environmental Physics for support, advices and fruitful discussions, particularly the FTIR- and RAM-group, and especially all those who knew when I had to be cheered up with chocolates, tea or other distractions.

Special thanks to Tine Weinzierl for the support in technical aspects and her efforts sharing her knowledge about the FTIR instruments, even if necessary per skype-phone to Suriname. Many thanks also to Peter Grupe for rescuing my computer and his support, especially during measurement campaigns in Suriname.

I wish to thank Cor Becker and his team of the Meteorological Service of Suriname and Dennis Wip and Bing Tan from the Anton-de-Kom-University of Suriname for their support and cooperation during the measurement campaigns. I especially acknowledge my guest-family Bernadetta and Henk Guilhuis in Suriname for their hospitality and warm welcoming during my stays in Paramaribo and their prayers to support me with the thesis.

Many thanks to the Atmospheric Chemistry group at the University of Wollongong, especially to Travis Naylor, Martin Riggenbach, Graham Kettlewell and Francis Philips for support during my project, and to all others who made me feel home in Wollongong. I would like to acknowledge the Australian Government

and the Endeavour Programme, which funded my stay in Wollongong, Australia and made it possible for me to experience the Australian way of life and work and to realize my project together with the group of David Griffith. I am also grateful to the German Academic Exchange Service (DAAD) for support. I kindly acknowledge the company Manildra and its staff members at Nowra, Australia for willingly providing the land, cattle and infrastructure support during the measurement campaign on their farm. Many thanks to Glenys Lugg for her cooperation and dedicated support. Without her, the field campaign in Nowra would not have been possible. I also thank Mike Harvey and Murray Smith from NIWA for assistance and support with the REA system.

I am grateful to Mark Lawrence and Tim Butler for providing the MATCH-MPIC model output and for their cooperation and fruitful discussions concerning the comparison of the FTIR data sets with the model.

I wish to thank Christian Frankenberg for providing the methane data from SCIAMACHY and Peter Bergamaschi and Jan Fokke Meirink for providing the TM5 methane data.

I kindly acknowledge Otto Schrems and the Alfred-Wegener Institute (AWI) Bremerhaven for support and cooperation with the Paramaribo-spectrometer.

Thanks to the MPI Jena, especially Christoph Gerbig, for the analysis of the flask samples from Suriname.

I thank John Burrows for providing the Bruker 125HR FTS for the laboratory cell measurements, Frank Hase (Forschungszentrum Karlsruhe) for his cooperation and Peter Spitz (University of Bremen) for his help with the measurement setup.

I acknowledge Peter van Velthoven for providing ECMWF data from 2004 for Paramaribo.

Financial support of the tropical measurement campaigns by the EU within STAR, HYMN and ACCENT is acknowledged.

I acknowledge the Zentrale Forschungsförderung (ZF) of the University Bremen for financial support.

Finally I would like to thank my family and friends, especially my parents Sophie Ehlert and Jens Petersen, for all their support and encouragements, especially during the last weeks of PhD-writing.